

Please note the color coding. **Green** was for Referee 1 and **Gray** for referee 2. I used **bold** for replies to referee 2 that are not inserted into the paper.

Interactive comment on “NO₂ and HCHO measurements in Korea from 2012 to 2016 from Pandora Spectrometer Instruments compared with OMI retrievals and with aircraft measurements during the KORUS-AQ campaign” by Jay Herman et al.

Anonymous Referee #2 Received and published: 10 June 2018

General comments:

The manuscript entitled “NO₂ and HCHO measurements in Korea from 2012 to 2016 from Pandora Spectrometer Instruments compared with OMI retrievals and with aircraft measurements during the KORUS-AQ campaign” presents total vertical column measurements of NO₂ and HCHO with 9 Pandora instruments at 8 sites during a field campaign in Korea in 2016 (May-June) and from 1 to 5 years before, depending on the station. An investigation of the pollution levels at the 8 different sites, the diurnal pattern of NO₂ and HCHO as well as NO₂ long-term trends are presented.

During the campaign, additional measurements of the NO₂ column using the 4STAR airborne sun photometer and of the altitude profile of HCHO using the air-borne CAMS instrument have been performed, which are compared to the columns measured by the ground-based Pandora instruments. On a longer time series of 1 and 5 years, respectively, a comparison to OMI NO₂ satellite measurements is presented. At last, the Pandora HCHO measurements during the campaign are compared to HCHO measurements from OMI.

The paper highlights nicely the importance and advantages of ground-based measurements with a high temporal resolution for the investigation of local, surface near air pollution in comparison to satellite measurements, which cannot capture the diurnal cycle and tend to underestimate local pollution hotspots due to the large averaging area of the ground pixels.

The paper is well structured and the scientific approach is clearly described. However, the objective and aim of the campaign should be declared more clearly in the text and in some cases the interpretation of the results is lacking.

All in all, I believe this paper is in the scope of AMT and should be published, with some minor improvements, based on answering my specific comments below:

Specific comments:

Abstract, line 44: What kind of average is meant by the mentioned “PSI C(NO₂) averages” and “OMI averages”?

PSI C(NO₂) 30-day running averages

Introduction: Please mention that these are direct sun measurements.

I added: “The intent of the network was to integrate **direct-sun** column density observations of NO₂ and HCHO into a multi-perspective framework of observations including ground-based, satellite, and airborne measurements of air quality.”

The objective and aim of the campaign should be declared more clearly in the text. **Done**

Although the cited reference Spinei et al., 2018 discusses the analysis procedure very extensively, please mention in the introduction at least briefly the retrieval algorithm (DOAS?), what kind of reference spectrum is used and how the measured slant columns from the direct sun measurements are converted into vertical columns.

The following has been added

“The retrieval algorithm is based a **direct-sun spectral fitting method similar to the well-accepted DOAS (Differential Optical Absorption Spectroscopy, Platt, et al., 1979 and Platt, 1994). NO₂ absorption cross sections were obtained from the laboratory measurements of Vandaele et al., 1998, and HCHO cross sections from Meller and Moortgat (2000). The PSI reference solar spectrum is constructed from a high resolution extraterrestrial spectrum from 270 nm to 1000 nm merged from different sources (Bernhard et al. (2004). Solar spectrum sources are from: Kurucz (2005) normalized to Thuillier et al. (2004), SUSIM/Atlas-3 spectrum (VanHoosier et al., 1996), and the spectrum from Gueymard (2004). One of the advantages of using direct-sun observations is the accurate conversion to vertical column based on a geometric calculation of the slant path air mass factor AMF for a known solar zenith angle SZA is with a slight correction to the function Secant(SZA) (Herman et al., 2009 eqn. 3). A complete description of the retrieval algorithms and PSI operations are given in the PSI software manual (Cede, 2017). Accuracy in the DOAS-type retrieval is obtained using careful measurements of the spectrometer’s slit function, wavelength calibration, knowledge of atmospheric absorption cross sections, and the solar spectrum at the top of the atmosphere. Accuracy for C(NO₂) has been estimated to be ±0.05 DU. A recent addition of anti-reflection coatings to the PSI optics has improved accuracy and precision by reducing the residuals associated with spectral fitting using trace gas absorption cross sections. The reduced residuals are necessary for the retrieval of formaldehyde and bromine oxide that absorb in spectral regions dominated by ozone and NO₂. Other DOAS-type measurements have been made in Korea based on observations of sky radiance ratios (e.g., Multi Axis MAX-DOAS: Kanaya, et al., 2014) and direct-sun DOAS using a PSI in Seoul, Korea (Park et al., 2018).”**

Since it is mentioned later on in Section 2 for the measurements in Anmyeondo, please discuss briefly the contribution of the stratosphere to the presented total vertical columns.

How large is the contribution and does it change over the day? Can stratosphere and troposphere be separated?

The measurement from the PSI is for total column (stratosphere + troposphere). For NO_2 , the stratospheric contribution is approximately 0.1 DU and it does change during the day by about 0.05 DU. The direct sun measurement does not permit separation of troposphere and stratosphere

A sentence was added, "Of these sites, Anmyeondo frequently (40%) retrieves values of $\text{C}(\text{NO}_2)$ that are close to the typical stratospheric values of 0.1 ± 0.05 DU. Other sites occasionally have clean days with similar low values."

Please mention briefly what other work on ground-based (DOAS type) Korean/Asian air pollution measurements has been published in other studies in the past to put the aim of the campaign/study into context.

There are other DOAS measurements, but they are all MAX-DOAS, which are quite different than direct sun. I added a brief comment, "Other DOAS-type measurements have been made in Korea based on observations of sky radiance ratios (e.g., Multi Axis MAX-DOAS: Kanaya, et al., 2014) and direct-sun DOAS using a PSI in Seoul, Korea (Park et al., 2018)."

Fig. 2a, page 5: The agreement between the instruments is quite impressive. But what happened at 17:30-18:00 local time? Are these real differences or has the Pan27 instrument some missing data gaps and the connected data points convey a wrong impression?

These are differences caused by low signal from increasing cloud cover that affects the retrieval algorithm. There are small differences between instruments that introduce different amounts of noise in the signal for small signals.

Section 2, line 195f, page 8: See comment on stratospheric contribution above.

The most frequently occurring $\text{C}(\text{NO}_2)$ value at Anmyeondo is 0.15 – 0.2 DU, which means that the measured NO_2 amount are partly from the stratosphere (0.1 ± 0.05 DU) with very little tropospheric or boundary layer NO_2 . There are occasional $\text{C}(\text{NO}_2)$ plumes that could be from industrial activity to the north, and, perhaps, from China. Transport of NO_2 from China occurs episodically in significant amounts (Lee et al., 2014).

Section 3: Please explain in more detail why the observed NO_2 daily patterns fit so well to automobile and power generation emissions.

The pattern measured by PSI in Korea during the spring KORUS-AQ campaign differed from other non-Korean locations in that there usually a weaker morning peak in Korea compared to the afternoon. The strong afternoon peak does not occur every day, but is often enough to be notable. The meteorological effects certainly play a role, but at this time the appropriate model studies are not available.

In many of the studies on the NO₂ diurnal cycle in polluted urban regions two NO₂ peaks in the morning and afternoon are observed corresponding to the morning and afternoon traffic rush hour. Do you have an explanation why the morning rush hour is hardly visible in the presented measurements and why the afternoon peak is so pronounced? Do you also observe a weekly cycle in your NO₂ measurements, like it has been observed in polluted regions and discussed for example in Beirle et al. (GRL, 2003) or Ialongo et al. (AMT, 2016)?

Yes, there is a weekly cycle in that Sundays usually have less pollution than Wednesdays.

Section 4: About the seasonal cycles: Please discuss briefly why the seasonal cycle of NO₂ has its minimum in August/September and its maximum in winter/early spring. Is there more heating during winter times in Korea or is it just due to less OH radicals because of less light in winter?

Winter in Korea is complicated with quite a bit of cloud cover and precipitation. This certainly would affect the chemistry. Plus the cold winter weather certainly increases the amount of energy used, which produces more NO₂. Since I did not do the model studies, I preferred to just leave the data without a “hand waving” explanation.

Section 4, line 291, page 13: The “strong effect on local air quality” is an improvement of local air quality, right?

The strong effect on local air quality mentioned in the paragraph concerns large amounts of total column NO₂, most of which is near the surface. This probably makes the air quality worse.

Section 6, line 531f, page 27: What is the reason for this seasonal increase during May and June?

Unfortunately, there are no long term measurements of C(HCHO), so there is no way of determining if the increase is from sources or VOC chemistry. The PSI was not capable of measuring HCHO prior to late 2016.

Technical corrections:

Line 43, page 2: please add “local time” or LT

Added: “OMI overpass local times (LT = 13.5 ± 0.5 hours).”

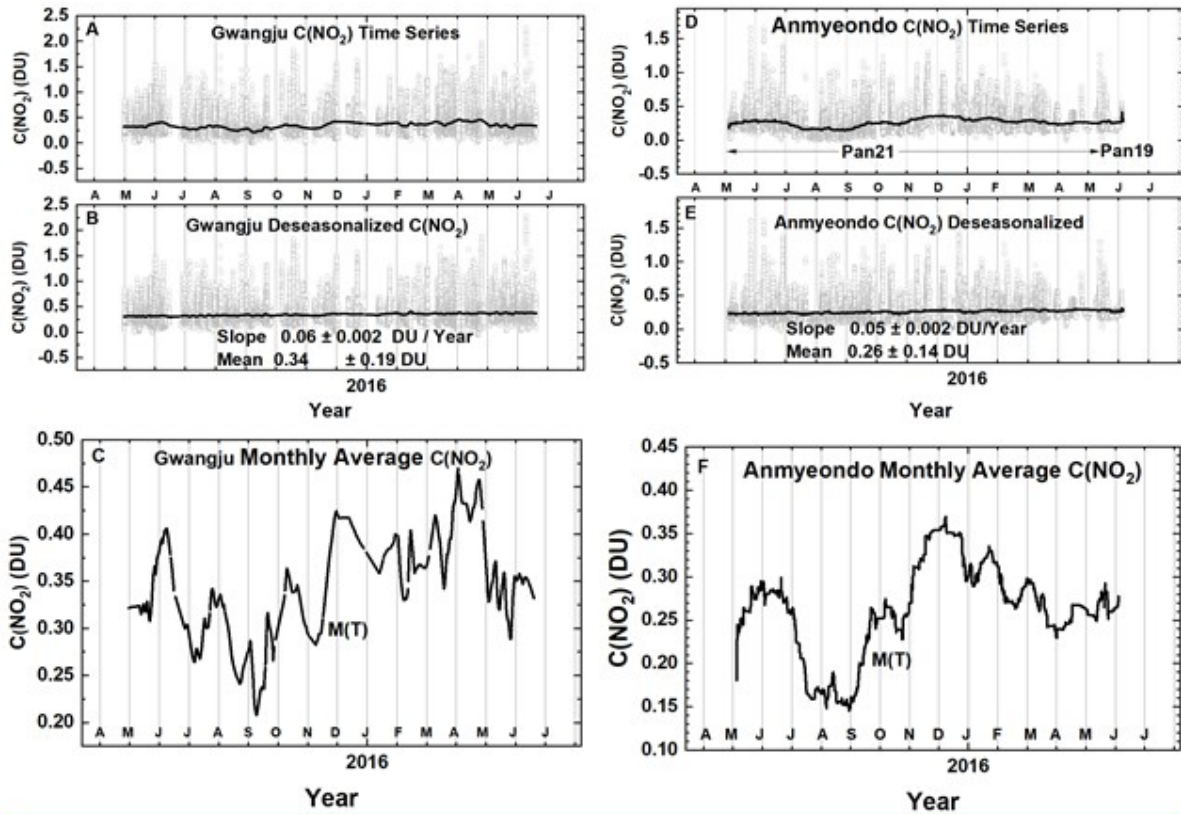
Line 48, page 2: please enclose “FOV” in brackets **OK**

Tab. 1: The degree symbol is missing for latitude and longitude values **OK**

Line 229, page 10: Please round off the values for H₂O and CO₂. Six significant(?) digits are unnecessary here, since this paragraph is only about getting a general impression on the order of magnitude of the emissions from automobiles. **OK** “containing H₂O (144 ppm) and CO₂ (122 ppm)”.

Fig. 6: Between Panel A and Panel B the x axis tick labels A, M, J and J (April, May, June, July) are missing.

Fixed



Line 298, page 13: please add “local time” or LT Fig. 9a: Seoul (left panel): Why does the 3-month average (solid lines) show values where around 6 month of data are missing? Or is it just a linear interpolation between the values before and after the gap?

Missing data are represented by linear interpolation in the plots, but not any analysis. I have added a statement in the caption. “Fig. 9a Comparisons between the daily values of C(NO₂) for OMI (black) and PSI (red) at Seoul and Busan for a 5-year period. Solid lines show the average seasonal variation (Lowess(0.1)), see also Fig. 9b. **Linear interpolation is used where there are missing data points.**”

Line 429, page 19 and Fig. 14: The numbers in “Integ(0.026, 7.2)” are given in kilometers?

Yes. Added: “Integ(0.026, 7.2 km)”

Tab. 2.: "PSI HCHO" is missing the "DU" (like in "DC8 HCHO DU")

Table 2 is now

Table 2 Taehwa Mtn DC8 compared to PSI measurements (see 10 Jun in Fig. 18)

Date	LT	DC8 HCHO DU	PSI HCHO (DU)	Percent
11 May	08:25:19	0.4	0.6	67
18 May	08:34:26	0.4	0.5	80
30 May	12:05:00	0.5	0.9	56
10 Jun	08:22:45	1	1.16	86
10 Jun	12:22:53	1	1.5	67
10 Jun	15:46:03	1	1.3	77

Line 545, page 29: "... very high amounts of urban pollution from NO₂ and HCHO *, and more moderate, but still high values, away from the urban centers." *close to the urban centers

Changed to , " but still high values in Mt Taewha and Yeogju, which are some distance from the major urban centers, . An exceptional location was Amnyeondo"

1 **NO₂ and HCHO measurements in Korea from 2012 to 2016 from Pandora Spectrometer Instruments**
2 **compared with OMI retrievals and with aircraft measurements during the KORUS-AQ campaign**

3 **Jay Herman¹, Elena Spinei², Alan Fried³, Jhoon Kim⁴, Jae Kim⁵, Woogyung Kim³, Alexander Cede⁶, Nader**
4 **Abuhassan¹, Michal Segal-Rozenhaimer^{7,8}**

5

6

7

8

9

10

11

12

13

14

15

16

17

18 **Correspondence email: jay.r.herman@nasa.gov**

19 **¹University of Maryland Baltimore County JCET**

20 **²Virginia Polytechnic Institute and State University, Blacksburg, VA 24061, USA**

21 **³Institute of Arctic & Alpine Research, University of Colorado, Boulder, Colorado**

22 **⁴Dept. of Atmospheric Sciences, Yonsei University, Seoul Korea**

23 **⁵Department of Atmospheric Science, Pusan University, Busan, Korea**

24 **⁶Goddard Earth Sciences Technology & Research (GESTAR) Columbia, Columbia, MD 21046, USA**

25 **⁷Earth Science Division, NASA Ames, Mountain View, California**

26 **⁸Bay Area Environmental Research Institute, Petaluma, California**

27

28

29 **NO₂ and HCHO measurements in Korea from 2012 to 2016 from Pandora Spectrometer Instruments**
30 **compared with OMI retrievals and with aircraft measurements during the KORUS-AQ campaign**

31
32 **Abstract**

33
34 Nine Pandora Spectrometer Instruments (PSI) were installed at 8 sites in South Korea as part of
35 the KORUS-AQ (Korea U.S.-Air Quality) field study integrating information from ground, aircraft,
36 and satellite measurements for validation of remote sensing air-quality studies. The PSI made
37 direct-sun measurements of total vertical column NO₂, C(NO₂), with high precision (0.05 DU,
38 where 1DU = 2.69x10¹⁶ molecules/cm²) and accuracy (0.1 DU) that were retrieved using
39 spectral fitting techniques. Retrieval of Formaldehyde (HCHO) total column amounts were also
40 obtained at five sites using the recently improved PSI optics. The HCHO retrievals have with
41 high precision, but possibly lower accuracy than for NO₂ because of uncertainty about the
42 optimum spectral window for all ground-based and satellite instruments. PSI direct-sun
43 retrieved values of C(NO₂) and C(HCHO) are always significantly larger than OMI (AURA satellite
44 Ozone Monitoring Instrument) retrieved C(NO₂) and C(HCHO) for the OMI overpass local times
45 (LT = 13.5 ± 0.5 hours). In urban areas, PSI C(NO₂) 30-day running averages are at least a factor
46 of two larger than OMI averages. Similar differences are seen for C(HCHO) in Seoul and nearby
47 surrounding areas. Late afternoon values of C(HCHO) measured by PSI are even larger, implying
48 that OMI early afternoon measurements underestimate the effect of poor air quality on human
49 health. The primary cause of the OMI underestimate is the large OMI field of view (FOV) that
50 includes regions containing low values of pollutants. In relatively clean areas, PSI and OMI are
51 more closely in agreement. C(HCHO) amounts were obtained for five sites, Yonsei University in
52 Seoul, Olympic Park, Taehwa Mtn., Amnyeondo, and Yeosu. Of these the largest amounts of
53 C(HCHO) were observed at Olympic Park and Taehwa Mountain, surrounded by significant
54 amounts of vegetation. Comparisons of PSI C(HCHO) results were made with the Compact
55 Atmospheric Multispecies Spectrometer CAMS during overflights on the DC-8 aircraft for
56 Taehwa Mtn and Olympic Park. In all cases, PSI measured substantially more C(HCHO) than
57 obtained from integrating the CAMS altitude profiles. PSI C(HCHO) at Yonsei University in Seoul
58 frequently reached 0.6 DU and occasionally exceeded 1.5DU. The semi-rural site, Mt. Taehwa,
59 frequently reached 0.9 DU and occasionally exceeded 1.5DU. Even at the cleanest site,
60 Amnyeondo, HCHO occasionally exceeded 1 DU.

61
62 Keywords: Pandora, KORUS-AQ, NO₂, HCHO, Formaldehyde, Korea

63

64 **1 Introduction**

65 The purpose of this paper is to present the retrieved amounts of nitrogen dioxide and
66 formaldehyde, NO₂ and HCHO, obtained from Pandora Spectrometer instruments (PSI) direct-sun
67 observations during the KORUS-AQ campaign (Korea US Air Quality: May – June 2016). Quoting from a
68 NASA website: “Korea U.S.-Air Quality (KORUS-AQ) is a joint field study between NASA and the Republic
69 of Korea to advance the ability to monitor air pollution from space. The campaign will assess air quality
70 across urban, rural and coastal South Korea using observations from aircraft, ground sites, ships and
71 satellites to test air quality models and remote sensing methods. Findings will help develop observing
72 systems using models and data to improve air quality assessments for decision makers.” A thorough
73 description of the KORUS-AQ campaign and its motivations is given in a pre-campaign white paper,
74 https://espo.nasa.gov/korus-aq/content/KORUS-AQ_White_Paper.

75 Assessing air quality in South Korea is of interest because of the levels of pollution arising from
76 high densities of population and intense industrial activity associated with the production of NO₂.
77 Recent measurements of surface concentrations of NO₂ and comparisons with satellite data
78 demonstrate the need for high quality ground-based measurements to augment satellite observations
79 (Kim et al., 2017; Jung et al., 2017). The driving reason behind the interest is the effect of elevated levels
80 of NO₂ in Korea on human health (Kim and Song, 2017 and references therein). Measurements of N O₂
81 from aircraft have been used to obtain altitude profiles to compare with data obtained from fixed site
82 measurements and to obtain a national scale
83 estimate of pollutant exposure (Lee et al., 2015;
84 Kim and Song, 2017).

85 In addition to NO₂, PSI measurements
86 were used to assess the amount of Formaldehyde
87 (HCHO) present in the air. This is important
88 because of HCHO potential impact on health
89 (Zhang et al., 2013,) and because it plays a strong
90 role in tropospheric reactions leading to the
91 formation of boundary layer ozone. Sources of
92 HCHO are from atmospheric reactions with
93 volatile organic compounds (VOC) emitted from
94 ground sources and industrial activities (Lee at al.,
95 2009). A previous paper describes HCHO
96 retrievals from a PSI located at Yonsei University
97 in Seoul using a similar spectral fitting retrieval
98 algorithm used in the current study (Park et al.,
99 2018), but using a different wavelength fitting
100 range, 335 – 358 nm instead of 332 – 359 nm
101 used in this study. The choice of spectral fitting
102 window is discussed in Spinei et al. (2018).



Fig. 1 KORUS-AQ sites for 9 Pandora instruments at 8 sites.

103 As part of the KORUS-AQ campaign, a network of nine PSI was installed in Korea at 8 locations
 104 (Fig. 1 and Table 1). Five of the sites were selected to be “down-wind” from Seoul, an extremely NO₂
 105 polluted area. The intent of the network was to integrate **direct-sun** column density observations of
 106 NO₂ and HCHO into a multi-perspective framework of observations including ground-based, satellite,
 107 and airborne measurements of air quality. Viewing air quality through these multiple perspectives is
 108 important for connecting observations from future geostationary satellites to air quality networks such
 109 that conditions both at the surface and aloft can be better understood and represented across
 110 unmonitored areas. The data are especially important for computer models used for forecasts and
 111 decision making. Five of the KORUS-AQ PSI had recently improved optics that permitted retrieval of total
 112 vertical column formaldehyde (C(HCHO)). Part of the network was installed in April 2015, a year before
 113 the start of the campaign. Three PSI continue to operate in Korea, one each, in Busan and Seoul since
 114 2012, and one in Gwangju operating since April 2015.

115
 116 Measurements of daytime total columns in Dobson Units, where 1 DU = 2.69 x 10¹⁶
 117 molecules/cm², C(NO₂), C(O₃) and C(HCHO) are obtained every 80 seconds, which enables the PSI to
 118 show rapid short term (minutes to hours) variations in most locations with significant pollution (e.g.,
 119 C(NO₂) > 0.2 DU). PSI measurements of the visible and UV wavelengths are obtained separately (40
 120 seconds each). A visible wavelength blocking filter, U340, reduces stray light for UV measurements.

121

Table 1 KORUS-AQ Locations (South to North)

Locations	Alt(m)	Latitude	Longitude
Gwangju	33	35.2260 ^o N	126.8430 ^o W
Busan	228	35.2353 ^o N	129.0825 ^o W
Anmyeondo	41	36.5380 ^o N	126.3300 ^o W
Taehwa Mtn	160	37.3123 ^o N	127.3106 ^o W
Yeoju-1 & 2	90	37.3385 ^o N	127.4895 ^o W
Songchon	49	37.4100 ^o N	127.5600 ^o W
Olympic Park	26	37.5232 ^o N	127.1260 ^o W
Seoul	181	37.5644 ^o N	126.9340 ^o W

122

123 Details on the Pandora spectrometer instrument can be found in Herman et al., (2009 and 2015)
 124 as well as a NASA Pandora website
 125 https://avdc.gsfc.nasa.gov/pub/DSCOVER/Pandora/Web_Pandora/index.html and the data used are
 126 available from <https://avdc.gsfc.nasa.gov/pub/DSCOVER/Pandora/DATA/KORUS-AQ/>

127

128 The PSI consists of a small Avantes low stray light spectrometer (280 – 525 nm with 0.6 nm
 129 spectral resolution with 4 times oversampling) connected to an optical head by a 400 micron single
 130 strand fiber optic cable. The spectrometer is temperature stabilized at 20^oC (68^oF) inside of a weather
 131 resistant container. The optical head consists of a collimator and lens giving rise to a 1.6^o FOV (field of
 132 view) FWHM (Full Width Half Maximum) with light passing through two filter wheels containing
 133 diffusers, a UV340 filter (blocks visible light), neutral density filters, and an opaque position (dark
 134 current measurement). When the diffuser is used, the FOV is increased to over 2^o. The optical head is

135 connected to a small suntracker capable of accurately following the sun's center using software running
136 on a small computer-data logger contained in a weatherproof outer box along with the spectrometer in
137 a second inner temperature controlled box. The PSI is capable of obtaining C(NO₂), C(HCHO) and C(O₃)
138 amounts sequentially over a period of 80 seconds including two dark current determinations. The
139 integration time for NO₂ in bright sun is about 4 milli-seconds that is repeated and averaged for 20
140 seconds (up to 4000 measurements) to obtain very high signal to noise ratios and very high precision
141 (precision < 0.01 DU). Similar comments apply to C(O₃), but not to C(HCHO), since formaldehyde
142 absorption spectrum is mixed in with absorption from NO₂ and O₃. This causes cross-correlation effects
143 in the retrieval algorithm that make C(HCHO) retrievals sensitive to the selection of the wavelength
144 range. The main source of noise in the measurement comes from the presence of clouds or haze in the
145 FOV, which increases the exposure time and reduces the number of measurements in 20 seconds.

146
147 The retrieval algorithm is based a direct-sun spectral fitting method similar to the well-accepted
148 DOAS (Differential Optical Absorption Spectroscopy, Platt, et al., 1979 and Platt, 1994). NO₂ absorption
149 cross sections were obtained from the laboratory measurements of Vandaele et al., 1998, and HCHO
150 cross sections from Meller and Moortgat (2000). The PSI reference solar spectrum is constructed from a
151 high resolution extraterrestrial spectrum from 270 nm to 1000 nm merged from different sources
152 (Bernhard et al. (2004). Solar spectrum sources are from: Kurucz (2005) normalized to Thuillier et al.
153 (2004), SUSIM/Atlas-3 spectrum (VanHoosier et al., 1996), and the spectrum from Gueymard (2004).
154 One of the advantages of using direct-sun observations is the accurate conversion to vertical column
155 based on a geometric calculation of the slant path air mass factor AMF for a known solar zenith angle
156 SZA is with a slight correction to the function Secant(SZA) (Herman et al., 2009 eqn. 3). A complete
157 description of the retrieval algorithms and PSI operations are given in the PSI software manual (Cede,
158 2017). Accuracy in the DOAS-type retrieval is obtained using careful measurements of the
159 spectrometer's slit function, wavelength calibration, knowledge of atmospheric absorption cross
160 sections, and the solar spectrum at the top of the atmosphere. Accuracy for C(NO₂) has been estimated
161 to be ±0.05 DU. A recent addition of anti-reflection coatings to the PSI optics has improved accuracy and
162 precision by reducing the residuals associated with spectral fitting using trace gas absorption cross
163 sections. The reduced residuals are necessary for the retrieval of formaldehyde and bromine oxide that
164 absorb in spectral regions dominated by ozone and NO₂. Other DOAS-type measurements have been
165 made in Korea based on observations of sky radiance ratios (e.g., Multi Axis MAX-DOAS: Kanaya, et al.,
166 2014) and direct-sun DOAS using a PSI in Seoul, Korea (Park et al., 2018).

167
168 This paper discusses the distribution of C(NO₂) and C(HCHO) over Korea at the sites where the
169 PSI were located (Fig. 1). Section 2 shows the amounts of NO₂ observed by PSIs at the 8 KORUS-AQ
170 sites. Section 3 discusses the diurnal variation of NO₂. Section 4 looks at longer term changes in NO₂
171 obtained from PSIs that were deployed before the beginning of the KORUS-AQ campaign. Section 5
172 evaluates the disagreement with **Ozone Monitoring Instrument** (OMI) satellite C(NO₂) retrievals (Kramer
173 et al., 2008). Section 6 compared PSI C(NO₂) retrievals with the aircraft overpass retrievals from the
174 4STAR instrument (Segal-Rozenhaimer et al., 2014). Section 6 discusses retrievals of C(HCHO) amounts
175 for five PSI sites, the diurnal variation of C(HCHO), and comparisons with the Compact Atmospheric
176 Multispecies Spectrometer CAMS (Richter et al., 2015) from DC-8 aircraft overflights of 5 PSI sites.

177
178

179 2 NO₂ during the KORUS-AQ Campaign (May – June 2016)

180 An example of NO₂ retrieval from two independently calibrated Pandoras that were initially
181 located at the same site (Yeosu, Korea, 37.3385°N, 127.4895°W) are compared in Fig. 2a showing that
182 the difference in C(NO₂) amount is less than 0.05 DU even in the presence of thin afternoon clouds (Fig.
183 2b) that decrease the measured solar irradiance by more than a factor of 2. Though Yeosu is a relatively
184 clean site in Korea (located to the southeast of Seoul Lat=37.5644°N, Long=126.934°W), C(NO₂) amounts
185 frequently reach moderately high values (e.g., 1 DU on 3 June 2016), and occasionally even higher (2-3
186 DU). However, Yeosu has much less C(NO₂) compared to Seoul, less than 30 km distant, where PSI
187 measurements were found to reach over 3 DU (Fig. 3) during the campaign period from mid-April to
188 early June, 2016. Typical C(NO₂) amounts are 0.3 to 0.5 DU in polluted regions.

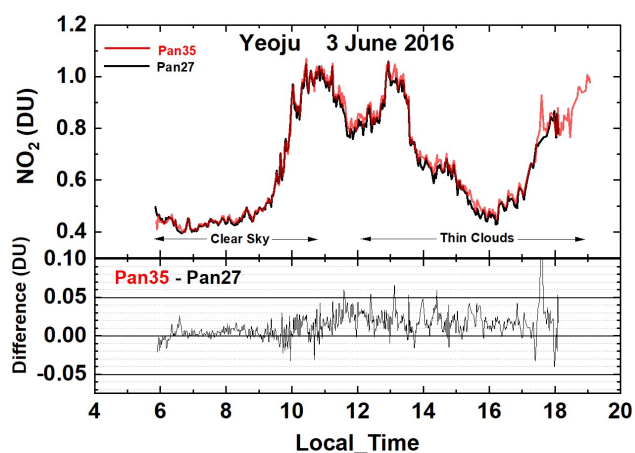


Fig. 2a C(NO₂) amounts from Pandora 27 and 35 in Yeosu, Korea during 3 June 2016 and their difference |Pan35 – Pan27| < 0.05 DU.

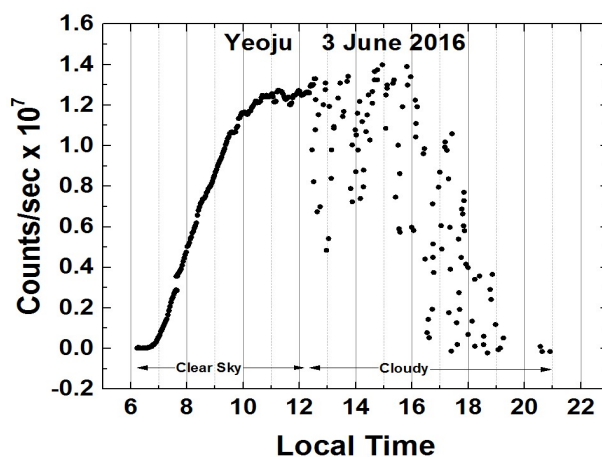


Fig. 2b Pandora 35 estimate of cloud or aerosol reduced measured counts/second at approximately 500 nm.

189 In a manner similar to Fig. 2a, C(NO₂) amounts can show large variability from day-to-day and
190 intraday, as well as between different sites. The largest amounts of C(NO₂) are in the north (Seoul and
191 Olympic Park) associated with the largest population and industry concentrations, while the southern
192 cities of Busan and Gwangju have smaller amounts of C(NO₂). The smallest C(NO₂) amounts are at
193 Anmyeondo (an island on west coast of Korea 42 km south of Seoul, usually not downwind of Seoul),
194 and Songchon to the east of Seoul.

195
196 Figure 2b shows the effect of thin clouds in terms of reduced measured count rates for a single
197 spectrometer pixel near 500 nm showing a near noon count rate of 1.26 x 10⁷ counts/second followed
198 by a reduced count rate as clouds move in front of the sun. The cloud plus aerosol cover estimate is
199 from the same date 3 June 2016 as the C(NO₂) amounts shown in Fig.2a. The effect of thin clouds for
200 C(NO₂) retrieval (Fig. 2a) is increased noise (reduced precision) with a very small impact on accuracy.
201 There are two effects on PSI observations to consider in association with thin clouds. First, is multiple

202 scattering within the cloud affecting the optical path and effective air mass factor AMF. This has a very
203 small effect on AMF, since most of the NO₂ is near the surface well below the clouds. Second, is the
204 reduction in the number of measurements during a fixed 20 second measuring period causing a
205 decrease in the signal to noise ratio. The weather during the campaign was occasionally very cloudy,
206 which caused some missing NO₂ and O₃ data. However, most of the cloudy days were light to moderate
207 cloud cover, which permitted C(NO₂) amounts to be determined, but with lower precision compared to
208 clear-sky direct sun measurements (e.g., Fig.s 2a and b). When the cloud cover becomes sufficiently
209 thick, precision is reduced (increased point-to-point scatter) and the spectral fitting error increases. A
210 small percentage of data points with high retrieval error, C(NO₂ Error) > 0.1 DU, have been removed
211 from the data set.

212

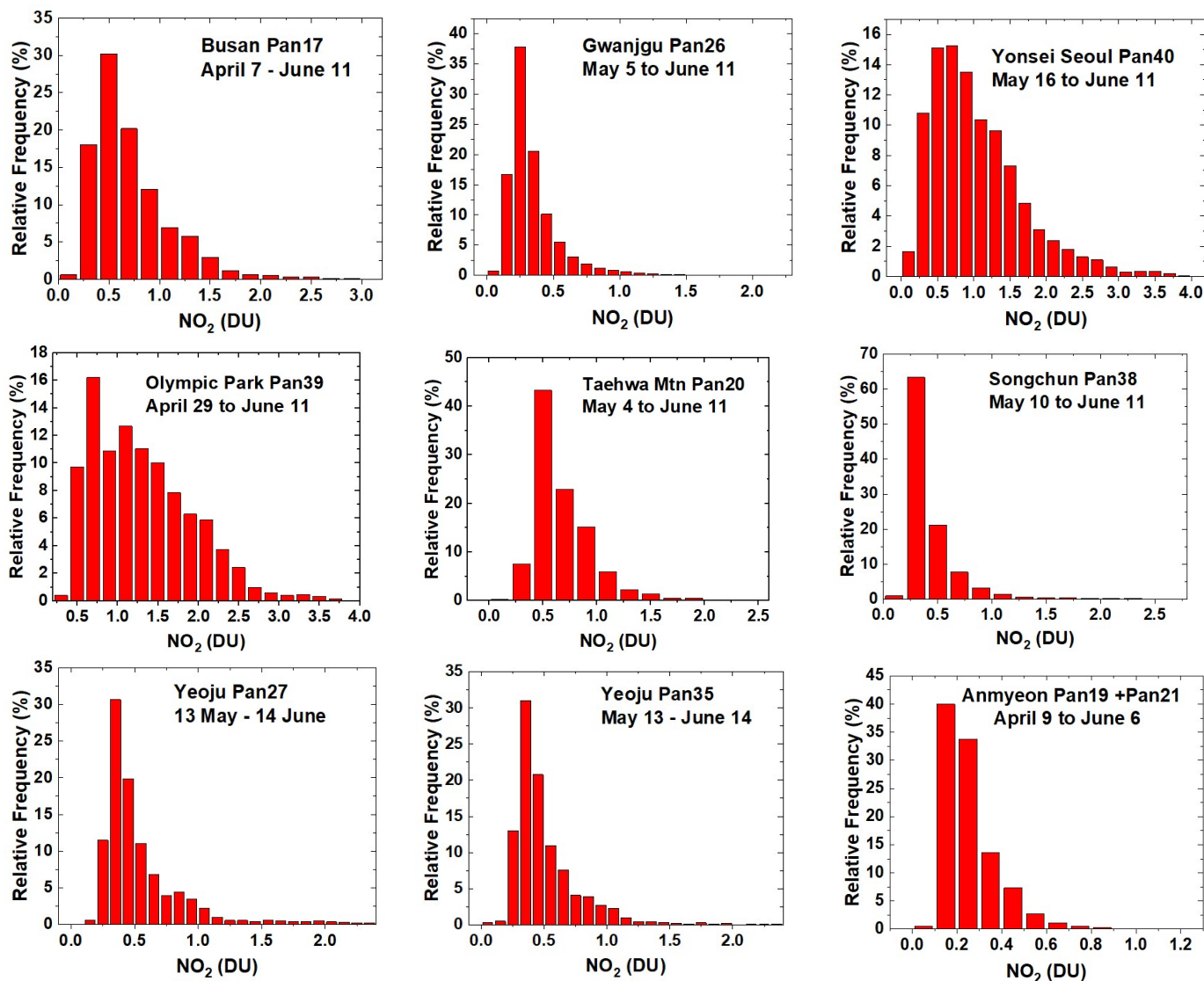


Fig. 3. Frequency distributions of $C(\text{NO}_2)$ across the KORUS-AQ PSI network: April 20 to Jun 6 2016, except as labelled. The axes vary for different sites.

213
214
215
216
217
218
219
220
221

Figures 3 and 4 summarize all of the Pandora $C(\text{NO}_2)$ data obtained during the KORUS-AQ campaign. Figure 3 presents histograms in percent frequency of occurrence for all nine sites. All of the sites located within or downwind of major cities have production of NO_x mainly from transportation and power generation as its major sources. The ratio of transportation NO_x production compared to all other sources is estimated as up to a factor of three (Kim et al., 2013). Of these sites, Anmyeondo frequently (40%) retrieves values of $C(\text{NO}_2)$ that are close to the typical stratospheric values of 0.1 ± 0.05 DU. Other sites occasionally have clean days with similar low values.

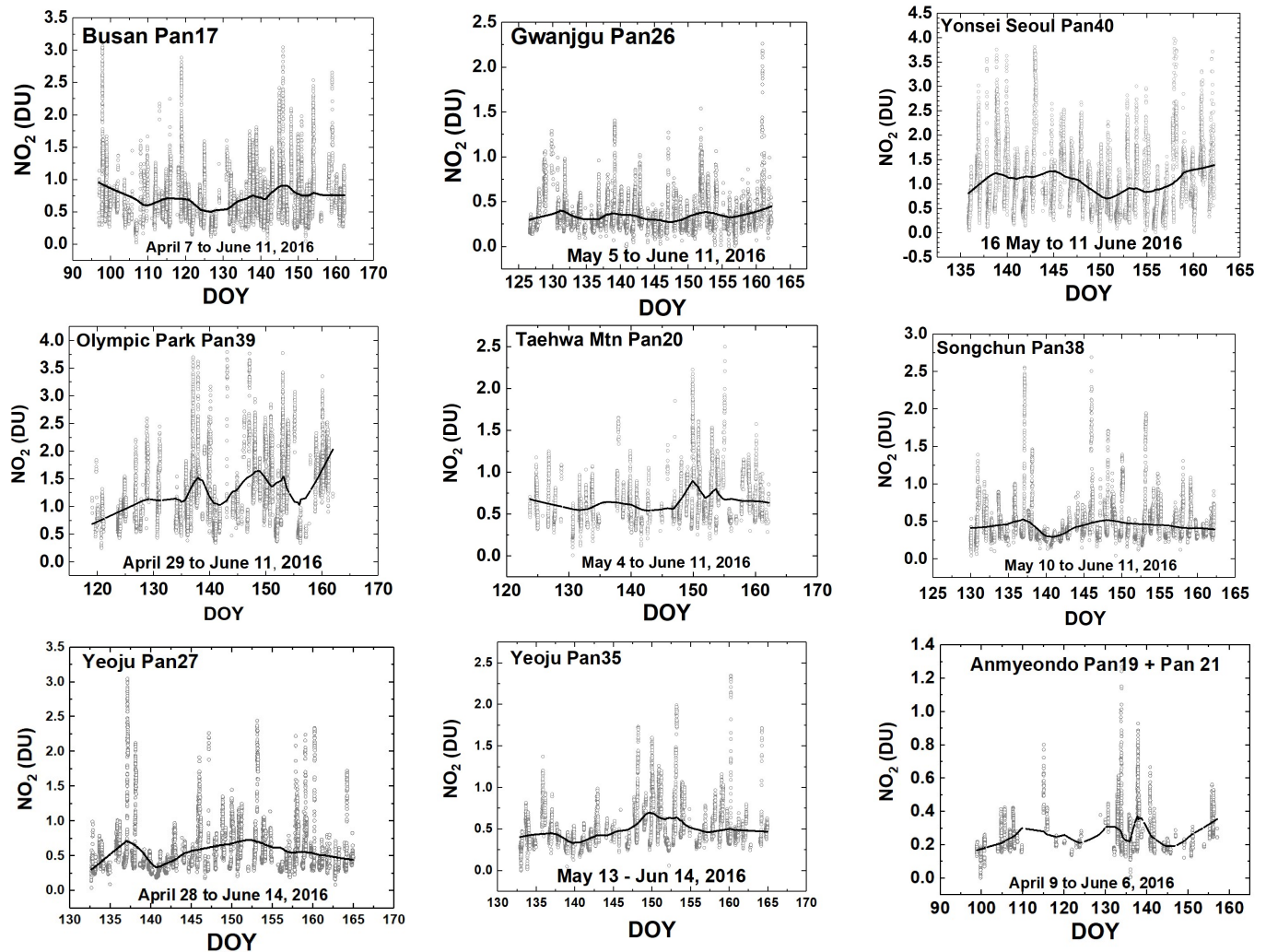


Fig. 4 NO₂ time series vs day of the year (DOY) and diurnal variability (daily vertical extent) at 9 Pandora sites. Notice the very high NO₂ amounts in Seoul and nearby Olympic Park. The black curves are approximately weekly least squares running averages. The daily vertical extent corresponds to diurnal variation (Fig. 2). Note: the vertical scales are different for each site to show the daily variability relative to the running average.

222

223 The Seoul site frequently has amounts of C(NO₂) greater than 2 DU. The same is true of Olympic
 224 Park, located in the eastern part of the Seoul metropolitan area. For locations increasingly distant from
 225 Seoul, the amount of C(NO₂) decreases in response to smaller local emissions, since the short chemical
 226 lifetime of NO₂ normally precludes long distance transport. Compared to Seoul, the two smaller
 227 southern cities, Gwangju and Busan, have relatively low levels of C(NO₂) on most days, with the most
 228 typical values ranging from 0.3 to 0.5 DU, although high values exceeding 2 DU can occur on rare
 229 occasion.

230

231 Figure 4 shows the same data as Fig. 3, but in the form of a time series covering the KORUS-AQ
 232 period. The daily variation (at least one point every two minutes) is shown in the vertical extent
 233 corresponding to each day's data. Figures 3 and 4 show that sites near Seoul metropolitan (Olympic
 234 Park) area have larger amounts of pollution compared to those further away (Taehwa, Songchon, and

235 **Yeosu**. Even though average $C(\text{NO}_2)$ amounts are much lower at Songchon and Yeosu, there are times
236 when the pollution levels are quite high ($C(\text{NO}_2) > 2$ DU, **Figs. 4 and 5**). There are days when the amount
237 of $C(\text{NO}_2)$ gets close to 4 DU in Seoul, 3 DU in Olympic Park and Busan, and 4 DU for one day in Yeosu
238 (April 27). The southern cities, Busan and Gwangju are much less polluted on average, which results in a
239 much smaller effect on adjacent regions. **Busan is located on the southeastern coastline, so that some of**
240 **its NO_2 pollution dissipates over the ocean, except for occasional days when very high amounts (3 DU)**
241 **occur.** Anmyeondo is quite clean, since it is located on the western coast well south of Seoul. **The most**
242 **frequently occurring $C(\text{NO}_2)$ value at Anmyeondo is 0.15 – 0.2 DU, which means that the measured NO_2**
243 **amount are partly from the stratosphere (0.1 ± 0.05 DU) with very little tropospheric or boundary layer**
244 **NO_2 . There are occasional $C(\text{NO}_2)$ plumes that could be from industrial activity to the north, and,**
245 **perhaps, from China. Transport of NO_2 from China occurs episodically in significant amounts (Lee et al.,**
246 **2014).**

247

248 **3 Diurnal Variation of $C(\text{NO}_2)$**

249

250 Grouping the diurnal variation together from multiple days (Fig. 5) reveals a pattern to NO_2
251 emissions and accumulation related to the main NO_2 emission sources (automobiles and power
252 generation) for the 3 largest cities in Korea: Seoul (Pan40), Busan (Pan17), and Gwangju (Pan26). For
253 Seoul, the amounts of $C(\text{NO}_2)$ during the morning (1 DU at 10:00) are much less than later in the
254 afternoon (over 2 -3 DU at 16:00) on almost every day with values occasionally reaching as high as 6 DU.
255 Even the relatively low morning values of $C(\text{NO}_2)$ represent a significant amount of pollution. The 6 DU
256 $C(\text{NO}_2)$ amount in Seoul is unusual, but coincides with the peak values frequently occurring in the late
257 afternoon. $C(\text{NO}_2)$ behavior at nearby Olympic Park to the east of Seoul is very similar to Yonsei
258 University in the heart of Seoul, even though Olympic Park's traffic density is lower than Seoul. Olympic
259 Park is close enough to the metropolitan Seoul area for the transport of NO_2 combined with local
260 production from traffic to produce a very similar diurnal pattern. The moderately large city of Busan also
261 has high values of NO_2 , occasionally reaching 3 DU in the afternoon. Busan has relatively low values of
262 NO_2 in the morning, having peaks in the mid-afternoon and declining in the late afternoon. Gwangju,
263 located in the southwest, is a smaller city with less pollution (peak values = 1.6 DU) and does not have as
264 distinct an afternoon maximum.

265

266

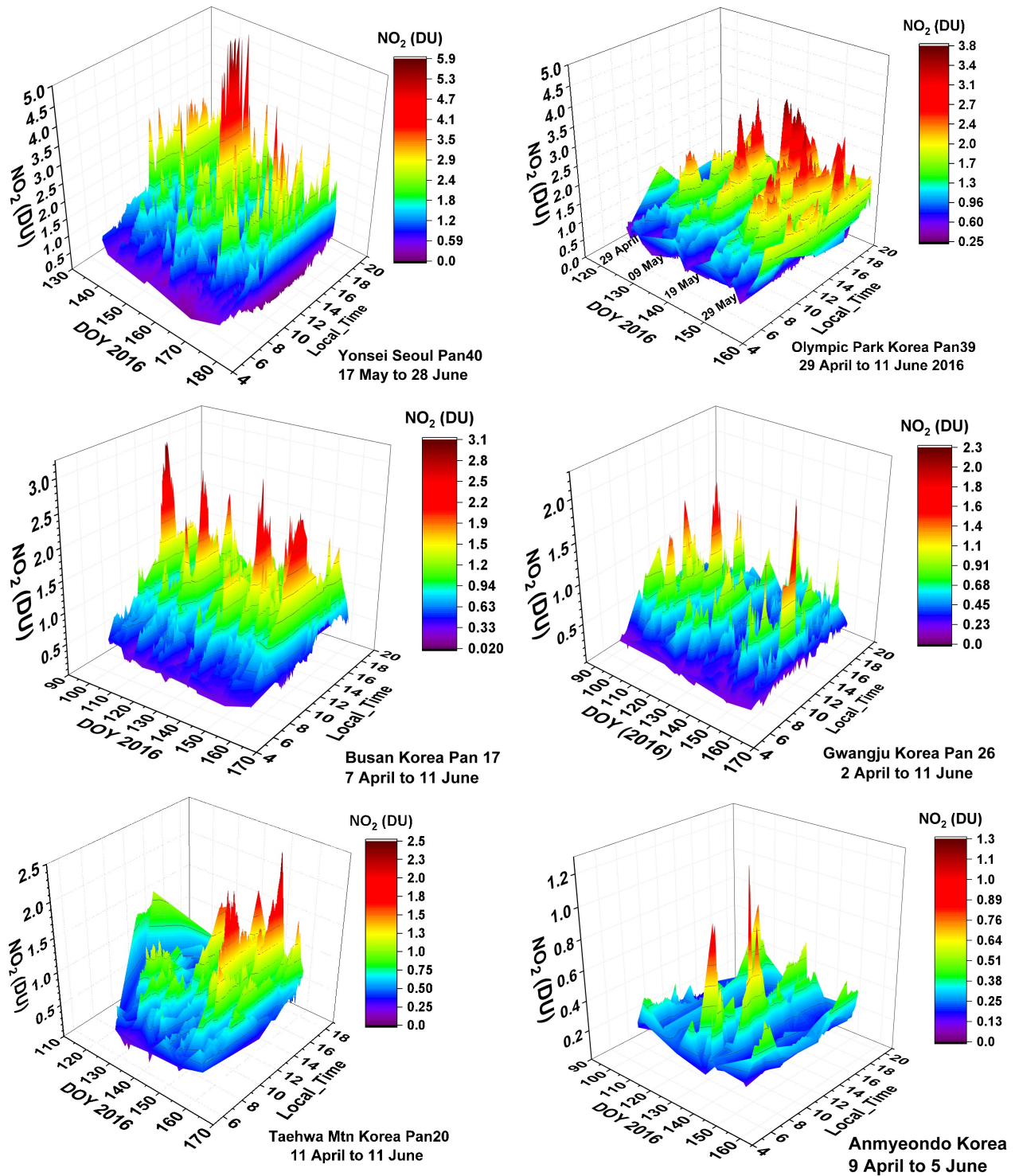


Fig. 5 NO₂ amounts vs Day of the Year (DOY) and Local Time for six sites as labeled in each panel. Day 120=April 29, Day 130=May 9, Day 140=May 19, Day 150=May 29, Day 160=June 8, Day 170 =June18.

268 The panels in Fig. 5 for Taehwa Mtn. and Anmyeondo show regions outside the Seoul
269 metropolitan area that still show substantial amounts of NO₂. Compared to Seoul, the Taehwa site is a
270 semi-rural location with only a small amount of car traffic in the immediate area. However, there are
271 major highways about 6 km from the site that are close enough to permit transport of NO₂ to the
272 Taehwa Mountain site. All of the sites showed a tendency to have peak NO₂ occur in the late afternoon.
273 Anmyeondo on the west central coast of Korea shows C(NO₂) amounts that are quite low with
274 occasional plumes arriving from the north or the west (China).

275 The basic daily pattern of C(NO₂) in urban Korea arises from large amounts of automobile traffic
276 and power plants emitting NO_x (for modern automobiles, roughly 99 % NO and 1 % NO₂). An FTIR
277 analysis of automobile exhaust shows that NO is emitted at 127 ppm, NO₂ at 1.6 ppm, HCHO at 39 ppm,
278 and CH₃OH at 139 ppm as part of the main emissions containing H₂O (144 ppm) and CO₂ (122 ppm).
279 (<https://tools.thermofisher.com/content/sfs/brochures/D10248~.pdf>); see also Walters et al., 2015).

280 NO quickly converts into NO₂ in the presence of ozone and volatile organic compounds VOCs in
281 the atmosphere and can convert back to NO by solar photolysis. KORUS-AQ results frequently show
282 increasing NO₂ during the day with peaks in the afternoon. For these days the measurements imply that
283 the amount of locally produced NO_x and conversion into NO₂ dominates the losses of NO₂ by photolysis
284 and transport out of the region. Other days occasionally show a different behavior, with NO₂ peaks in
285 the morning and a decline thereafter suggesting transport out of the region.

286 4 Longer-Term Changes in C(NO₂)

287 Some of the sites used for the KORUS-AQ campaign (Gwangju and Anmyeondo) had PSIs set up
288 in April 2015, about one year before the start of the campaign. Two other sites (Seoul and Busan) have
289 PSI C(NO₂) data starting in 2012. The extended data sets for Seoul and Busan provide the opportunity to
290 estimate 5-year changes in C(NO₂) amount and seasonal dependence.

291 In Fig. 6, the daily variation over one year at Gwangju and Anmyeondo are evaluated to estimate
292 one year secular trends. The vertical extent in the time series is not noise or uncertainty, but rather the
293 80 second per data point variability throughout each day (e.g., see Fig. 2). Before calculating linear least
294 squares slopes, the unadjusted time series (grey data points in Panels A and D) were deseasonalized
295 (grey data points in Panels B and E) by subtracting a function with zero slope derived from a 30 day
296 running average (dark line in panels A and D or the identical curves in C and F). The running average
297 curves in panels A and D are shown with expanded scale in panels C and F to clearly show the seasonal
298 variation. The “zero slope functions” ZM(t) are obtained by subtracting a linear least squares fit L(t) to
299 monthly running average curves M(t) in panels C and F to form zero slope functions ZM(t) = M(t) – L(t).
300 The results ZM(t) are functions that look similar to the M(t) plots in panels C and F, but with zero slopes.
301 The resulting ZM(t) are then subtracted from the respective original time series (grey circles) in panels A
302 and D. The results are the grey circles in Panels B and E. Similar monthly running means are shown in
303 Panels B and E that have almost no monthly variations (see appendix Fig. A1).

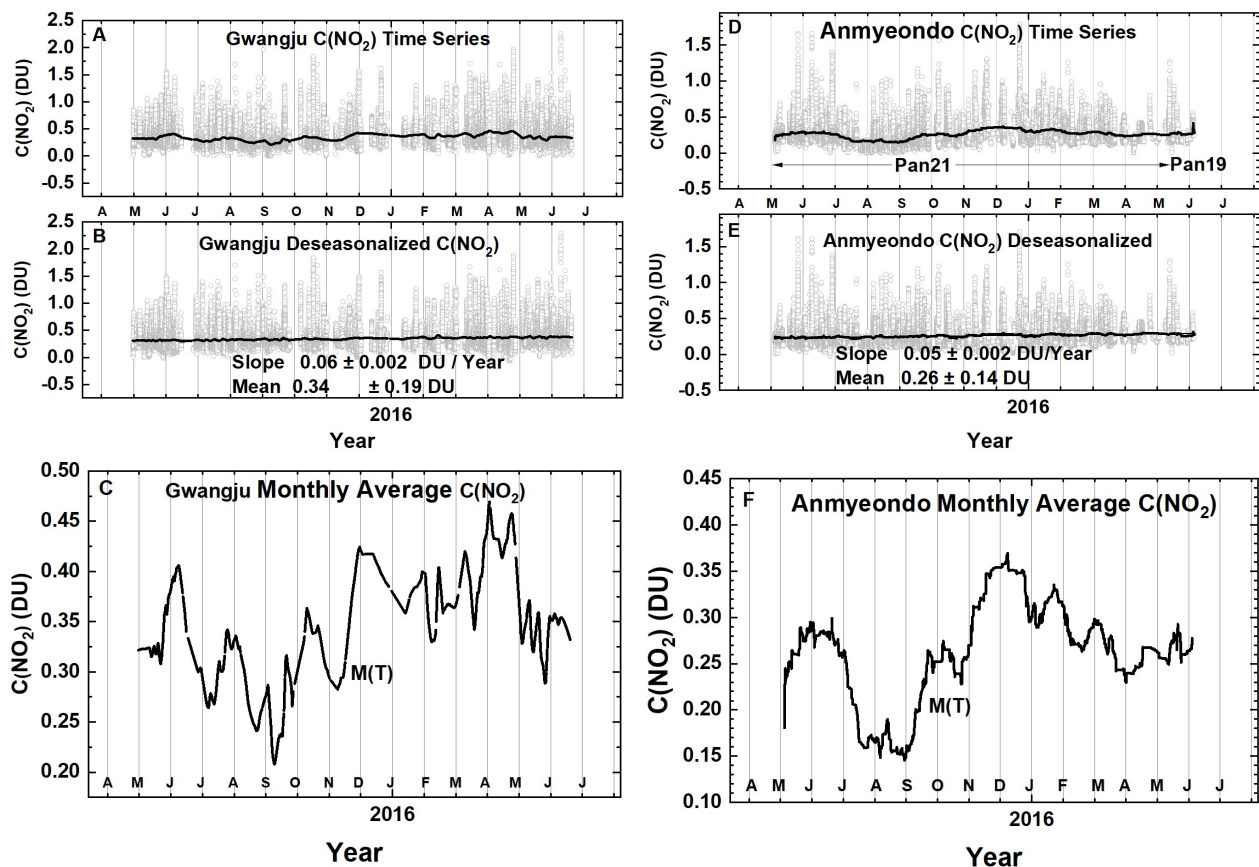


Fig. 6 Approximately 1 year of daily column $C(\text{NO}_2)$ amount data (Panels A and D) and the monthly running average amount (dark plot in Panels A and D). The data are from GIST at Gwangju and Anmyeondo. Panels A and D are the original time series with one data point every 80 seconds, panels B and E are the deseasonalized time series. Panels C and F are an expanded scale of the monthly running averages $M(t)$ of $C(\text{NO}_2)$ that are identical to the solid lines in panels A and D. The vertical extent (panels A, B, D, and E) on a given day is the range of diurnal variation from early morning to late afternoon.

304 The linear trends in Figs. 6B and 6E suggest that there was an increase in pollution levels in
 305 Gwangju and Anmeondo over the period of observation. The southern city of Gwangju (Pan 26) has
 306 higher average $C(\text{NO}_2)$ amounts, 0.34 ± 0.19 DU, compared to the relatively clean coastal site
 307 Anmyeondo, 0.26 ± 0.14 DU. Gwangju seasonal cycle has a minimum in $C(\text{NO}_2)$ amount in September-
 308 October and a very broad maximum from December to May. The Gwangju PSI is located away from
 309 major city traffic on a university campus (Gwangju Institute of Science and Technology, GIST) so that the
 310 average amount of NO_2 (about 0.34 DU) is moderate with some days reaching 1.5 DU. The slopes are
 311 statistically significant at the 2-standard deviation level ($p < 0.05$) and imply that $C(\text{NO}_2)$ was increasing
 312 at a substantial rate. However, the period of observation was too short to estimate multi-year long-term
 313 trends. Additional long-term monitoring of these sites would be desirable for air quality purposes.

314 The PSI on Anmyeondo was located away from a commercial area with moderate traffic and
 315 very near the shore of the Yellow Sea at a regional Global Atmosphere Watch (GAW) station. For
 316 Anmyeondo there is a clear seasonal cycle similar to that in Gwangju with a minimum in September-

317 October and a broad maximum during the winter-spring months. Amnyeondo had an average amount
 318 of 0.25 DU, which is lower than observed at Gwanjgu.

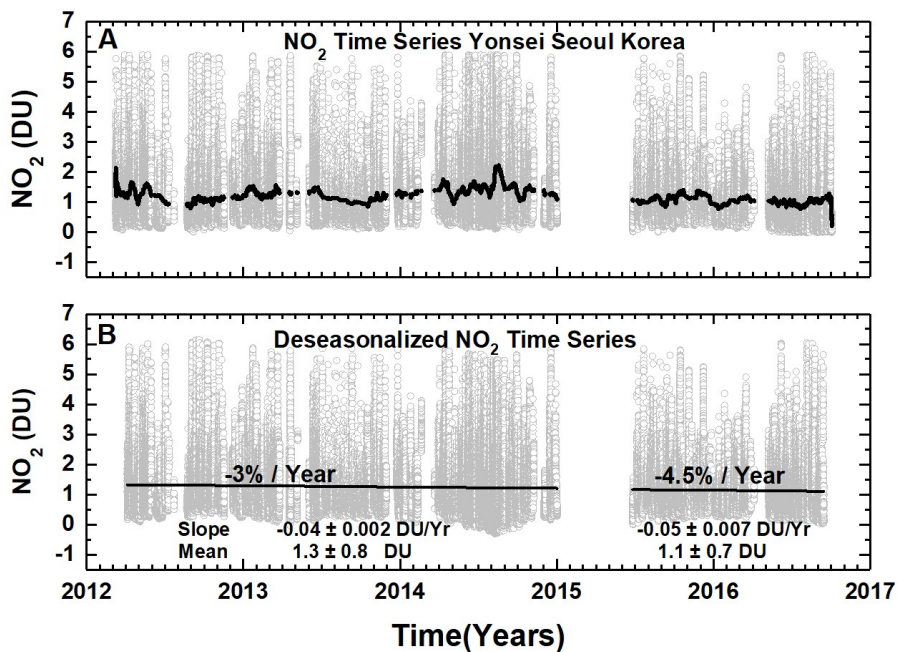


Fig. 7 (A) NO₂ time series at Yonsei University in Seoul NO₂(grey) and (B) deseasonalized time series. Combined slope = -0.05 ± 0.001 DU/Year and Mean = 1.2 ± 0.8 DU or the decrease is -4 ± 0.08 % / Year. Seoul has no clear seasonal cycle.

319

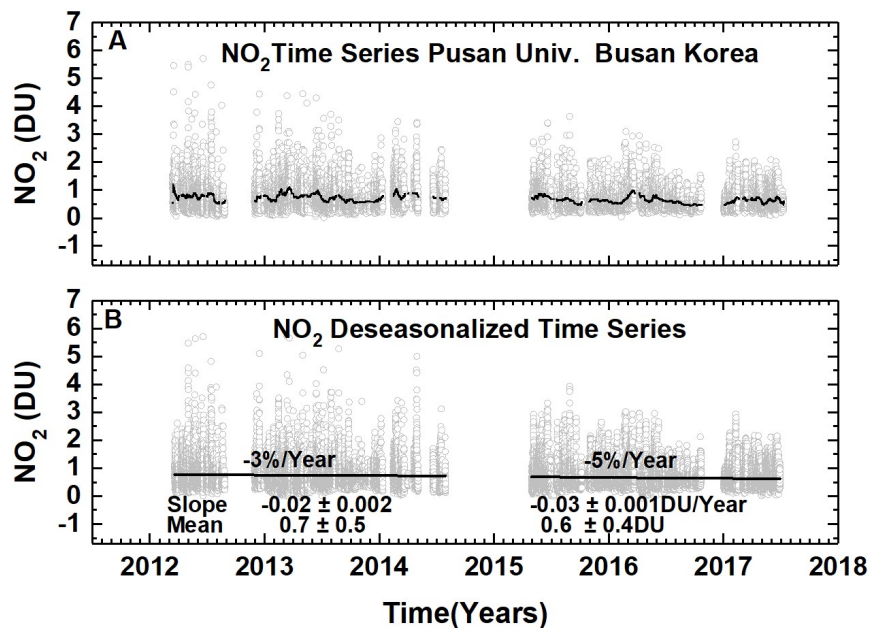


Fig. 8 (A) Pusan University in Busan NO₂ daily time series (grey) and (B) deseasonalized time series with linear trends.

320 Figures 7 and 8 each contain an approximately 5-year daily time series (grey) for Seoul (Yonsei
321 University) and Busan (Pusan University) and a linear fit to a deseasonalized version of the time series.
322 Since the observations at both sites had an extended period of missing data, the slopes were estimated
323 separately for each segment and for the combined time series. Both Seoul and Busan show a steady
324 reduction in NO₂ air pollution with an average reduction of about -4 % per year. A recent paper by
325 Duncan et al., (2016) estimated a decrease in C(NO₂) for Seoul in about a 10 x 10 km box of about 1.6 ±
326 1.4 % per year over the 2004 to 2013 period based on a 2014 average C(NO₂) amount of 0.6 DU, or
327 about half of the average value 1.3 ± 0.8 DU observed by the PSI. The larger reduction in C(NO₂)
328 measured by the PSI is caused by a reduction in higher than average afternoon C(NO₂) amounts that are
329 rarely observed by OMI overpass at 13:30 local time. OMI is a polar orbiting push broom hyperspectral
330 instrument (300 – 500 nm with resolution of 0.45 nm in the UV and 1 nm in the visible and a spatial
331 resolution of 13 x 24 km²) onboard the AURA satellite. The high observed late afternoon values are not
332 restricted to Seoul, but occur for all of the urban areas where the PSI has been deployed. The high late
333 afternoon values do not regularly occur in remote rural areas such as Amnyeondo.

334 Seoul and Busan C(NO₂) measurements are remarkable for the large peak amounts that are seen
335 on most days compared to the 1.5 to 2 DU peak values for Gwangju and Amnyeondo. For Yonsei, the
336 peak values range above 5 to 6 DU in the years 2012 to 2015, but decrease somewhat in 2015 to 2016.
337 In 2015 - 2016, the decrease appears to be large, but is only 0.2 DU relative to a mean of about 1.2 DU.
338 A smaller decrease appears for Busan (Fig. 8) relative to a mean of about 0.6 DU. All of the PSI
339 measurements show very high values of NO₂ during almost every day when measurements were
340 possible. Since the NO₂ concentrations represented by these large column amounts are probably in the
341 boundary layer near the sources of NO₂, there is a strong effect on local air quality.

342

343 5 Comparison with OMI Satellite Overpass Data

344

345 Seoul and Busan have 5-year PSI data records (Figs. 9a and 9b), and Gwangju has a 1-year data
346 record (Figs. 6 and 10) spanning the KORUS-AQ campaign. The PSI C(NO₂) can be matched in time (± 8
347 minutes) with the overpass time from OMI (Ozone Monitoring Instrument) onboard the AURA satellite
348 (mid-day overpass times 13:30 ± 90 minutes). Figure 9a shows the C(NO₂) daily variation at the OMI
349 overpass time with far more high values of C(NO₂) from the PSI than observed by OMI. The solid lines
350 represent the seasonal dependence, which are shown separately in Fig. 9b along with the C(NO₂)
351 differences, PSI - OMI. The result is that the average PSI values are double those observed by OMI's
352 large FOV. (OMI Version 03: <https://avdc.gsfc.nasa.gov/index.php?site=666843934&id=13>)

353

354 The seasonal dependence (Fig. 9b) of C(NO₂) from OMI for both Seoul and Busan is fairly
355 regular, with maxima in January of each year and minima in July-August. The seasonal behavior of
356 C(NO₂) obtained from the PSI for Seoul varies with high values extending from January into the summer
357 months and with minima varying from August in 2012, September-October in 2013, missing in 2014, July
358 in 2015, and June in 2016. For Busan, the maxima occur in the Spring for 2013 and 2014, October for
359 2015, and in the Spring for 2016. The minima are also variable. The difference between OMI and PSI
360 retrievals depends on local conditions for PSI and on an area average for OMI.

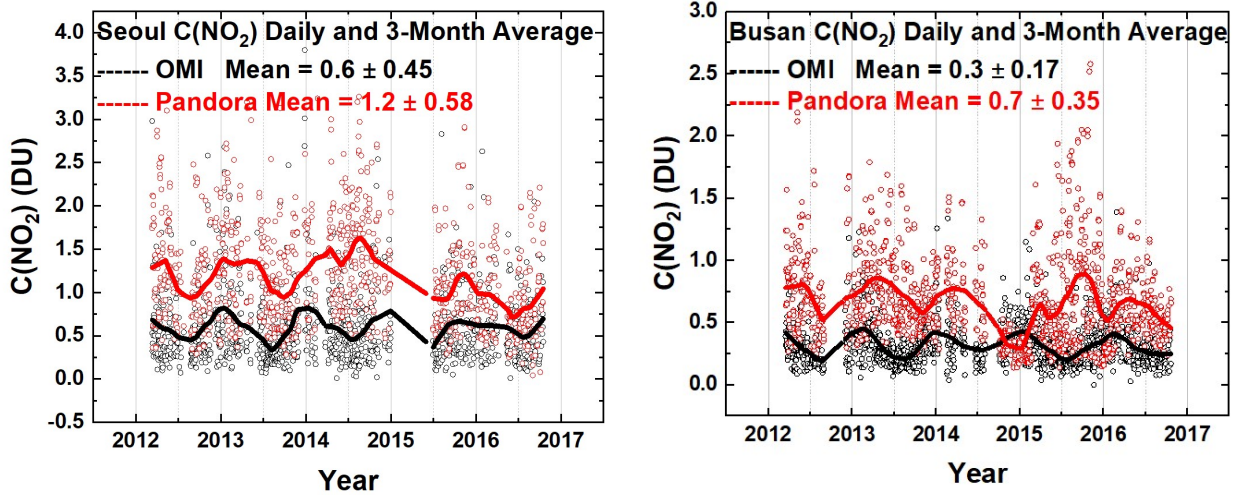


Fig. 9a Comparisons between the daily values of $C(\text{NO}_2)$ for OMI (black) and PSI (red) at Seoul and Busan for a 5-year period. Solid lines show the average seasonal variation (Lowess(0.1)), see also Fig. 9b. Linear interpolation is used where there are missing data points.

361

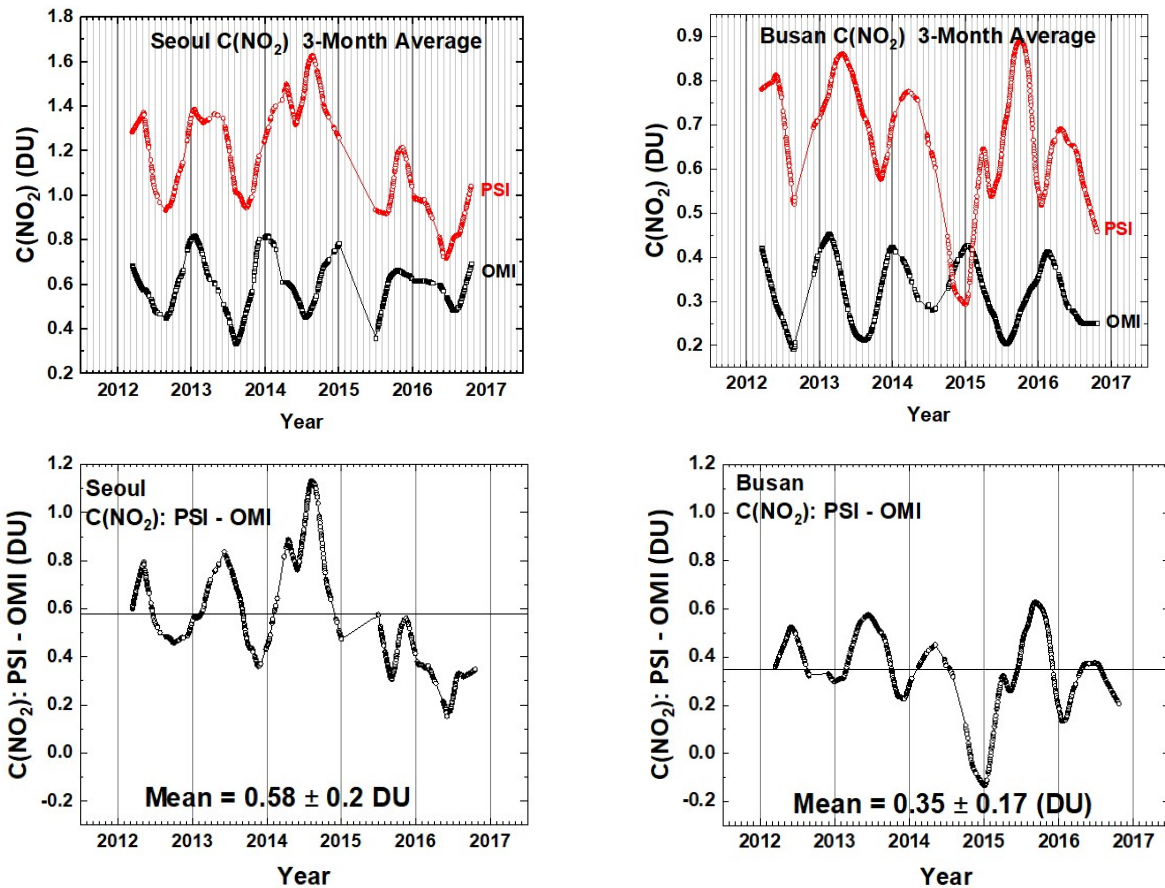


Fig. 9b Comparisons between the seasonal averages for $C(\text{NO}_2)$ from OMI (black) and PSI (red) at Seoul and Busan for a 5-year period. The lower panels show the seasonal difference between the PSI and OMI. The individual data points are shown derived from a Lowess(0.1) smoothing, approximately a 3-month running averages of the daily data. Interpolation used where there are missing data points.

362
363
364
365
366
367
368
369
370

Figure 9b shows that the PSI has a mean difference compared to OMI in Busan of 0.35 DU and peak values (up to 2.5 DU at 13:30 and 4 DU in the late afternoon). The differences are important when considering pollution effects on human health (Krafta et al., 2005; Latza et al., 2009). Even larger differences are observed in Seoul, where the mean difference is 0.58 DU between Pandora and OMI at the satellite overpass time. **The results from PSI suggest that local ground-based monitoring of pollution is important for estimating their impact on human health, particularly since amounts of C(NO₂) occurring later in the afternoon exceed the amounts at the time of the satellite overpass.**

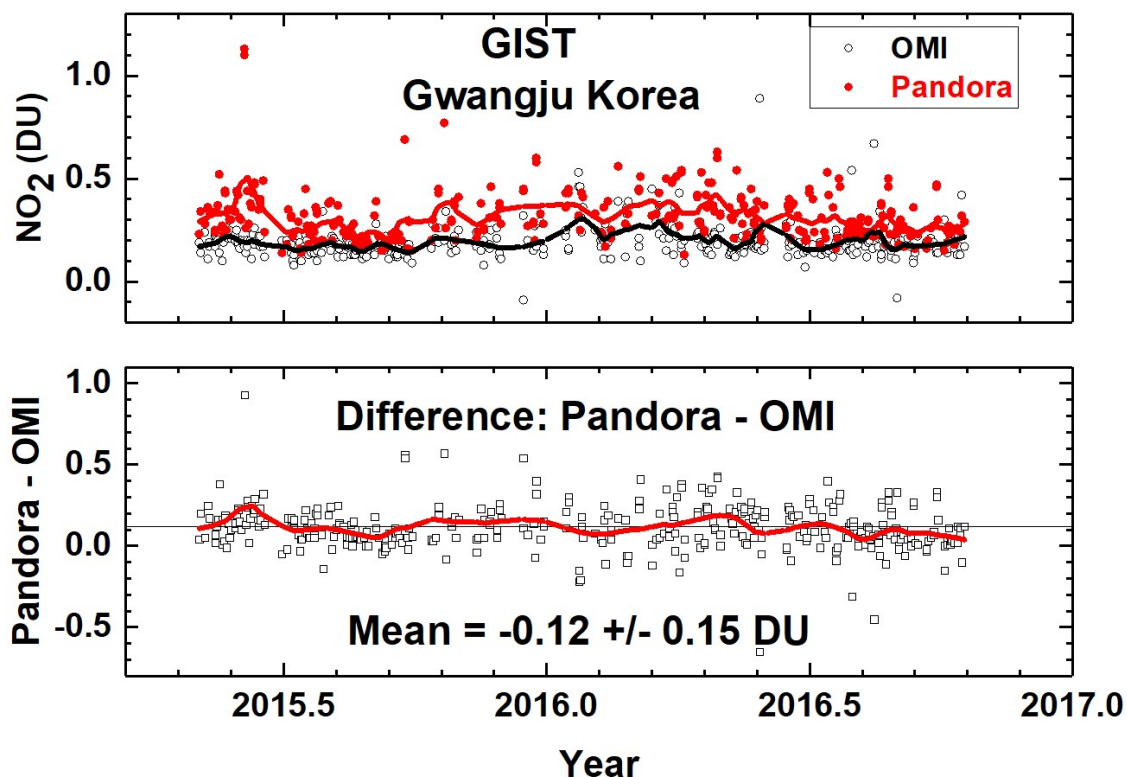


Fig. 10 C(NO₂) time series from Pandora (red) and OMI (black) for GIST University in Gwangju Korea and their differences. The comparison is formed from time coincidences between Pandora and OMI.

371 A comparison with Lowess(0.1) fits (Locally Weighted least squares fit to 0.1 of the data points,
372 (Cleveland, 1981)) to the matched Pandora vs OMI overpass data (about 3-month averages) shows that
373 PSI C(NO₂) is larger than OMI measured C(NO₂) mostly because of its much smaller 2^o field of view (a
374 circle of 35 meters diameter at 1 km altitude) compared to OMI's FOV of 13 x 24 km² at nadir, which
375 may encompass areas outside of the city or the adjacent ocean areas. For example, the center of Seoul
376 is about 48 km from the Yellow Sea, while the OMI overpass file lists FOV center distances of over 60 km
377 from Seoul. Another possible reason for the differences is that OMI C(NO₂) retrievals use NO₂ vertical
378 profile shape factors from the low resolution (~110 x 110 km) Global Model Initiative (GMI) model
379 simulation to calculate air mass factors that are used to determine observed tropospheric NO₂ vertical
380 columns, while much finer resolution profiles are needed to more accurately represent highly polluted

381 urban areas such as Seoul. Increases in OMI retrieved tropospheric column NO₂ up to 160 % are found
382 when using model derived 1.33 x 1.33 km² profile shape factors (Goldberg et al., 2017). The effect of
383 moderate amounts of cloud or aerosol have little effect on the PSI direct-sun spectral fitting retrieval of
384 C(NO₂) as shown in Fig. 2. OMI and MAXDOAS retrievals are sensitive to the presence of aerosols and
385 clouds (Kanaya et al., 2014), which may contribute to the underestimate of C(NO₂) by OMI even after
386 corrections are made for retrieved aerosol and cloud amounts (Chimot, et al. 2016).

387
388 The implications for assessing clean air indices suggest that OMI underestimates the human
389 health effect from trace gases such as NO₂, especially in highly populated urban areas. Figure 5 gives a
390 much clearer picture of the degree of pollution than is possible with just the 13:30 OMI comparison
391 measurements, since the late afternoon is the time of maximum pollution.

392
393 The city of Gwangju is much smaller than Busan, with less industrial activity, especially
394 automobiles. PSI observations at GIST show much closer agreement with OMI (Fig. 10), especially since
395 GIST is located within the city boundaries, but in an area with much less concentrated industrial activity
396 compared to the center of Gwangju. The large OMI FOV over a relatively clean area reduce the OMI
397 difference in measured NO₂ amount compared to the PSI C(NO₂) amounts. OMI still measures less than
398 the PSI (0.12 ± 0.15 DU), but the mean difference is not statistically significant. However, OMI clearly
399 misses the high values of C(NO₂) that are present in the PSI observations.

400
401

402 **5.1 Comparison with 4STAR DC-8 Overpass Data**

403
404 C(NO₂) results were obtained by the Spectrometer for Sun-tracking Sky-Scanning Atmospheric
405 Research (4STAR) flown on-board the DC-8 during KORUS-AQ and compared with the PSI (Fig. 11). The
406 4STAR is an airborne sunphotometer, capable of measuring total C(NO₂), C(O₃), water vapor and AOD
407 columns in its direct-sun mode (Segal-Rozenhaimer et al., 2014; Shinozuka et al., 2013), which is similar
408 to the mode used by the PSI network.

409
410 A detailed description of 4STAR is given in Dunagan et al., (2013). In brief, the instrument has
411 two structurally rigid grating array spectrometers that are combined to yield continuous spectra
412 between 300-1700 nm. The instrument sampling rate is 1 Hz, and the nominal integration time used for
413 C(NO₂) retrievals is 50 ms (with six spectra averaged per one sampling period). Dark counts are
414 measured every 20 min using a shutter mechanism. The 4STAR light collection system has fiber optic
415 bundle foreoptics that is connected to the spectrometers. A two-axis motion control system with analog
416 feedback provides active tracking of the solar disk. The instrument full field of view (FOV) is ~1.25°.
417 C(NO₂) is retrieved following a method described in Segal-Rozenhaimer et al. (2014), but using the 460-
418 490 nm spectral range. A series of 4STAR columnar NO₂ values above aircraft (for legs below 300 m)
419 taken from DC8 “missed approach” maneuvers overflying Olympic Park PSI station, within a radius of 5
420 km, are shown in Fig. 11. There is a relatively good correlation (R²=0.7), with a slight positive bias of
421 4STAR compared with the PSI values. This might result from higher noise effects (i.e. small amount of
422 spectra averages) for 4STAR during the fast change of altitude when the aircraft performs its “missed

423 approach” overpasses over the PSI stations. Relaxing the altitude constraint to include legs below 500 m
 424 showed good agreement with the PSI station at Taewha Mountain, but with an overall lower correlation
 425 coefficient ($R^2=0.54$), which is expected due to averaging of larger vertical range. As with PSI, 4STAR
 426 shows better agreement with OMI $C(NO_2)$ for low values of $C(NO_2)$, but considerable differences over
 427 polluted areas (Segal-Rozenhaimer et al., *in prep.*), when 4STAR $C(NO_2)$ values are averaged within each
 428 of the OMI pixels corresponding to the flight path for each of the days.
 429

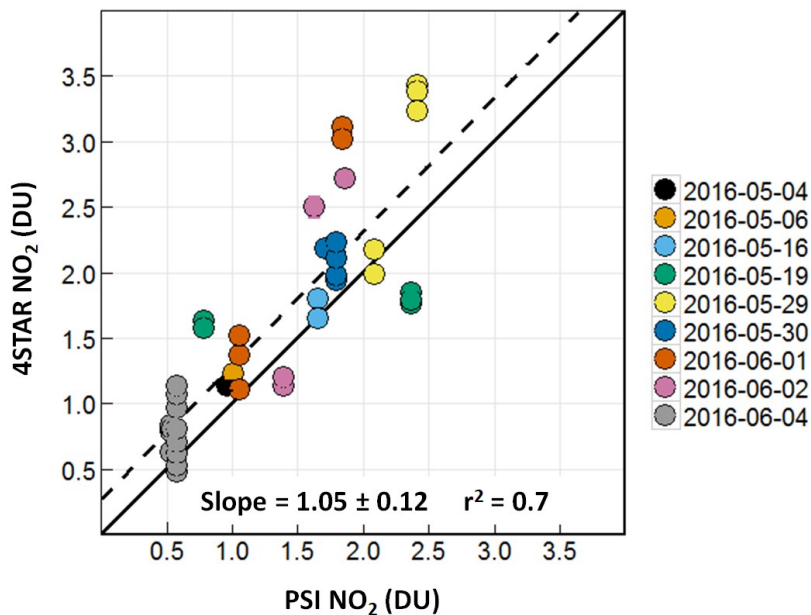


Fig. 11 A correlation plot of $C(NO_2)$ from 4STAR onboard the DC-8 compared to the $C(NO_2)$ amount measured by the PSI at Olympic Park on nine different days. The solid black line is the 1:1 line drawn for reference. The dashed line represents the data linear fit, with a slope of 1.05, and a correlation coefficient $r^2 = 0.7$, as shown on the plot.

430
 431
 432
 433

6 Formaldehyde from Five Korus-AQ Sites

434 PSI makes two sets of direct-sun measurements every 80 seconds. One set is for measurements
 435 in the visible range (380 – 525 nm used for NO_2) and the other is for the UV range (290 – 380 nm with a
 436 filter, U340, which blocks visible light). Formaldehyde is derived from the same set of spectral
 437 measurements used for ozone (i.e., with a U340 blocking filter), but using the spectral range 332 - 359
 438 nm. Sources of error in the $C(HCHO)$ retrieval arise from the selection of the fitting window and the
 439 amount of $C(HCHO)$ remaining in the reference spectrum after application of the modified Langley
 440 estimation (MLE) method of calibration (Herman et al., 2009, Spinei et al., 2018). The MLE extrapolation
 441 to zero $C(HCHO)$ could have an offset error of 0.1 to 0.2 DU. Selecting different fitting windows can also
 442 cause the $C(HCHO)$ retrievals to differ. For example, a wider alternate fitting window, 324 -360 nm,
 443 retrieves HCHO values that are about 8 % higher because of different amounts of interference from
 444 overlapping absorption by O_3 , NO_2 , and BrO at the spectral resolution of 0.5 to 0.6 nm currently in use.

445 Absolute offset errors do not affect the retrieval precision (relative column amounts), which is
446 approximately 0.1 DU. A detailed analysis of the algorithms and uncertainties is discussed by Spinei et
447 al., 2018.

448
449 The Olympic Park area has much more vegetation than central Seoul for the production of
450 isoprene (<http://www.olympicpark.co.kr>), which is a significant source of the chemicals needed for
451 formaldehyde production in the atmosphere (Luecken et al., 2012). Observations from PSI show that
452 C(HCHO) starts out every day at low levels 0.6 DU at about 08:00 and increases to over 2 DU until 18:00
453 (Fig.s 12 and 13). Most HCHO arises from photochemical production, while a significant fraction is
454 chemically derived from automotive emissions in densely populated urban areas (Friedfeld et al., 2002;
455 Garcia et al., 2006; Lei et al., 2009; Liteplo et al., 2010). Regardless of the precursor source, HCHO forms
456 in the atmosphere primarily by photochemistry, which causes HCHO to usually be a minimum early in
457 the day, increase into the afternoon, and decline towards evening. The PSI C(HCHO) observations (Figs.
458 12 and 13) support this pattern of daily variation.

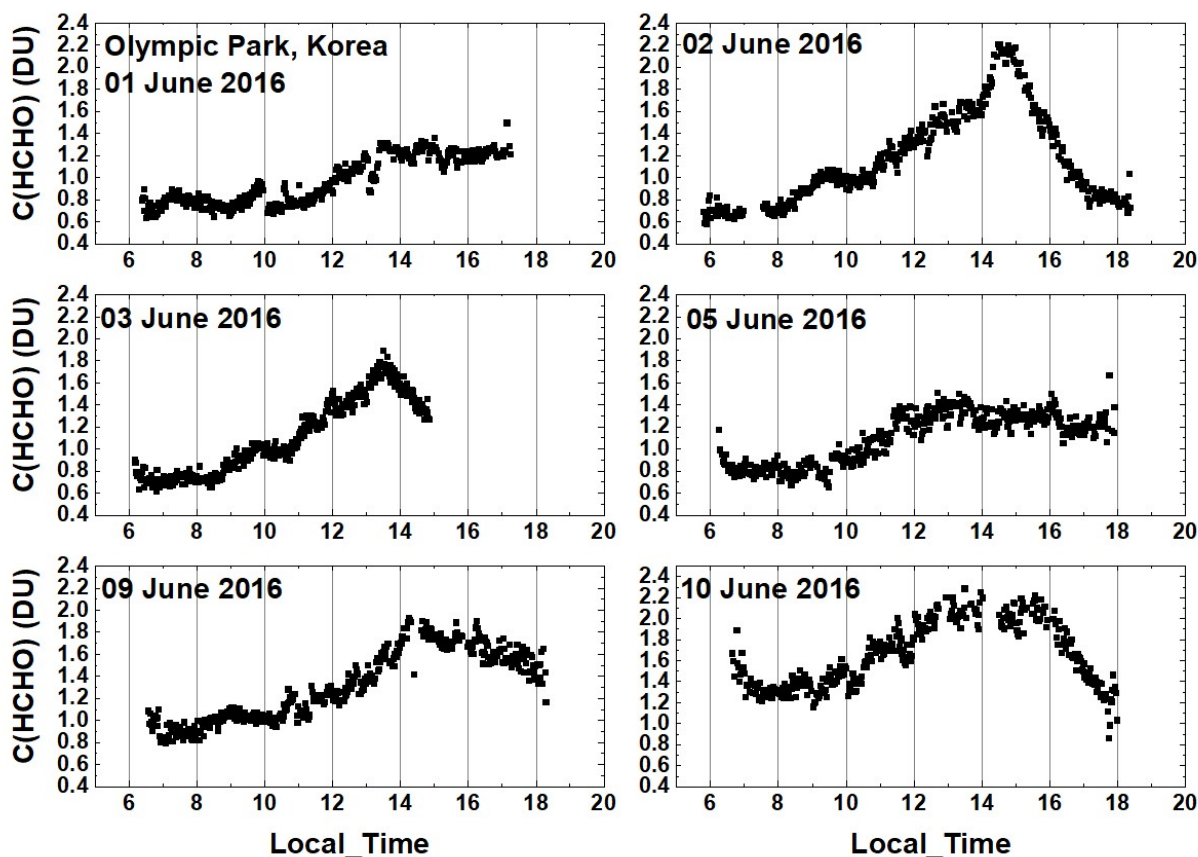


Fig. 12 C(HCHO) from PSI at Olympic Park for 6 days in June 2016. C(HCHO) on 2 June 2016 has a peak value of 2.3 DU at 14:30 hours.

460
461 A summary of the daily time dependence of C(HCHO) at Olympic Park during the entire
462 KORUS-AQ campaign is shown in Fig. 13. As in Fig. 12, minimum values are observed in the

463 morning (06:00 – 08:00) before the chemical and direct sources of HCHO are significant. There
464 is strong buildup during the day that reached a maximum between 15:00 to 16:00, and then
465 diminished towards sunset. As with NO₂, the daily pattern of late afternoon peaking of HCHO
466 amounts presents a problem for polar orbiting satellite observations (e.g., OMI observations at
467 13:30) assessing air quality.

468
469
470

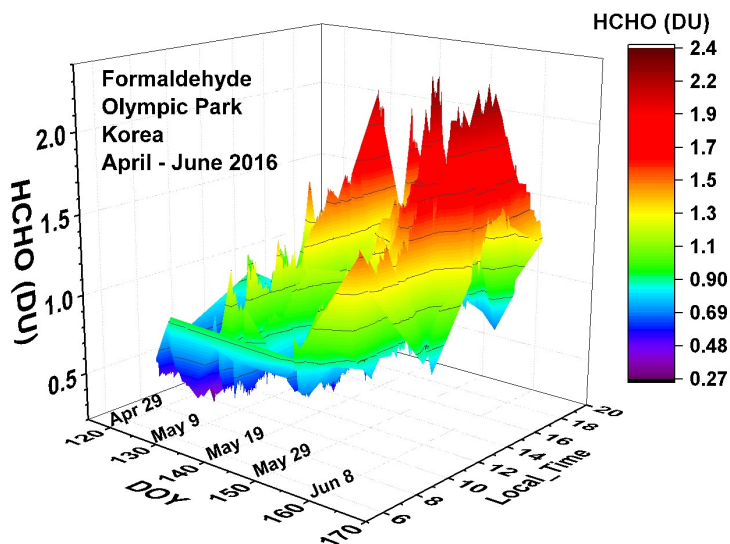


Fig. 13 Pandora measured formaldehyde amounts vs day of the year and local time for 29 April 2016 to 11 June 2016 in Olympic Park.

471
472
473
474
475
476
477
478
479

Figure 14 shows two altitude profiles acquired by the Compact Atmospheric Multispecies Spectrometer (CAMS) (Richter et al., 2015) onboard the DC-8 aircraft as it spiraled over the Olympic Park area on 4 May 2016 in the morning and at midday. Quoting from Richter et al., (2015), “CAMS is a multi-species spectrometer configured for the simultaneous detection of ethane (C₂H₆) and formaldehyde (CH₂O). The spectrometer utilizes a tunable, fiber optically pumped difference frequency generation laser source in combination with a Herriott type multi-pass absorption cell with an effective path length of 89.6 m”

480 The morning integrated amount on 4 May was 1.02×10^{16} molecules cm^{-2} (0.38 DU) and the
481 afternoon amount was 6.95×10^{15} molecules cm^{-2} (0.26 DU), both substantially less than the PSI
482 measured values of 0.48 DU and 0.42 DU, respectively. There were no surface measurements of HCHO
483 mixing ratio on 4 May at Olympic Park. On 2 June at 11:40 there was a surface measurement 3.94 ppb.
484 Including the surface measurement in the profile integral yields $\text{Integ}(0.026, 7.2 \text{ km}) = 0.55 \text{ DU}$, while PSI

485 measured 1.2 DU, which is consistent with the differences shown in Fig. 14. The notation in Fig 14 is

486
$$\text{Integ}(z_1, z_2) = \int_{z_1}^{z_2} \text{HCHO}(z) dz$$
 for the altitudes z_1 to z_2 .

487

488

489

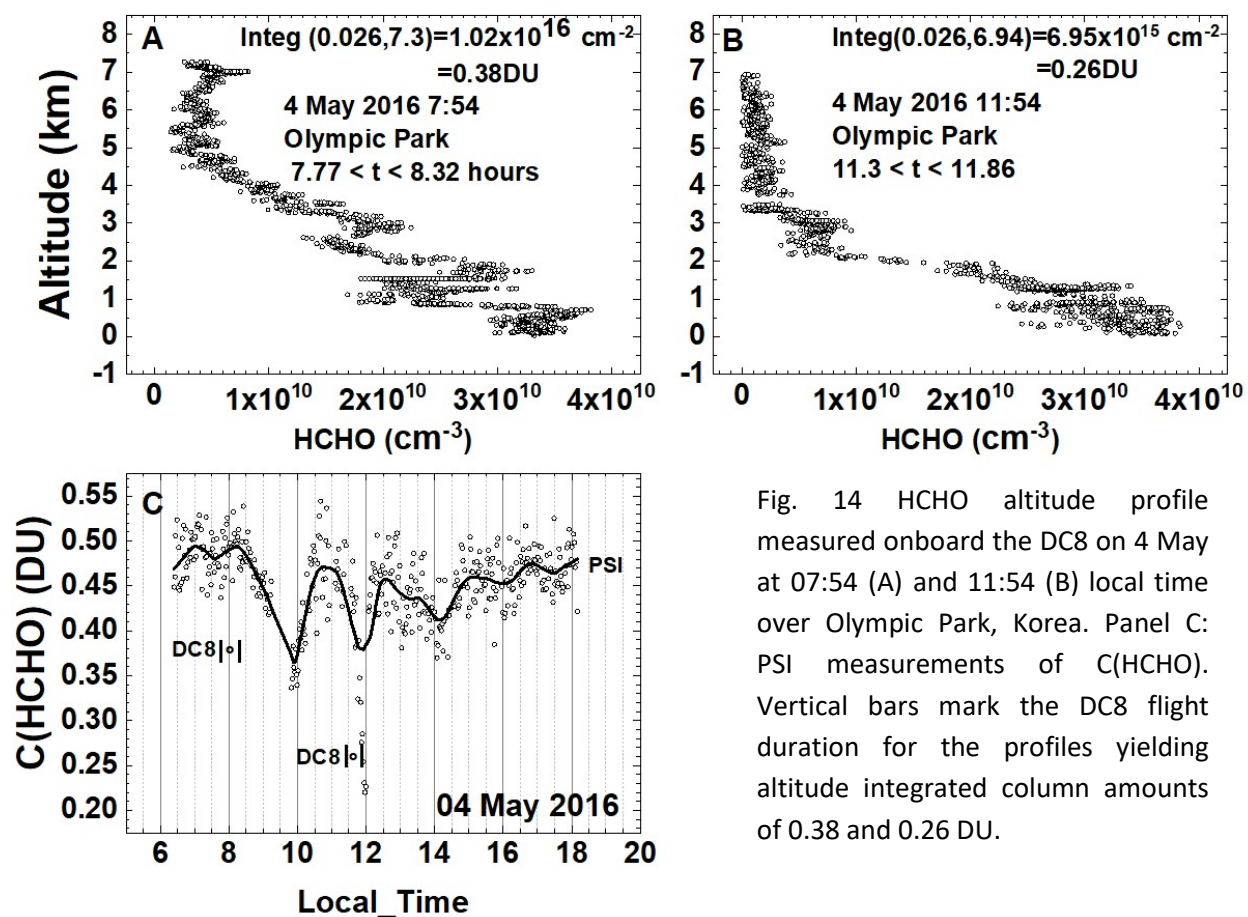


Fig. 14 HCHO altitude profile measured onboard the DC8 on 4 May at 07:54 (A) and 11:54 (B) local time over Olympic Park, Korea. Panel C: PSI measurements of C(HCHO). Vertical bars mark the DC8 flight duration for the profiles yielding altitude integrated column amounts of 0.38 and 0.26 DU.

490 The profiles used data for lower altitudes obtained from aircraft “missed approach”
 491 maneuvers at a nearby Seoul Airbase, 8.5 km from Olympic Park, (Fig. 15). When available, a
 492 single surface altitude point was added using ground-based volume mixing ratio measurements
 493 obtained from US Environmental Protection Agency measurements using quantum cascade
 494 laser instruments (Hottle et al., 2009, Spinei et al., 2018 and references therein). The DC-8 minimum
 495 altitude exactly over Olympic Park was typically around 0.4 km above the surface (black circles
 496 Fig. 15). Large vertical DC-8 HCHO gradients were observed as the DC8 descended to lower
 497 altitudes over Seoul Airbase. A comparison of 10-second DC-8 HCHO averages at the points of
 498 closest spatial approach to the Olympic Park (black circles) site on June 4, for example, to peak
 499 HCHO measurements during missed approaches at the nearby Seoul Airbase (20 – 40 meters
 500 above the ground) revealed ratios in the observed HCHO (black circles) ranging between 75 % to

501 83 % of the maximum values near the surface. Since Olympic Park DC-8 overpasses miss
 502 significant near surface HCHO amounts, the profiles shown in Figs. 14 and 16 incorporate the
 503 HCHO amounts down to the surface at an altitude of 0.026 km asl derived from the “missed
 504 approach” at Seoul airbase. HCHO measurements above the maximum altitude over Olympic
 505 Park (see Fig. 14 and 16) were taken from the closest time over the Taewha Mtn. site, 28 km
 506 from Olympic Park. The assumption is that the horizontal gradients above 2.2 km (Fig. 15) can
 507 be neglected,
 508

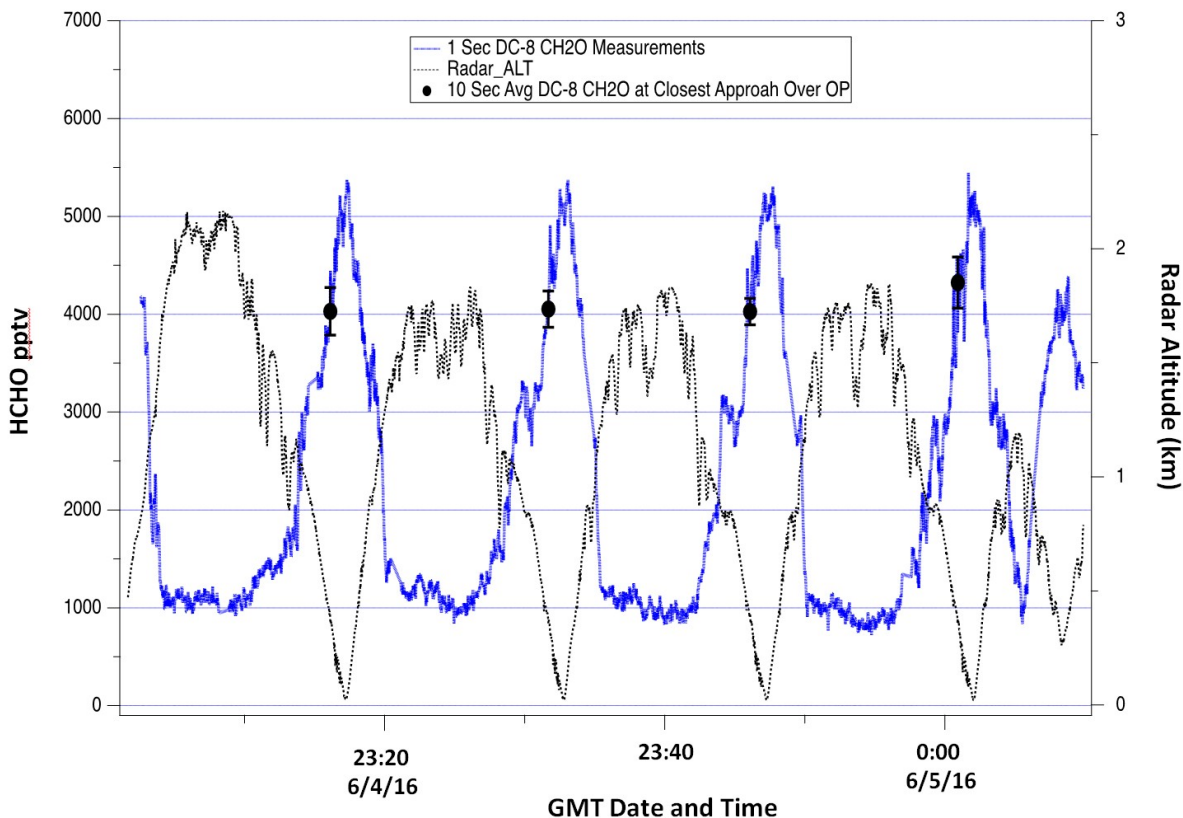


Fig. 15 DC-8 HCHO measurements over Olympic Park on June 4. The continuous blue profiles show the 1-second HCHO data while the black points with error bars show the 10-second average and standard deviation of this data at points of closest approach above the Olympic Park site.

509
 510 After conversion from mixing ratio to molecules/cm³ using the measured atmospheric
 511 density, the resulting profile data were integrated from the minimum (0.026 km asl, Table 1) to
 512 the maximum heights indicated in Fig. 14. The result is 0.38 DU at 07:54 and 0.26 DU at 11:54
 513 compared to the measurements from the Pandora instrument 0.48 and 0.38 DU The derived
 514 vertical HCHO columns from the DC8 data in Fig. 14 A and B are 79 % of PSI measured C(HCHO) in the
 515 morning and 68 % of PCI C(HCHO) at midday (Fig 14 C).
 516

517 A similar comparison is shown in Fig. 16 for 5 June 2016 where the amount of C(HCHO)
 518 is much larger than on 4 May. Integration of the measured profiles yields column densities of
 519 0.60 and 0.82 DU at 08:30 and 15:21 hours. For this case, at both times the DC8 values are
 520 about 77 % and 63 % of the PSI measured column amounts, 0.78 and 1.3 DU. For both cases in
 521 Figs. 14 and 15 the 23 % to 37 % differences are outside of the expected error from PSI fitting
 522 window selection and from residual HCHO included in the MLE calibration method.
 523

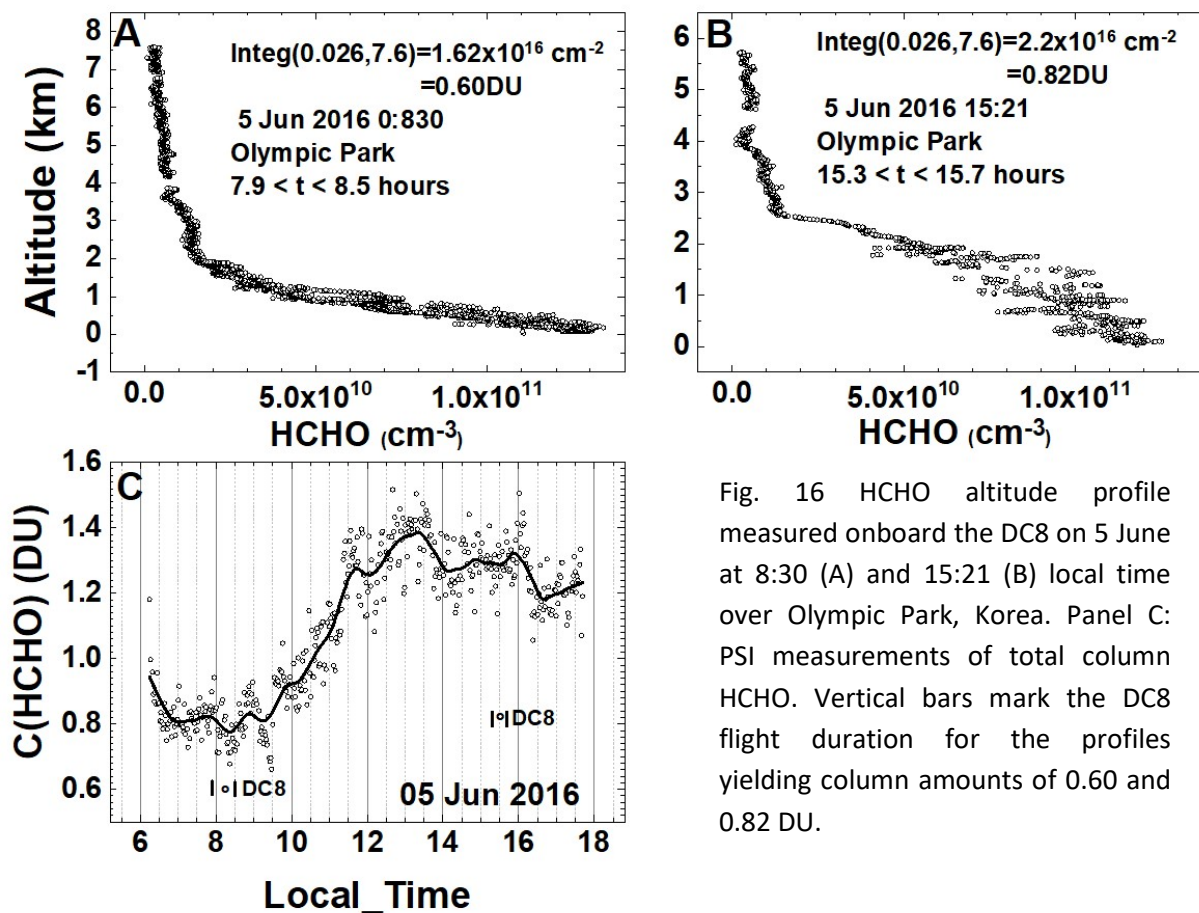


Fig. 16 HCHO altitude profile measured onboard the DC8 on 5 June at 8:30 (A) and 15:21 (B) local time over Olympic Park, Korea. Panel C: PSI measurements of total column HCHO. Vertical bars mark the DC8 flight duration for the profiles yielding column amounts of 0.60 and 0.82 DU.

524
 525 Another Olympic Park case on 9 June 2016 shows DC8=0.79 vs PSI=1 DU at 08:06,
 526 DC8=0.74 vs PSI=1.3 DU at 12:12, and DC8=1.13 vs PSI=1.9DU, or the DC8 measurements are 79
 527 % and 57 % less than the PSI total column HCHO. All of the remaining comparisons of DC8
 528 profile results with PSI C(HCHO) show similar results. The reasons for the disagreement between
 529 C(HCHO) measured by direct sun observations (PSI) and the integrated column density from aircraft
 530 measurements of HCHO VMR are not known. Contributions to the differences include the selection of
 531 the PSI wavelength window (332 - 359 nm) and possible interference from overlapping NO₂ and O₃
 532 absorption that are not properly included, and, more likely, the use of CAMS measured volume mixing
 533 ratios at the lowest altitudes from the nearby Seoul airbase, 8.5 km from Olympic Park, where spatial

534 variation may affect the calculation of C(HCHO). The use of Taehwa Mtn. data for higher altitudes over
535 Olympic Park contributes 25 % for 3 of the above cases and 50 % for 4 May 2016 at 07:54 (Fig.
536 14A). This is probably not the reason for the disagreement between CAMS and PSI, since the percent
537 underestimate for CAMS over Taewha is about the same magnitude (Table 2) as over Olympic Park.

538
539 PSI measurements show that Olympic Park produces more HCHO almost every day than
540 observed at the Yonsei University in Seoul and Taehwa Mountain sites (Figs. 12, 17, 18). The
541 hourly variations observed during the KORUS-AQ campaign at the Yonsei University in Seoul
542 and at Taehwa Mountain sites are similar to Olympic Park even though most of the HCHO is
543 locally produced by photochemistry, but has a relatively short lifetime of a few hours in
544 polluted air where there is significant ozone and OH. However, at typical wind speeds of 10 -20
545 km/hour and a chemical lifetime of 2.5 hours (Dufour et al., 2009), HCHO can be transported
546 about 25 – 50 km, which is far enough for some transport of HCHO between the PSI sites at
547 Yonsei, Olympic Park, and Taehwa Mtn. DC8 CAMS results over the Taehwa Mtn. site compared
548 to PSI are given in Table 2 with differences similar to Olympic Park
549

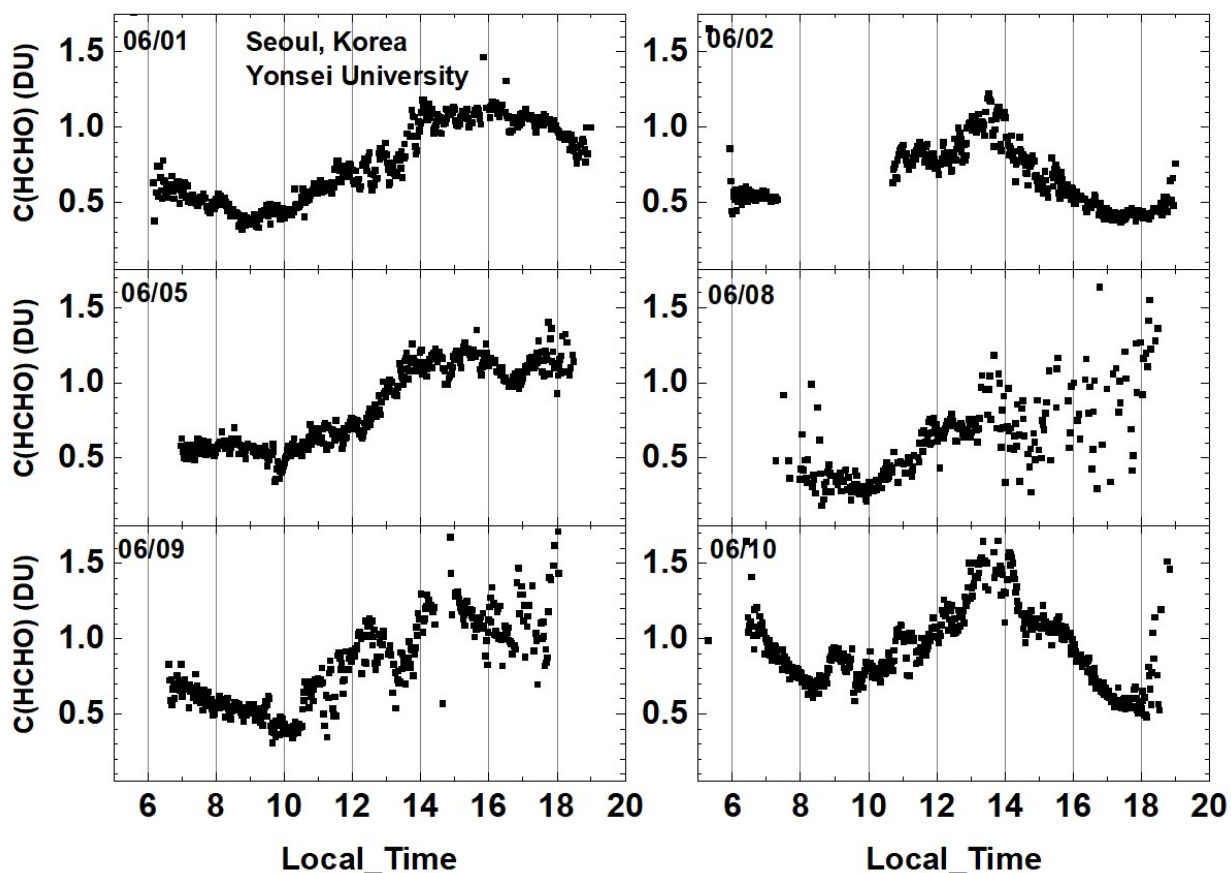


Fig. 17 Total column HCHO from Pandora Yonsei University, Seoul for 6 days in June 2016. C(HCHO) on 2 June 2016 has a peak value of 1.2 DU at 13:30 hours.

550
 551
 552
 553
 554

Table 2 Taehwa Mtn DC8 compared to PSI measurements (see 10 Jun in Fig. 18)

Date	LT	DC8 HCHO DU	PSI HCHO (DU)	Percent
11 May	08:25:19	0.4	0.6	67
18 May	08:34:26	0.4	0.5	80
30 May	12:05:00	0.5	0.9	56
10 Jun	08:22:45	1	1.16	86
10 Jun	12:22:53	1	1.5	67
10 Jun	15:46:03	1	1.3	77

555

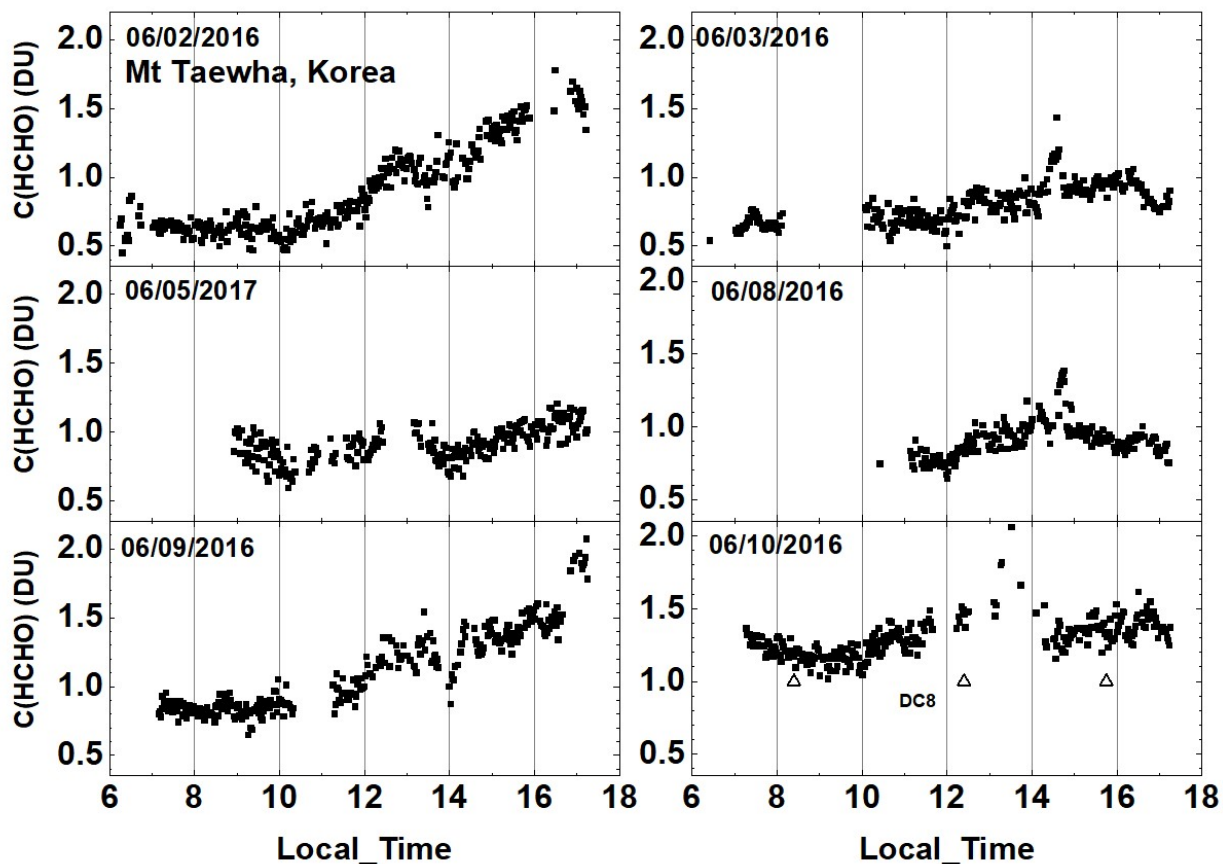


Fig. 18 Total column HCHO from Pandora at Taehwa Mountain for 6 days in June 2016. C(HCHO) on 2 June 2016 has a peak value of 1.7 DU at 16:20. △ are DC8 measurements on 10 June

556
 557

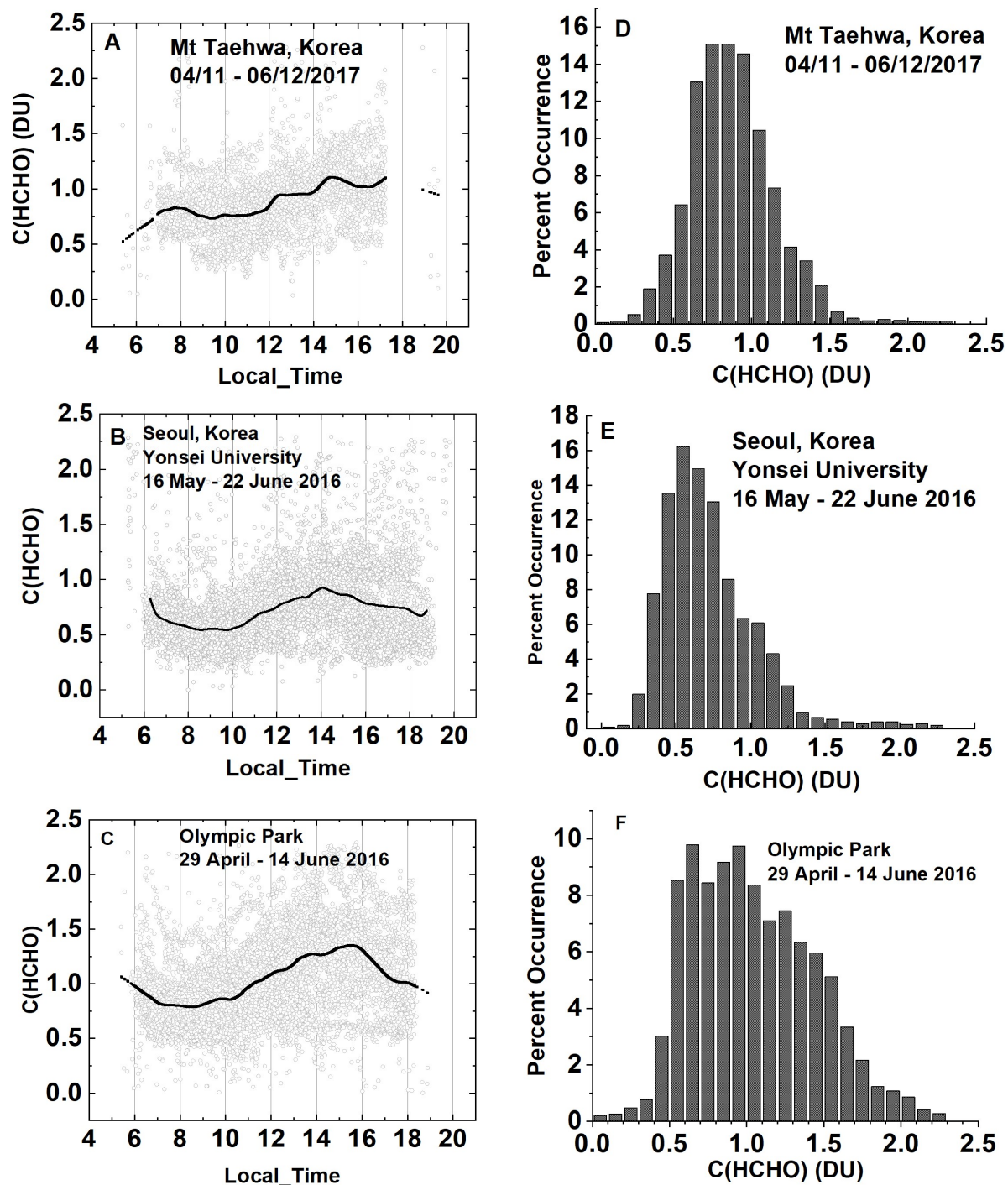


Fig. 19a Summary of total column HCHO for the stated dates during the KORUS-AQ campaign. The solid line is a Lowess(0.1) fit to the data. The sharp cutoffs in panel A, B, and C were caused by obstructions of the direct sun from the PSI FOV in the afternoon.

558

559

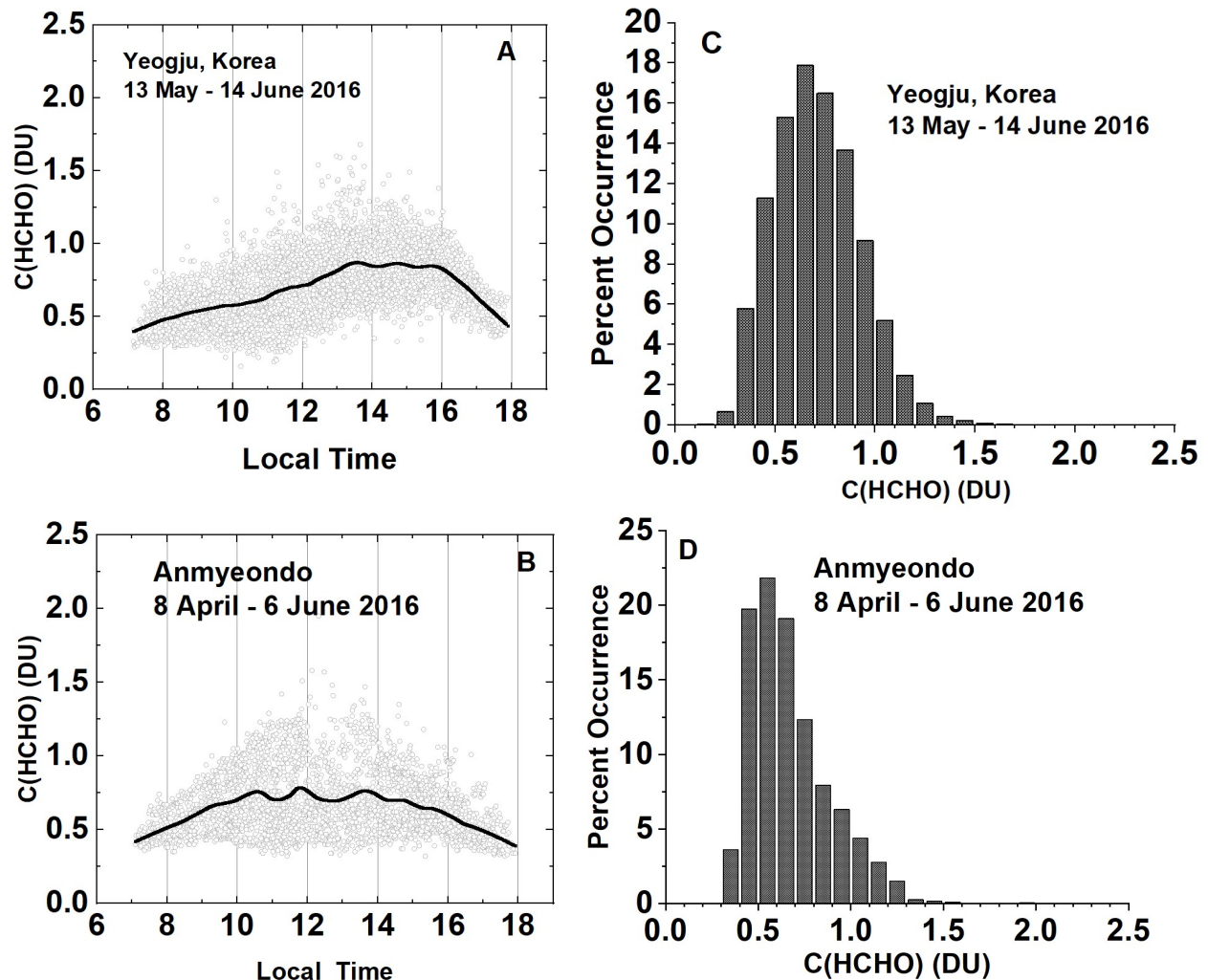


Fig. 19b Summary of total column HCHO for the stated dates during the KORUS-AQ campaign. Panels A and B represent the daily variation at a given local time. The solid line is a Lowess(0.1) fit to the data. Panels C and D show the frequency of occurrence (%) for different amounts of HCHO.

560 Figure 19a and 19b summarizes all of the C(HCHO) data obtained during KORUS-AQ at
 561 the five sites. The graphs on the left show all of the data points (light gray circles) as a function
 562 of the local time and a Lowess(0.1) fit to the data showing the average hourly behavior. The
 563 spread of the data about the Lowess(0.1) fit represents the day-to-day variation at a given local
 564 time. On average, Mt. Taehwa tends to increase throughout each day, while Yonsei and
 565 Olympic Park show maxima at 14:00 and 15:30, respectively. Similarly, in Fig. 18b Yeogju
 566 increases during the day having a maximum at 17:42 while Anmyeondo has a broad peak with
 567 maxima at 12:00 and 13:42.
 568

569 The histograms on the right side of Fig. 19 represent the percent frequency of
 570 occurrence of C(HCHO) in 0.1 DU bins. C(HCHO) at Mt. Taehwa and Seoul rarely exceeds 1.5 DU

571 compared to Olympic Park where C(HCHO) > 2 DU for a significant fraction of time. The most
 572 frequent values are 0.6 DU for Seoul, 0.9 DU for Mt Taehwa, and over 1 DU for Olympic Park.
 573 Olympic Park also has a broader distribution towards higher values of C(HCHO) than other sites.

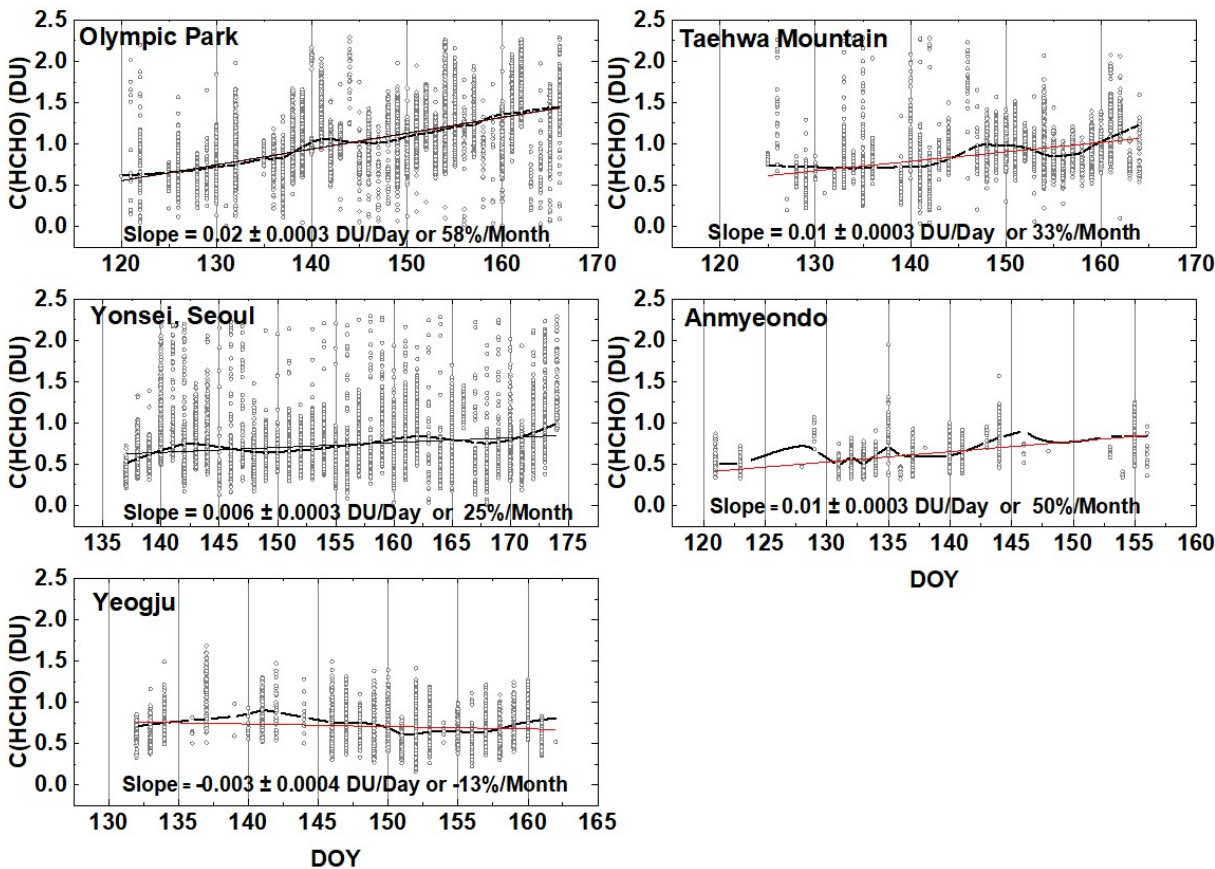


Fig. 20 The springtime change in C(HCHO) over about a 40 day period depending on the site. The “vertical bars” are the diurnal variation within each day of data. The thicker red curve is a Lowess(0.3) fit to the data, while the thin red line is a linear least squares fit. The Lowess(0.3) fit is approximately a 10-day local least-squares average.

574

575 The general intra-day C(HCHO) time dependence and C(HCHO) percent occurrence are
 576 shown for two additional sites (Fig. 19b), Yeogju and Anmyeondo. Yeogju shows an increase in
 577 C(HCHO) from morning to a peak value of 0.85 DU at 14:42, which then declines after 16:00. In
 578 contrast, Anmyeondo is almost symmetric with the sun position, having a maximum of about
 579 0.77 DU near 12:00 and 13:42 hours.

580 The average change in C(HCHO) during the spring campaign at the five sites is
 581 summarized in Fig. 20. Of the sites, Olympic Park showed the largest change rate, 58 %/Month
 582 followed by Anmyeondo at 50 %/Month, then Taehwa (33 %/Month), Yonsei Seoul (25
 583 %/Month), and Yeogju (-13 %/Month). Anmyeondo tends to have lower C(HCHO) amounts

584 because of its relatively isolated coastal location. These 2-month trends include seasonal
585 increases during the campaign months May and June, 2016.

586 It is difficult to compare PSI C(HCHO) with OMI for the KORUS-AQ period, since OMI
587 overpass C(HCHO) data for 2016 have some missing days (Fig. 21). For days with matching
588 data points over Seoul, PSI C(HCHO) (approximately 0.8 DU) is almost always larger than the
589 OMI values (0.2 DU) plus a few very high PSI values and two high OMI values. The general
590 day-to-day variations are similar.

591

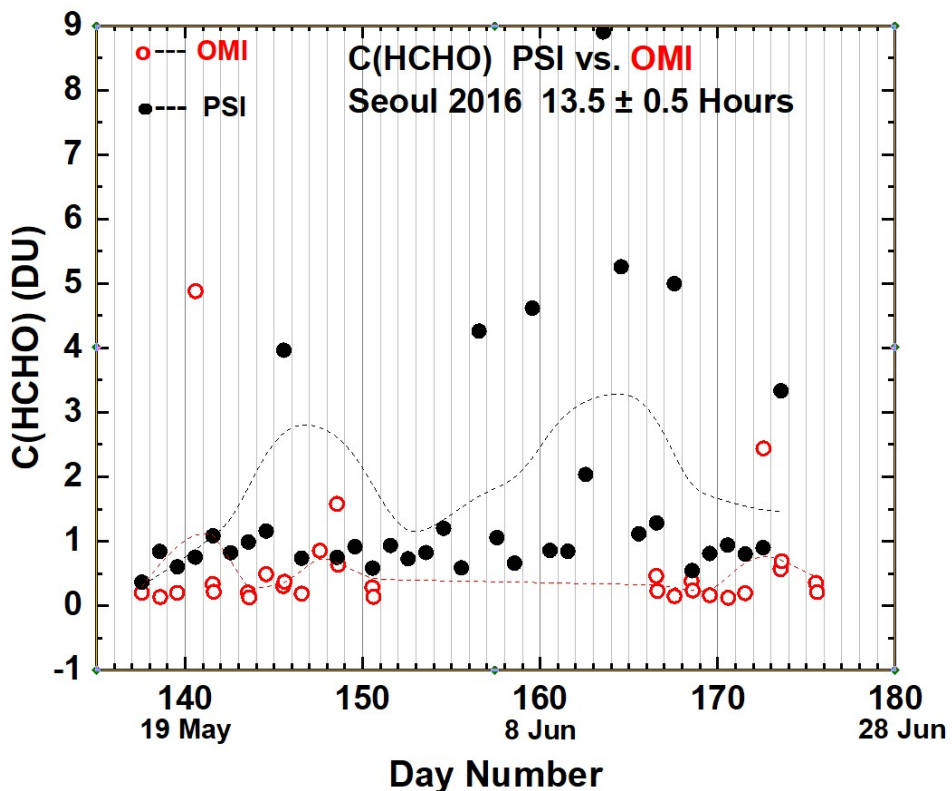


Fig. 21 Compare PSI • and OMI ◦ retrievals of C(HCHO) at 13.5 ± 0.5 hours. OMI overpass data, V03, are from <https://avdc.gsfc.nasa.gov/index.php?site=1113974256&id=81>

592

593

594

595

596

597 **7 Summary**

598

599 Nine Pandora Spectrometer Instruments, PSI, were installed at 8 sites in South Korea as part of
600 the KORUS-AQ ground, aircraft, and satellite measurements for air-quality studies. The measurements
601 made during the months of April to June by PSI showed that are very high amounts of urban pollution
602 from NO₂ and HCHO, and more moderate, but still high values in Mt Taewha and Yeogju, which are
603 some distance from the major urban centers,. An exceptional location was Amnyeondo, which is located
604 on a west-coastal island adjacent to the Yellow Sea about 100 km south of Seoul. The urban areas show
605 minimum values in the morning that rise rapidly throughout the day, peaking in the late afternoon for
606 both C(NO₂) and C(HCHO).

607

608 PSI direct-sun retrieved values of C(NO₂) and C(HCHO) are always larger than OMI retrieved
609 C(NO₂) and C(HCHO) for the OMI overpass times (13.5 ± 0.5 hours). In urban areas, PSI C(NO₂) averages
610 are at least a factor of two larger than OMI averages. Similar differences are seen for C(HCHO) in Seoul.
611 However, late afternoon values measured by PSI are even larger, implying that OMI measurements
612 underestimate the effect of poor air quality on human health. The primary cause of the OMI
613 underestimate is the large OMI FOV that includes regions containing low values of pollutants. In
614 relatively clean areas, PSI and OMI are more closely in agreement.

615

616 PSI retrieved C(NO₂) amounts for Seoul frequently exceed 2 DU and occasionally reach 6 DU.
617 Other urban centers in the south, Busan and Gwangju, have smaller C(NO₂) amounts, but exhibit a
618 similar strong diurnal pattern, namely low values in the morning and high values later during midday.
619 This behavior is expected because of the large number of urban automobiles and concentrated industry.
620 Urban areas downwind from Seoul show high C(NO₂) amounts, but also show daily minimum amounts in
621 the morning that increase later in the day. Two of the sites, Seoul and Busan, have long-term C(NO₂)
622 data records, 2012 – 2016, that suggest a gradual decrease in C(NO₂) amounts in Korea. When
623 compared with OMI, both ground-based PSI's and the 4STAR aircraft instrument onboard the DC8 show
624 that the correlation is best for small values of C(NO₂), most often seen in the troposphere and
625 stratosphere and worst for high values that are usually in the boundary layer near their local sources. In
626 Olympic Park, the measurements of significant values of C(HCHO) and high values of C(NO₂) in the
627 afternoon suggest that there are increased boundary layer amounts of ozone.

628

629 C(HCHO) amounts were obtained for five sites, Yonsei University in Seoul, Olympic Park, Taehwa
630 Mtn., Amnyeondo, and Yeosu. Of these the largest amounts of C(HCHO) were observed at Olympic Park,
631 and Taehwa Mountain, both surrounded by significant amounts of vegetation. Comparisons of PSI
632 results were made with overflights on the DC8 aircraft for Taehwa Mtn and Olympic Park showing a
633 significant difference in total column HCHO. In all cases, PSI measured substantially more C(HCHO) than
634 obtained from integrating the altitude profiles measured from the DC8 overflights.

635

636 Appendix

637
638 Figure A1 illustrates the deseasonalization of the time series in Fig.6. The left panel reproduces
639 the solid black curve in Fig. 6A or 6C in the inset. The right panel reproduces the solid curve in Fig. 6B
640 and is magnified in the inset. The seasonal dependence in the left panel inset is almost non-existent in
641 the right panel inset
642

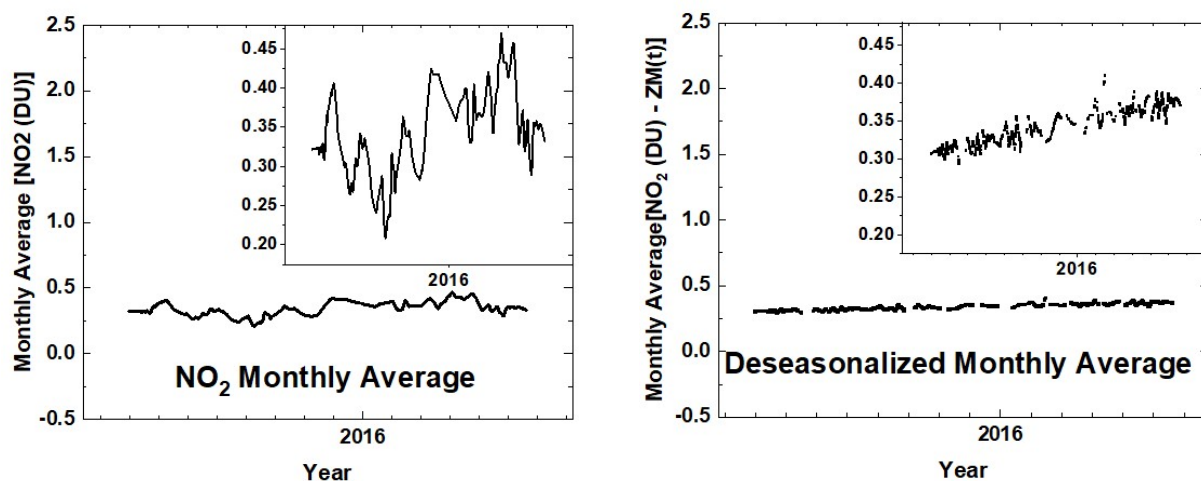


Fig. A1 An illustration of the deseasonalization (right panel) of the monthly running average of NO₂ for the Gwangju site (left panel) shown in Fig. 6. The insets are magnifications of the main plots.

643
644

645

646

647 **Data Sources**

648 **OMI Formaldehyde HCHO Version 03:** <https://avdc.gsfc.nasa.gov/index.php?site=1113974256&id=81>

649 **OMI Nitrogen Dioxide NO₂ Version 03** <https://avdc.gsfc.nasa.gov/index.php?site=666843934&id=13>

650 **Pandora KORUS-AQ** <https://avdc.gsfc.nasa.gov/pub/DSCOVER/Pandora/DATA/KORUS-AQ/>

651

652 **Author Contributions**

653

654 Jay Herman: Wrote most of the paper and performed the analysis and comparisons with the DC-8
655 aircraft measurements

656 Elena Spinei: Derived the formaldehyde altitude profiles suitable for comparison with Pandora data

657 Alan Fried: Obtained the HCHO profile data from the DC-8 CAMS instrument

658 Jhoon Kim: Provided support for the installation of Pandora instruments in Korea.

659 Jae Kim: Provided support for the Pandora located in Busan .

660 Woogyung Kim: Provided support in installing the Pandoras and analyzing the raw data

661 Alexander Cede: Provided calibration and data analysis support

662 Nader Abuhassan: Provided Pandora setup in Korea and provided the maintenance of calibration

663 Michal Segal-Rozenhaimer: Provided the 4STAR NO₂ data from the DC-8 flights and the comparison with
664 Pandora

665

666 The authors declare that they have no conflict of interest.

667 **8 References**

- 668 Boersma, K. F., D. J. Jacob, M. Trainic, Y. Rudich, I. DeSmedt, R. Dirksen, and H. J. Eskes, Validation of
669 urban NO₂ concentrations and their diurnal and seasonal variations observed from the SCIAMACHY and
670 OMI sensors using in situ surface measurements in Israeli cities, *Atmos. Chem. Phys.*, 9, 3867–3879,
671 2009.
- 672 Bernhard, G., C. R. Booth, and J. C. Eshamjian. Version 2 data of the National Science Foundation's
673 ultraviolet radiation monitoring network: South Pole. *Journal of Geophysical Research (Atmospheres)*,
674 109(D21), 2004
- 675 Cede, Alexander, Manual for Blick Software Suite1.3 Version 7, 20 Apr 2017
676 https://avdc.gsfc.nasa.gov/pub/DSCOVER/Pandora/Documents/BlickSoftwareSuite_Manual_v7.pdf
- 677 Chimot, J., Vlemmix, T., Veefkind, J. P., de Haan, J. F., and Levelt, P. F.: Impact of aerosols on the OMI
678 tropospheric NO₂ retrievals over industrialized regions: how accurate is the aerosol correction of cloud-
679 free scenes via a simple cloud model?, *Atmos. Meas. Tech.*, 9, 359-382, [https://doi.org/10.5194/amt-9-](https://doi.org/10.5194/amt-9-359-2016)
680 359-2016, 2016.
- 681 Cleveland, William S., LOWESS: A program for smoothing scatterplots by robust locally weighted
682 regression. *The American Statistician*. 35 (1): 54. [JSTOR 2683591](https://doi.org/10.2307/2683591). [doi:10.2307/2683591](https://doi.org/10.2307/2683591), 1981.
683
- 684 Dufour, G., F. Wittrock, M. Camredon, M. Beekmann, A. Richter, B. Aumont, and J. P. Burrows,
685 SCIAMACHY formaldehyde observations: constraint for isoprene emission estimates over Europe?,
686 *Atmos. Chem. Phys.*, 9, 1647–1664, 2009
687
- 688 Dunagan, S. E., R. Johnson, J. Zavaleta, P. B. Russell, B. Schmid, C. Flynn, J. Redemann, Y. Shinzuka, J.
689 Livingston, and M. Segal-Rosenhaimer, 4STAR spectrometer for sky-scanning Sun-tracking atmospheric
690 research: Instrument technology, *Remote Sens. (Special Issue*
691 "Optical Remote Sensing of the Atmosphere"), 5, 3872–3895, [doi:10.3390/rs5083872](https://doi.org/10.3390/rs5083872), 2013.
- 692 Fried, A., Walega, J. G., Olson, J. R., Crawford, J. H., Chen, G., Weibring, P., ... Millet, D. B. (2008).
693 Formaldehyde over North America and the North Atlantic during the summer 2004 INTEX campaign:
694 Methods, observed distributions, and measurement-model comparisons. *Journal of Geophysical*
695 *Research*, 113(D10). <https://doi.org/10.1029/2007JD009185>, 2008.
- 696 Friedfeld, S., M. Fraser, K. Ensor, S. Tribble, D. Rehle, D. Leleux, F. Tittel Statistical analysis of primary and
697 secondary atmospheric formaldehyde, *Atmospheric Environment*, 36, 4767-4775, 2002.
- 698 Garcia, A.R., R. Volkamer, L.T. Molina, M.J. Molina, J. Samuelson, J. Mellqvist, B. Galle, S.C. Herndon, C.E.
699 Kolb, Separation of emitted and photochemical formaldehyde in Mexico City using a statistical analysis
700 and a new pair of gas-phase tracers *Atmospheric Chemistry Physics*, 6, 4545-4557, 2006.
- 701 Goldberg D. et al., (2017), A High-Resolution And Observationally Constrained Omi NO₂ Satellite
702 Retrieval, *Atmos. Chem. Phys. Discuss.*, [doi:10.5194/acp-2017-219](https://doi.org/10.5194/acp-2017-219), 2017.

703 Gueymard, Christian A., The sun's total and spectral irradiance for solar energy applications and solar
704 radiation models. *Solar energy*, 76(4):423–453, 2004.

705 Herman, Jay, Alexander Cede, Elena Spinei, George Mount, Maria Tzortziou, Nader Abuhassan, NO₂
706 Column Amounts from Ground-based Pandora and MFDOAS Spectrometers using the Direct-Sun DOAS
707 Technique: Intercomparisons and Application to OMI Validation, *J. Geophys. Res.*, 114, D13307,
708 doi:10.1029/2009JD011848, 2009.

709 Jung, Jinsang, JaeYong Lee, ByungMoon Kim, SangHyub Oh, Seasonal variations in the NO₂ artifact from
710 chemiluminescence measurements with a molybdenum converter at a suburban site in Korea
711 (downwind of the Asian continental outflow) during 2015 - 2016, *Atmospheric Environment* 165, 290-
712 300, 2017.

713 Kanaya, Y., Irie, H., Takashima, H., Iwabuchi, H., Akimoto, H., Sudo, K., Gu, M., Chong, J., Kim, Y. J., Lee,
714 H., Li, A., Si, F., Xu, J., Xie, P.-H., Liu, W.-Q., Dzhola, A., Postlyakov, O., Ivanov, V., Grechko, E.,
715 Terpugova, S., and Panchenko, M.: Long-term MAX-DOAS network observations of NO₂ in Russia and
716 Asia (MADRAS) during the period 2007–2012: instrumentation, elucidation of climatology, and
717 comparisons with OMI satellite observations and global model simulations, *Atmos. Chem. Phys.*, 14,
718 7909-7927, <https://doi.org/10.5194/acp-14-7909-2014>, 2014.

719 Kim, Na Kyung, Yong Pyo Kim, Yu Morino, Jun-ichi Kurokawa, Toshimasa Ohara, Verification of NO_x
720 emission inventory over South Korea using sectoral activity data and satellite observation of NO₂ vertical
721 column densities, *Atmospheric Environment* , 77, 496-508, 2013.

722 Kim, Daewon, Hanlim Lee, Hyunkee Hong, Wonei Choi, Yun Gon Lee and Junsung Park, Estimation of
723 Surface NO₂ Volume Mixing Ratio in Four Metropolitan Cities in Korea Using Multiple Regression Models
724 with OMI and AIRS Data, *Remote Sens.* 2017, 9, 627; doi:10.3390/rs9060627, 2017.

725 Krafta, Martin, Thomas Eikmannb, Andreas Kapposc, Nino Künzlid, Regula Rappe, Klaus Schneiderf,
726 Heike Seitzb, Jens-Uwe Voss, H.-Erich Wichmannh, The German view: Effects of nitrogen dioxide on
727 human health – derivation of health-related short-term and long-term values, *International Journal of*
728 *Hygiene and Environmental Health*, 208, 305–318, 2005.

729 Kramer, L.J., R. J. Leigh, J. J. Remedios, et al., “Comparison of OMI and Ground-Based in situ and
730 MAXDOAS Measurements of Tropospheric Nitrogen Dioxide in An Urban Area,” *J. Geophys. Res.* **113**,
731 D16S39, 2008.

732 Kurucz. Robert L ., New atlases for solar flux, irradiance, central intensity, and limb intensity. *Memorie*
733 *della Societa Astronomica Italiana Supplementi*, 8:189, 2005.

734 Latza, Ute, , Silke Gerdes, and Xaver Baur, Effects of nitrogen dioxide on human health: Systematic review
735 of experimental and epidemiological studies conducted between 2002 and 2006, *International Journal*
736 *of Hygiene and Environmental Health* 212, Pages 271 - 287, doi.org/10.1016/j.ijheh.2008.06.003, 2009.

737 Lee, Grem, Hye-Ryun Oh, Chang-Hoi Ho, Jinwon Kim, Chang-Keun Song, Lim-Seok Chang, Jae-Bum Lee,
738 Seungmin Lee, Airborne Measurements of High Pollutant Concentration Events in the Free Troposphere
739 over the West Coast of South Korea between 1997 and 2011, *Aerosol and Air Quality Research*, 16,
740 1118–1130, 2016.

741 Lei, W., Zavala, M., de Foy, B., Volkamer, R., Molina, M. J., and Molina, L. T.: Impact of primary
742 formaldehyde on air pollution in the Mexico City Metropolitan Area, *Atmos. Chem. Phys.*, 9, 2607–2618,
743 2009.

744 Liteplo, R.G., R. Beauchamp, M.E. Meek, and R. Chénier. Formaldehyde. Geneva: International
745 Programme on Chemical Safety; 2002. [18 May 2010]. (Concise International Chemical Assessment
746 Document 40) (<http://www.inchem.org/documents/cicads/cicads/cicad40.htm>).

747 Luecken, D.J., W.T. Hutzell, M.L. Strum, G.A. Pouliot, Regional sources of atmospheric formaldehyde and
748 acetaldehyde, and implications for atmospheric modeling, *Atmospheric Environment* 47, 477-490,
749 doi:10.1016/j.atmosenv.2011.10.005, 2012.

750 Meller, Richard, and Geert K Moortgat. Temperature dependence of the absorption cross sections of
751 formaldehyde between 223 and 323 k in the wavelength range 225-375 nm. *Journal of Geophysical*
752 *Research: Atmospheres* (19842012), 105(D6):70897101, 2000.

753

754 Park. Junsung, Hanlim Lee, Jhoon Kim, Jay Herman, Woogyung Kim, Hyunkee Hong, Wonei Choi,
755 Jiwon Yang and Daewon Kim, HCHO column density retrieval using Pandora measurements in Seoul,
756 Korea: Temporal characteristics and comparison with OMI measurement, *Remote Sens.*, 10, 173;
757 doi:10.3390/rs10020173, 2018.

758

759 Platt, U., D. Perner, and H. W. Pätz, Simultaneous measurements of atmospheric CH₂, O₃ and NO₂ by
760 differential optical absorption, *J. Geophys. Res.* 84 (1979), 6329–6335, 1979.

761

762 Platt, U. Differential optical absorption spectroscopy (DOAS), *Air monitoring by Spectroscopic Techniques*
763 (M. Sigrist, ed.), John Wiley & Sons, Inc., 1994, pp. 27–84. [6] U. Platt, D. Perner, and H. W. Pätz,
764 Simultaneous measurements of atmospheric CH₂, O₃ and NO₂ by differential optical absorption, *J.*
765 *Geophys. Res.* 84 (1979), 6329–6335, 1994.

766

767 Richter D., P. Weibring, J. G. Walega, A. Fried, S. M. Spuler, M. S. Taubman: Compact highly sensitive
768 multi-species airborne mid-IR spectrometer, *Appl. Phys. B*, doi: 10.1007/s00340-015-6038-8, 2015.

769 Russell, A. R., Perring, A. E., Valin, L. C., Bucsela, E. J., Browne, E. C., Wooldridge, P. J., and Cohen, R. C.: A
770 high spatial resolution retrieval of NO₂ column densities from OMI: method and evaluation, *Atmos.*
771 *Chem. Phys.*, 11, 8543-8554, 2011.

772 Segal-Rosenheimer, M., P. B. Russell, B. Schmid, J. Redemann, J. M. Livingston, C. J. Flynn, R. R. Johnson,
773 S. E. Dunagan, Y. Shinozuka¹, J. Herman, A. Cede, N. Abuhassan, J. M. Comstock, J. M. Hubbe, A.
774 Zelenyuk³, and J. Wilson, (2014) Tracking elevated pollution layers with a newly developed

775 hyperspectral Sun/Sky spectrometer(4STAR): Results from the TCAP 2012 and 2013 campaigns, J.
776 Geophys. Res. Atmos., 119, 2611–2628, doi:10.1002/2013JD020884, 2014.

777 Shinozuka, Y., et al. , Hyperspectral aerosol optical depths from TCAP flights, J. Geophys. Res. Atmos.,
778 118, 12,180–12,194, doi:10.1002/2013JD020596, 2013.

779 Spinei, E., N. Abuhassan, A Cede, M. Tiefengraber, M. Mueller, J. Herman, N. Nowak, B. Poche, S. Choi,
780 A. Whitehill, J. Szykman, V. Lukas, D. Williams, R. Long, Jin Liao, Jason St. Clair, Glenn Wolfe, Thomas
781 Hanisco, Changmin Cho, Alan Fried, Petter Weibring, Dirk Richter, Robert Swap, James Walega, Pandora
782 formaldehyde measurements during KORUS-AQ over Olympic Park and Taehwa (South Korea, April-June
783 2016), (submitted to AMT), 2018.

784 Thuillier, G., L. Floyd, T.N. Woods, R. Cebula, E. Hilsenrath, M. Hersé, and D. Labs. Solar irradiance
785 reference spectra for two solar active levels. *Advances in Space Research*, 34(2):256–261, 2004.

786 Vandaele, A.C., C. Hermans, P. C. Simon, M. Carleer, R. Colin, S. Fally, M. F. Mérienne, A. Jenouvrier, and
787 B. Coquart. Measurements of the NO₂ absorption cross-section from 42,000 cm⁻¹ to 10,000 cm⁻¹ (238-
788 1000 nm) at 220 K and 294 K. *Journal of Quantitative Spectroscopy and Radiative Transfer*, 59: 171–184,
789 doi: 10.1016/S0022-4073(97)00168-4, 1998.

790 VanHoosier, Michael E. Solar ultraviolet spectral irradiance data with increased wavelength and
791 irradiance accuracy. In SPIE's 1996 International Symposium on Optical Science, Engineering, and
792 Instrumentation, pages 57–64. International Society for Optics and Photonics, 1996.

793 Walters, Wendell & Goodwin, Stanford & Michalski, Greg. (2015). The Nitrogen Stable Isotope
794 Composition ($\delta^{15}\text{N}$) of Vehicle Emitted NO_x. *Environmental science & technology*. 49.
795 10.1021/es505580v, 2015.

796 Zhang, Hongliang, Jingyi Li, Qi Ying, Birnur Buzcu Guven, and Eduardo P. Olaguer, Source apportionment
797 of formaldehyde during TexAQS 2006 using a source-oriented chemical transport model, *J. Geophys.*
798 *Res.*, 118, 1525–1535, doi:10.1002/jgrd.50197, 2013.

799 Zhu, Lei, Daniel J. Jacob, Frank N. Keutsch, Loretta J. Mickley, Richard Scheffe, Madeleine Strum, Gonzalo
800 González Abad, Kelly Chance, Kai Yang, Bernhard Rappenglück, Dylan B. Millet, Munkhbayar Baasandorj,
801 Lyatt Jaeglé, and Viral Shah, Formaldehyde (HCHO) As a Hazardous Air Pollutant: Mapping Surface Air
802 Concentrations from Satellite and Inferring Cancer Risks in the United States, *Environmental Science &*
803 *Technology* 51 (10), 5650-5657, DOI: 10.1021/acs.est.7b01356, 2017.

804

805

806

807

808 Acknowledgement

809 The author would like to thank the Pandora project for support in completing this study as well as
810 financial support from the KORUS-AQ project NNH15ZDA001N-KORUS. Dr. Jae Kim and Dr. Jhoon
811 Kim are supported by Korea Ministry of Environment as Public Technology Program based on
812 Environmental Policy (2017000160001). All data is available from a NASA data repository:
813 <https://avdc.gsfc.nasa.gov/pub/DSCOVER/Pandora/DATA/KORUS-AQ/>

814

815

816 **Tables**

Table 1 KORUS-AQ Locations (South to North)

Locations	Alt(m)	Latitude	Longitude
Gwangju	33	35.2260N	126.8430W
Busan	228	35.2353N	129.0825W
Anmyeondo	41	36.5380N	126.3300W
Taehwa Mtn	160	37.3123N	127.3106W
Yeoju-1 & 2	90	37.3385N	127.4895W
Songchon	49	37.4100N	127.5600W
Olympic Park	26	37.5232N	127.1260W
Seoul	181	37.5644N	126.9340W

817

818

Table 2 Taehwa Mtn DC8 compared to PSI measurements in Fig. 18

Date	LT	DC8 HCHO DU	PSI HCHO	Percent
11 May	08:25:19	0.4	0.6	67
18 May	08:34:26	0.4	0.5	80
30 May	12:05:00	0.5	0.9	56
10 Jun	08:22:45	1	1.16	86
10 Jun	12:22:53	1	1.5	67
10 Jun	15:46:03	1	1.3	77

819

820

821 **Figure Captions**

822 **Fig. 1** KORUS-AQ sites for 9 Pandora instruments at 8 sites.

823 **Fig. 2a** $C(NO_2)$ amounts from Pandora 27 and 35 in Yeosu, Korea during 3 June 2016 and their difference
824 $|Pan35 - Pan27| < 0.05$ DU.

825 **Fig. 2b** Pandora 35 estimate of cloud or aerosol reduced measured counts/second at approximately 500
826 nm.

827 Fig. 3. Frequency distributions of $C(NO_2)$ across the KORUS-AQ PSI network: April 20 to Jun 6 2016,
828 except as labelled. The axes vary for different sites.

829 Fig. 4 NO_2 time series vs day of the year (DOY) and diurnal variability (daily vertical extent) at 9 Pandora
830 sites. Notice the very high NO_2 amounts in Seoul and nearby Olympic Park. The black curves are
831 approximately weekly least squares running averages. Note: the vertical scales are different for each site
832 to show the daily variability relative to the running average.

833 Fig. 5 NO_2 amounts vs Day of the Year (DOY) and Local Time for six sites as labeled in each panel. Day
834 120=April 29, Day 130=May 9, Day 140=May 19, Day 150=May 29, Day 160=June 8, Day 170 =June18.

Fig. 6 Approximately 1 year of daily column $C(NO_2)$ amount data (Panels A and D) and the monthly
running average amount (dark plot in Panels A and D). The data are from GIST at Gwangju and
Amnyeondo. Panels A and D are the original time series with one data point every 80 seconds, panels B
and E are the deseasonalized time series. Panels C and F are an expanded scale of the monthly running
averages $M(t)$ of $C(NO_2)$ that are identical to the solid lines in panels A and D. The vertical extent (panels
A, B, D, and E) on a given day is the range of diurnal variation from early morning to late afternoon.

835 Fig. 7 (A) NO_2 time series at Yonsei University in Seoul NO_2 (grey) and (B) deseasonalized time series.
836 Combined slope = -0.05 ± 0.001 DU/Year and Mean = 1.2 ± 0.8 DU or the decrease is -4 ± 0.08 % / Year.
837 Seoul has no clear seasonal cycle.

838 Fig. 8 (A) Pusan University in Busan NO_2 daily time series (grey) and (B) deseasonalized time series with
839 linear trends.

840 Fig. 9a Comparisons between the daily values of $C(NO_2)$ for OMI (black) and PSI (red) at Seoul and Busan
841 for a 5-year period. Solid lines show the average seasonal variation (Lowess(0.1)), see also Fig. 9b. **Linear**
842 **interpolation is used where there are missing data points.**

843 Fig. 9b Comparisons between the seasonal averages for $C(NO_2)$ from OMI (black) and PSI (red) at Seoul
844 and Busan for a 5-year period. The lower panels show the seasonal difference between the PSI and
845 OMI. **The individual data points are shown derived from a Lowess(0.1) smoothing, approximately a 3-**
846 **month running averages of the daily data. Interpolation has been used where there are missing data**
847 **points.**

848 Fig. 10 C(NO₂) time series from Pandora (red) and OMI (black) for GIST University in Gwangju Korea and
849 their differences. The comparison is formed from time coincidences between Pandora and OMI.

850 Fig. 11 A correlation plot of C(NO₂) from 4STAR onboard the DC-8 compared to the C(NO₂) amount
851 measured by the PSI at Olympic Park on nine different days. The solid black line is the 1:1 line drawn for
852 reference. The dashed line represents the data linear fit, with a slope of 1.05, and a correlation
853 coefficient $r^2 = 0.7$, as shown on the plot.

854 Fig. 12 C(HCHO) from PSI at Olympic Park for 6 days in June 2016. C(HCHO) on 2 June 2016 has a peak
855 value of 2.3 DU at 14:30 hours.

856 Fig. 13 Pandora measured formaldehyde amounts vs day of the year and local time for 29 April 2016 to
857 11 June 2016 in Olympic Park.

858 Fig. 14 HCHO altitude profile measured onboard the DC8 on 4 May at 07:54 (A) and 11:54 (B) local time
859 over Olympic Park, Korea. Panel C: PSI measurements of total column HCHO. Vertical bars mark the DC8
860 flight duration for the profiles yielding altitude integrated column amounts of 0.38 and 0.26 DU.

861 Fig. 15 DC-8 HCHO measurements over Olympic Park on June 4. The continuous blue profiles
862 show the 1-second HCHO data while the black points with error bars show the 10-second
863 average and standard deviation of this data at points of closest approach above the Olympic
864 Park site.

865 Fig. 16 HCHO altitude profile measured onboard the DC8 on 5 June at 8:30 (A) and 15:21 (B) local time
866 over Olympic Park, Korea. Panel C: PSI measurements of total column HCHO. Vertical bars mark the DC8
867 flight duration for the profiles yielding column amounts of 0.60 and 0.82 DU.

868 Fig. 17 Total column HCHO from Pandora Yonsei University, Seoul for 6 days in June 2016. HCHO on 2
869 June 2016 has a peak value of 1.2 DU at 13:30 hours.

870 Fig. 18 Total column HCHO from Pandora Taehwa Mountain for 6 days in June 2016. HCHO on 2 June
871 2016 has a peak value of 1.2 DU at 12:45. ▲ are DC8 measurements on 10 June.

872 Fig. 19a Summary of total column HCHO for the stated dates during the KORUS-AQ campaign. The solid
873 line is a Lowess(0.1) fit to the data. The sharp cutoffs in panel A, B, and C were caused obstructions of
874 the direct sun from the PSI FOV in the afternoon.

875 Fig. 19b Summary of total column HCHO for the stated dates during the KORUS-AQ campaign. Panels A
876 and B represent the daily variation at a given local time. The solid line is a Lowess(0.1) fit to the data.
877 Panels C and D show the frequency of occurrence (%) for different amounts of HCHO.

878 Fig. 20 The springtime change in C(HCHO) over about a 40 day period depending on the site.
879 The “vertical bars” are the diurnal variation within each day of data. The thicker red curve is a
880 Lowess(0.3) fit to the data, while the thin red line is a linear least squares fit. The Lowess(0.3) fit
881 is approximately a 10-day local least-squares average.

882 Fig. 21 Compare PSI • and OMI o retrievals of C(HCHO) at 13.5 ± 0.5 hours. OMI overpass data, V03, are
883 from <https://avdc.gsfc.nasa.gov/index.php?site=1113974256&id=81>

884 Fig. A1 An illustration of the deseasonalization (right panel) of the monthly running average of NO_2 for
885 the Gwangju site (left panel) shown in Fig. 6. The insets are magnifications of the main plots.

886

887

888 Figures

889

890

891

892

893

894

895

896

897

898

899

900

901

902

903

904

905

906



Fig. 1 KORUS-AQ sites for 9 Pandora instruments at 8 sites.

F01

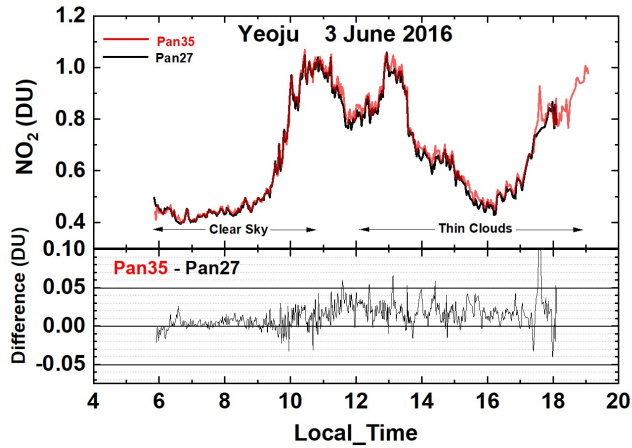


Fig. 2a $C(\text{NO}_2)$ amounts from Pandora 27 and 35 in Yeosu, Korea during 3 June 2016 and their difference $|\text{Pan35} - \text{Pan27}| < 0.05 \text{ DU}$.

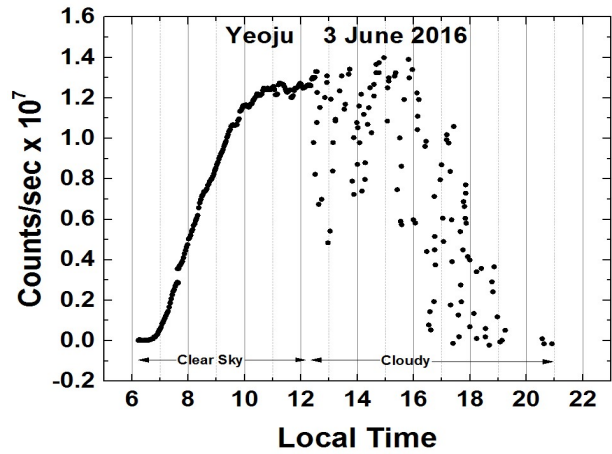


Fig. 2b Pandora 35 estimate of cloud or aerosol reduced measured counts/second at approximately 500 nm.

907

908 **F02**

909

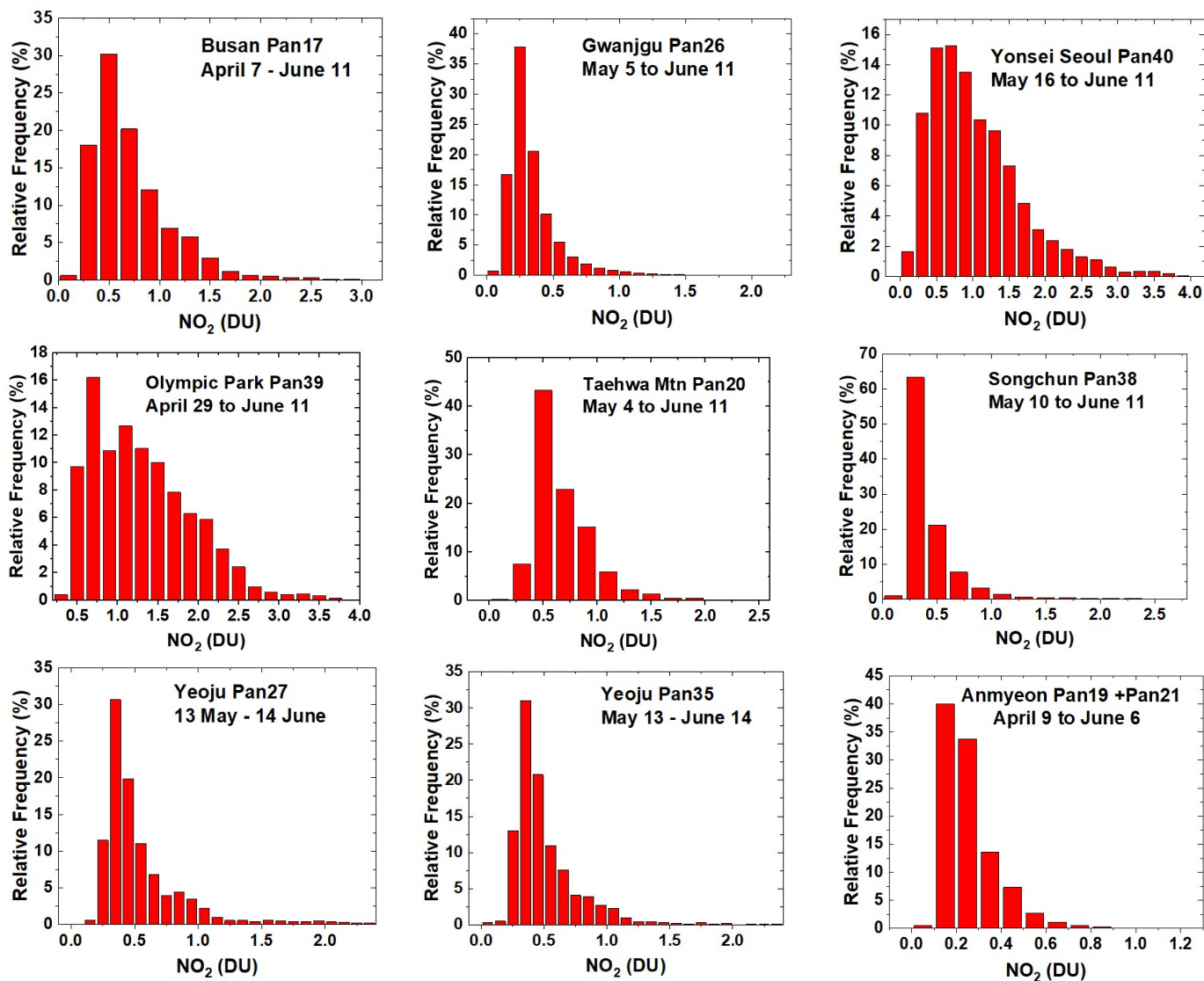


Fig. 3. Frequency distributions of $C(\text{NO}_2)$ across the KORUS-AQ PSI network: April 20 to Jun 6 2016, except as labelled. The axes vary for different sites.

910

911 **F03**

912

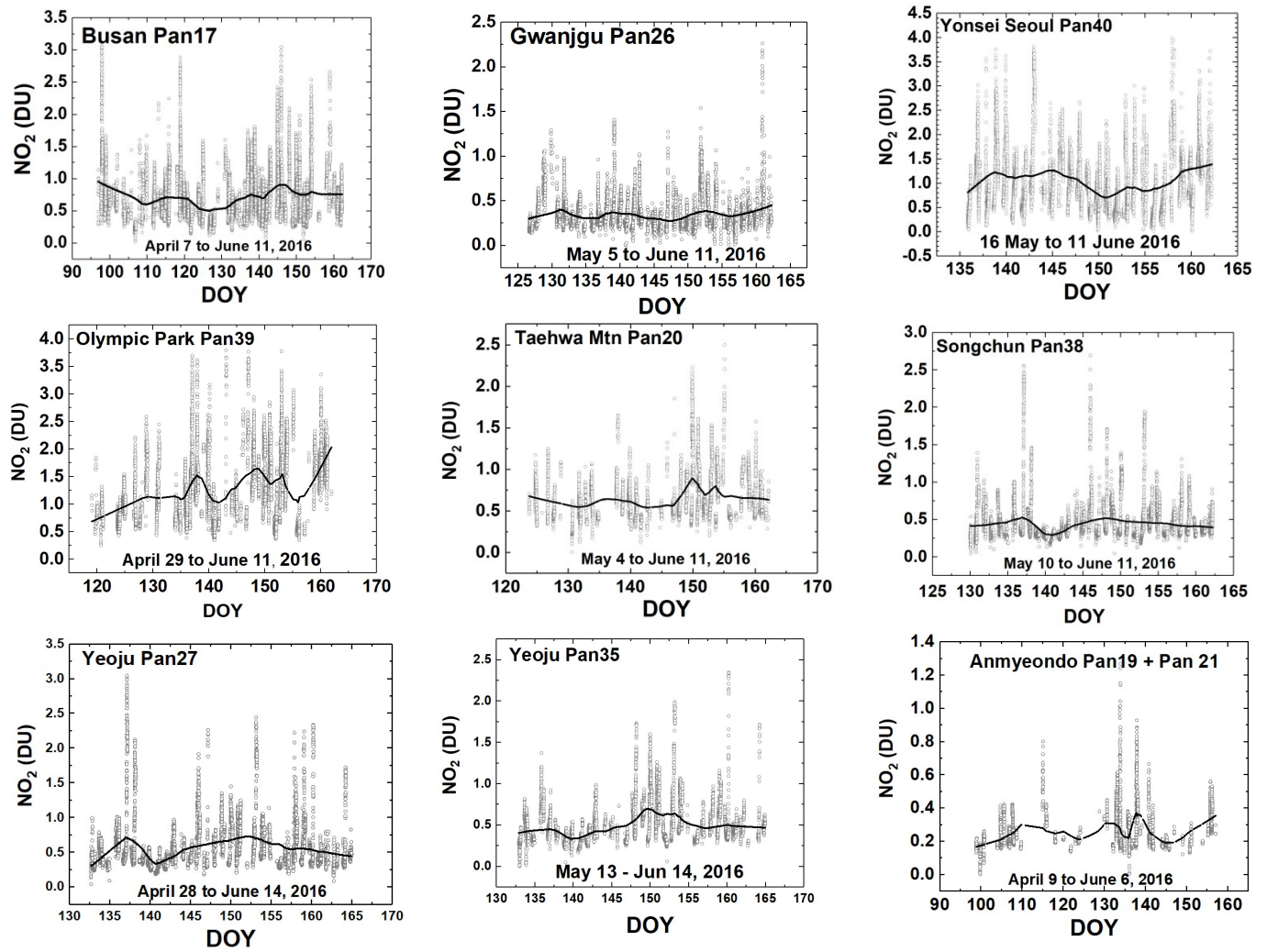


Fig. 4 NO₂ time series vs day of the year (DOY) and diurnal variability (daily vertical extent) at 9 Pandora sites. Notice the very high NO₂ amounts in Seoul and nearby Olympic Park. The black curves are approximately weekly least squares running averages. The daily vertical extent corresponds to diurnal variation (Fig. 2). Note: the vertical scales are different for each site to show the daily variability relative to the running average.

913

914 **F04**

915

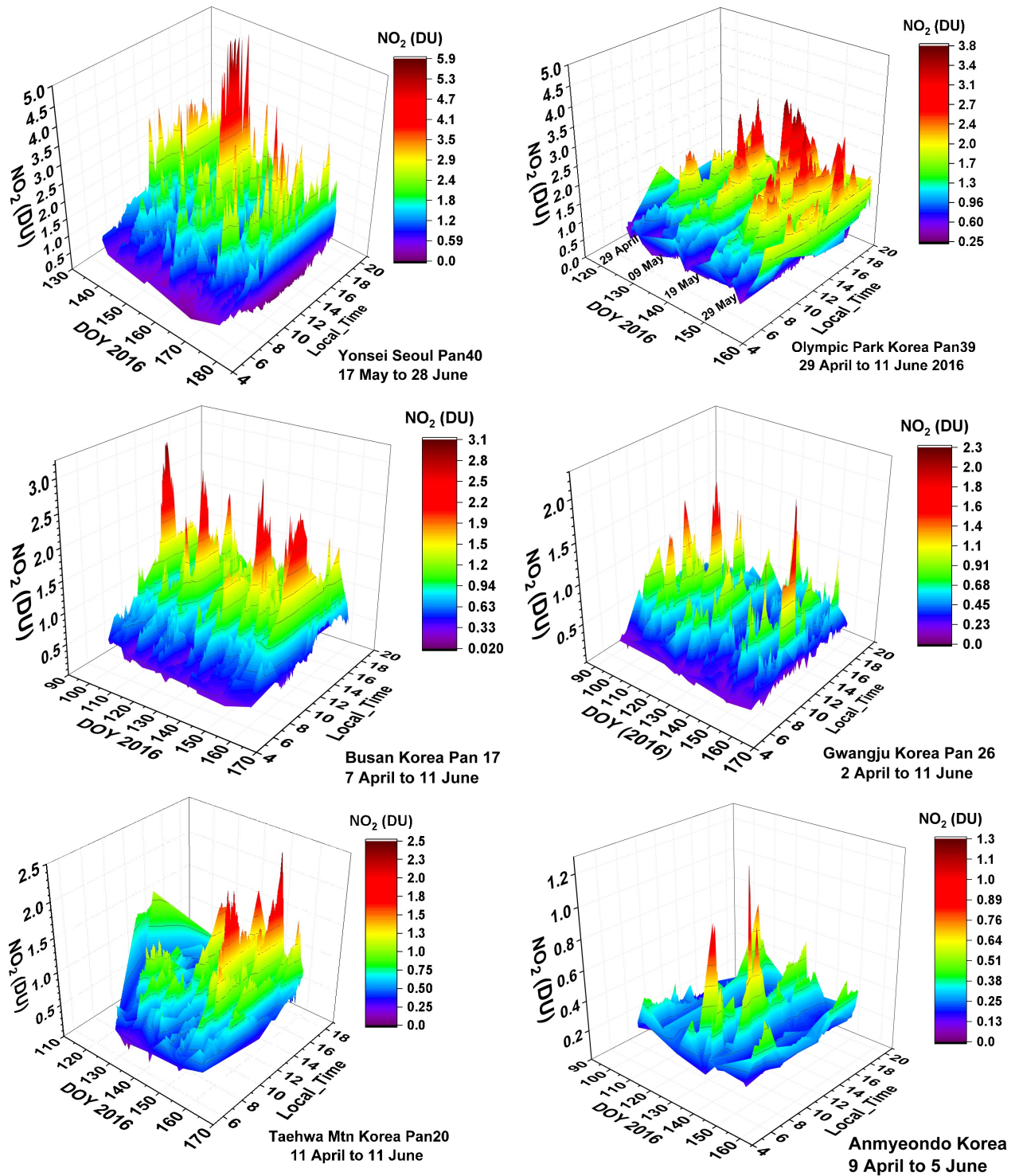


Fig. 5 NO₂ amounts vs Day of the Year (DOY) and Local Time for six sites as labeled in each panel. Day 120=April 29, Day 130=May 9, Day 140=May 19, Day 150=May 29, Day 160=June 8, Day 170 =June18.

916

917 **F05**

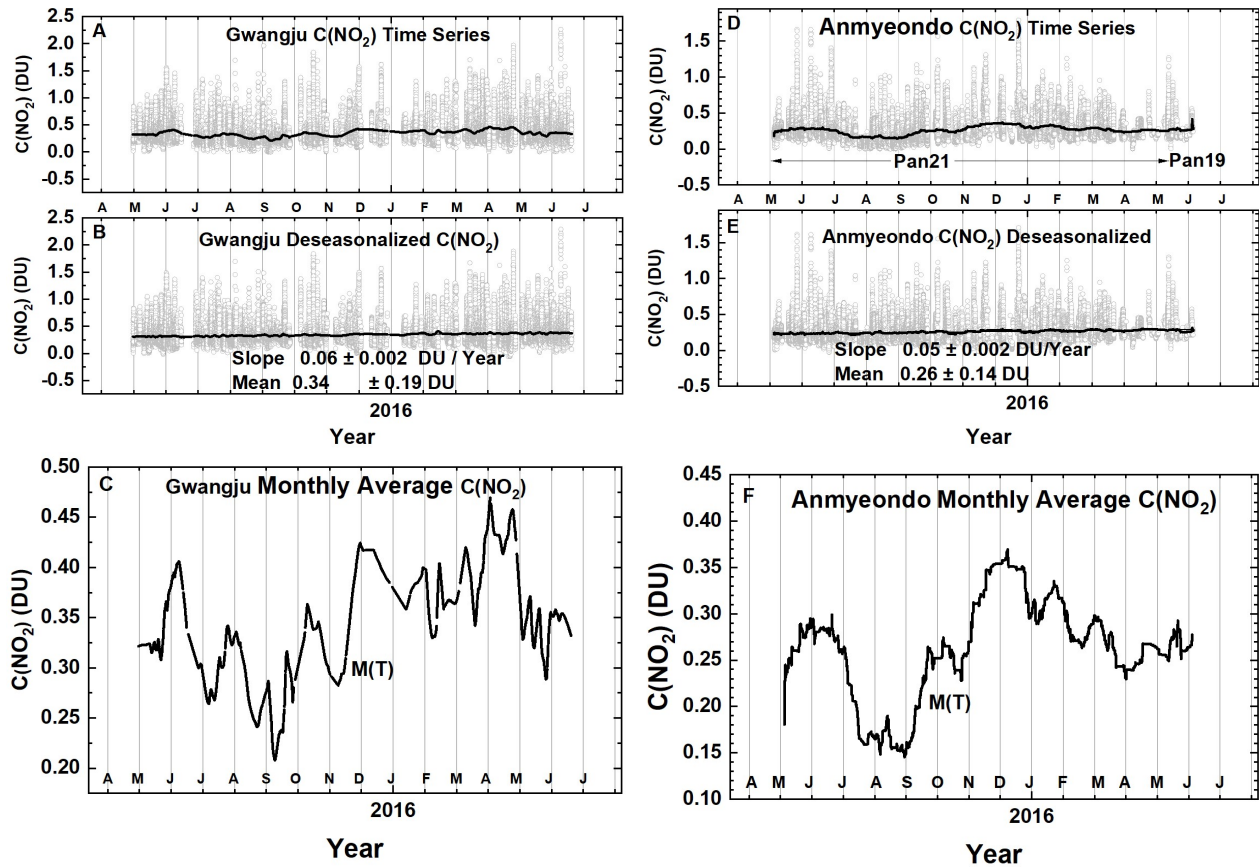


Fig. 6 Approximately 1 year of daily column $C(\text{NO}_2)$ amount data (Panels A and D) and the monthly running average amount (dark plot in Panels A and D). The data are from GIST at Gwangju and Anmyeondo. Panels A and D are the original time series with one data point every 80 seconds, panels B and E are the deseasonalized time series. Panels C and F are an expanded scale of the monthly running averages $M(t)$ of $C(\text{NO}_2)$ that are identical to the solid lines in panels A and D. The vertical extent (panels A, B, D, and E) on a given day is the range of diurnal variation from early morning to late afternoon.

918

919

920 **F06**

921

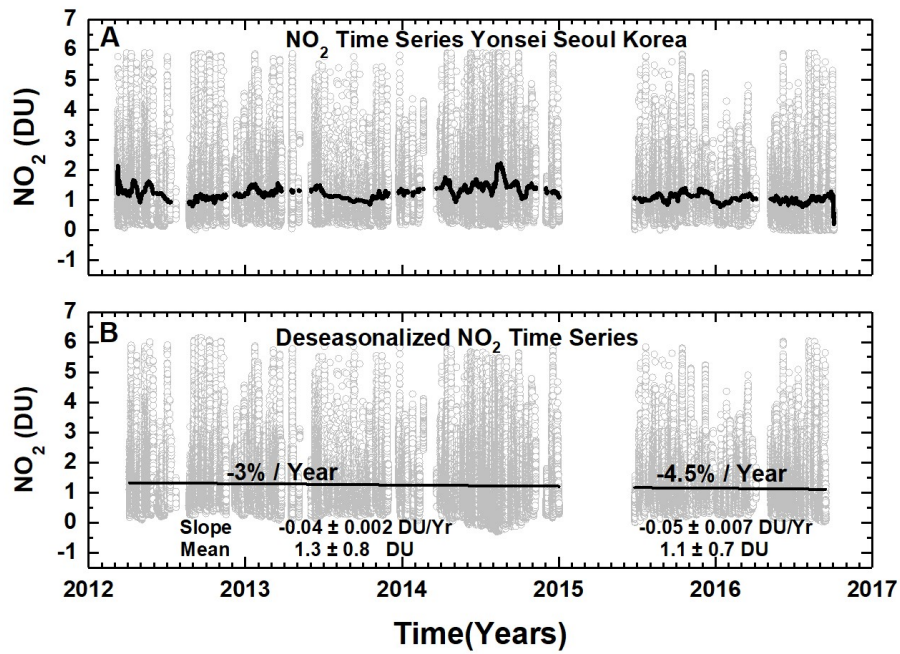


Fig. 7 (A) NO₂ time series at Yonsei University in Seoul NO₂(grey) and (B) deseasonalized time series. Combined slope = -0.05 ± 0.001 DU/Year and Mean = 1.2 ± 0.8 DU or the decrease is -4 ± 0.08 % / Year. Seoul has no clear seasonal cycle.

922

923 **F07**

924

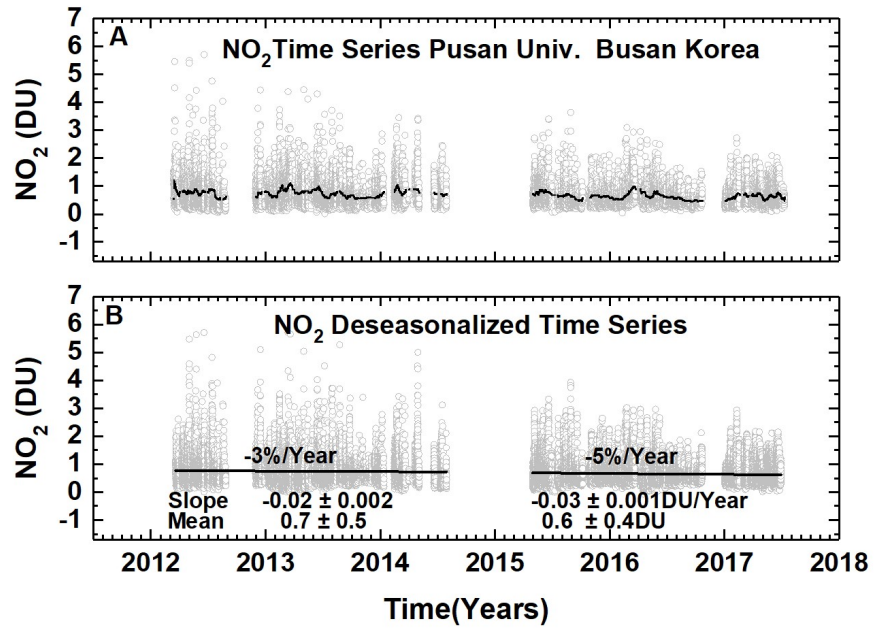


Fig. 8 (A) Pusan University in Busan NO₂ daily time series (grey) and (B) deseasonalized time series with linear trends.

925

926 **F08**

927

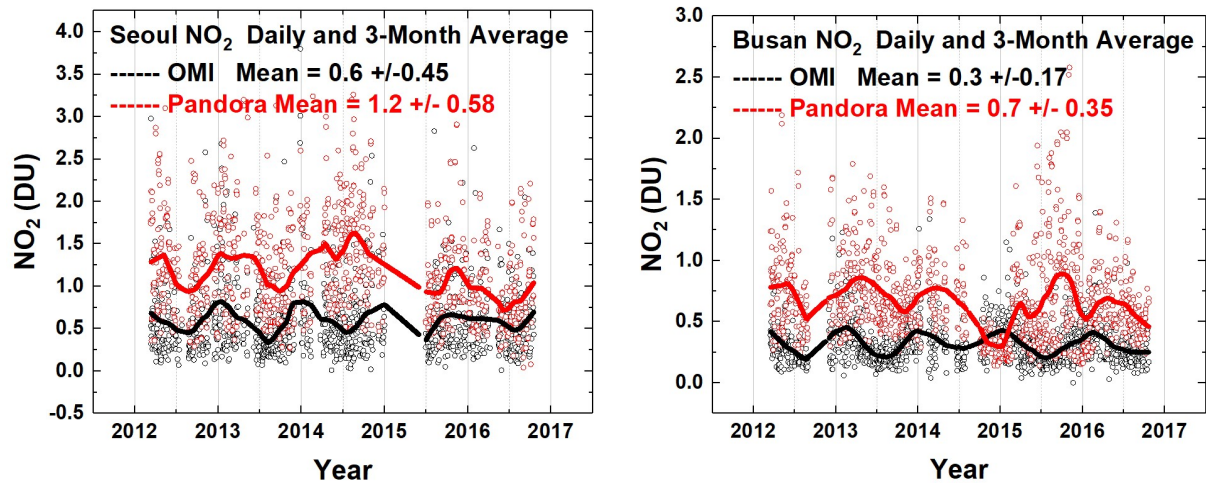


Fig. 9a Comparisons between the daily values of C(NO₂) for OMI (black) and PSI (red) at Seoul and Busan for a 5-year period. Solid lines show the average seasonal variation (Lowess(0.1)), see also Fig. 9b. Linear interpolation is used where there are missing data points.

928

929 **F09a**

930

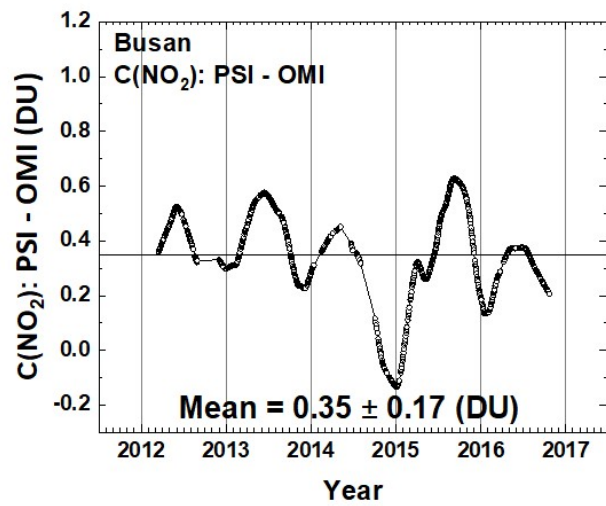
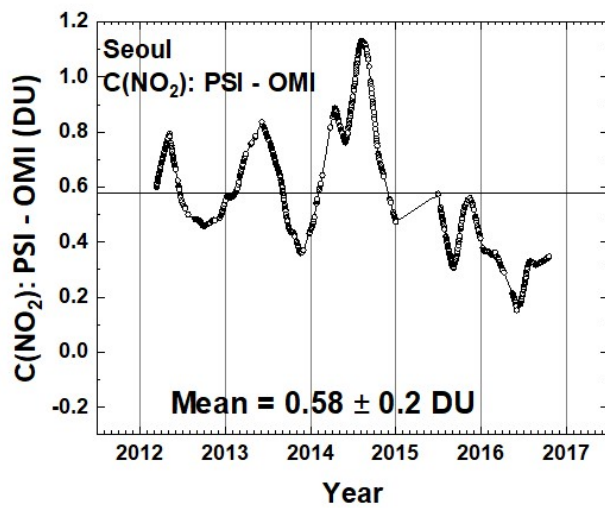
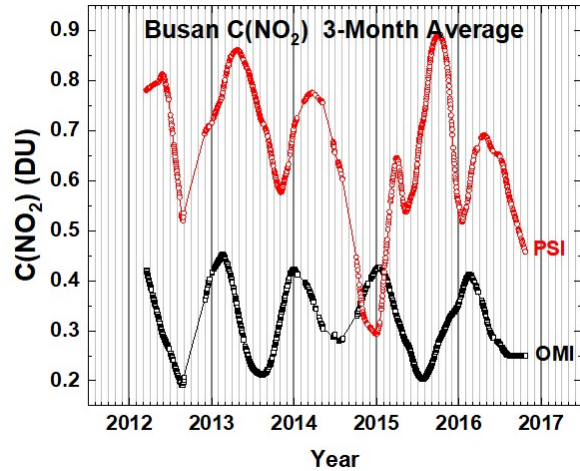
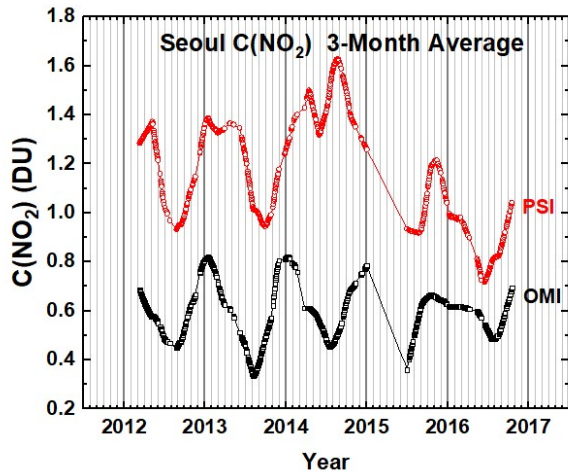


Fig. 9b Comparisons between the seasonal averages for C(NO₂) from OMI (black) and PSI (red) at Seoul and Busan for a 5-year period. The lower panels show the seasonal difference between the PSI and OMI. The individual data points are shown derived from a Lowess(0.1) smoothing, approximately a 3-month running averages of the daily data. Interpolation has been used where there are missing data points.

931

932 **F09b**

933

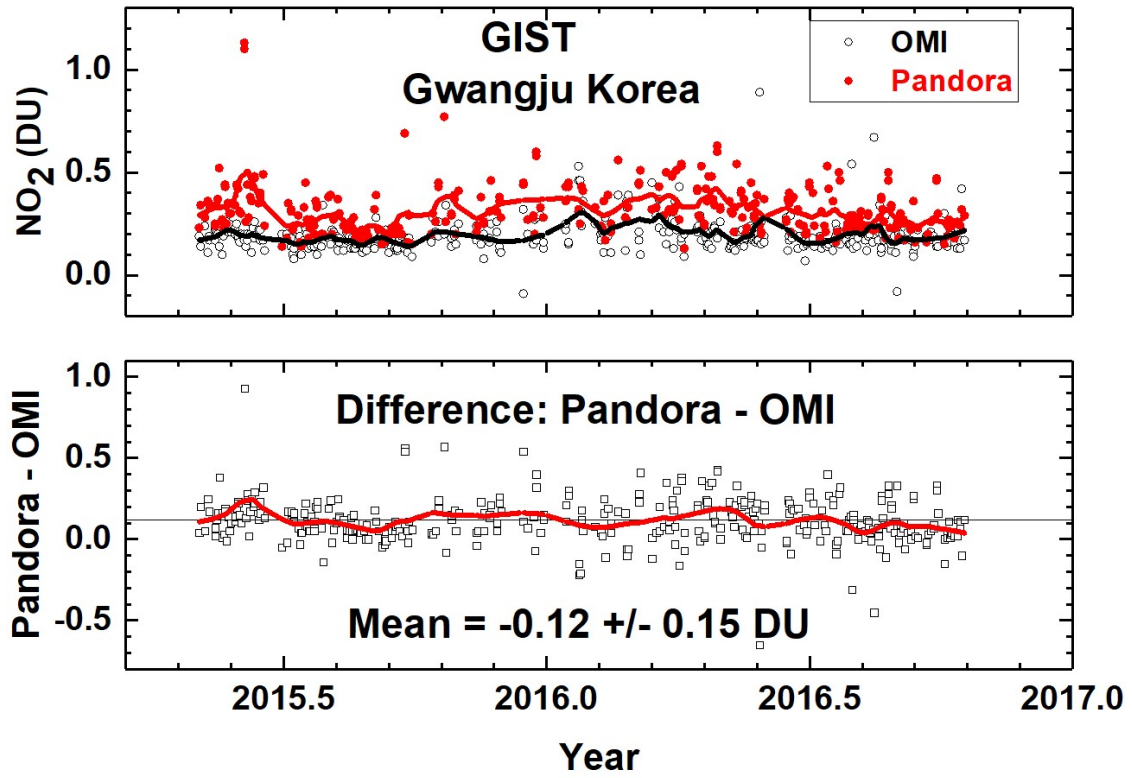


Fig. 10 C(NO₂) time series from Pandora (red) and OMI (black) for GIST University in Gwangju Korea and their differences. The comparison is formed from time coincidences between Pandora and OMI.

934

935 **F10**

936

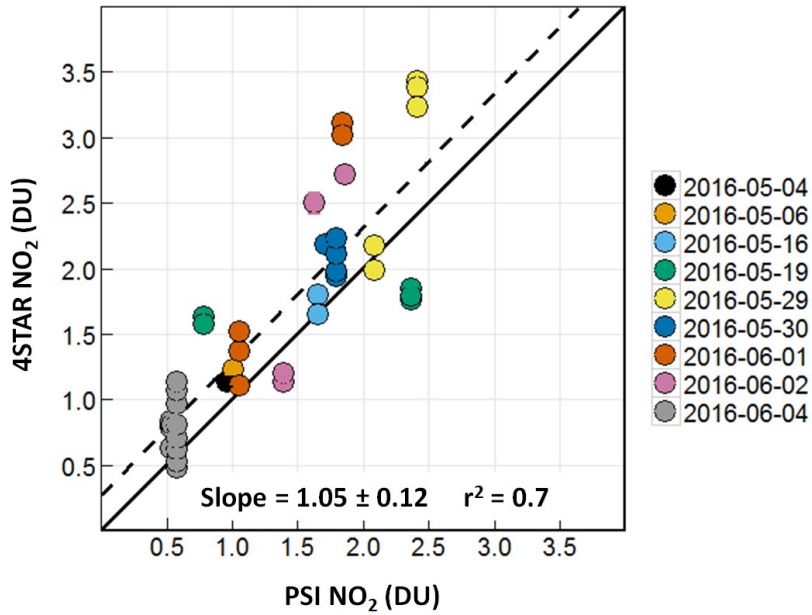


Fig. 11 A correlation plot of C(NO₂) from 4STAR onboard the DC-8 compared to the C(NO₂) amount measured by the PSI at Olympic Park on nine different days. The solid black line is the 1:1 line drawn for reference. The dashed line represents the data linear fit, with a slope of 1.05, and a correlation coefficient $r^2 = 0.7$, as shown on the plot.

937

938 **F11**

939

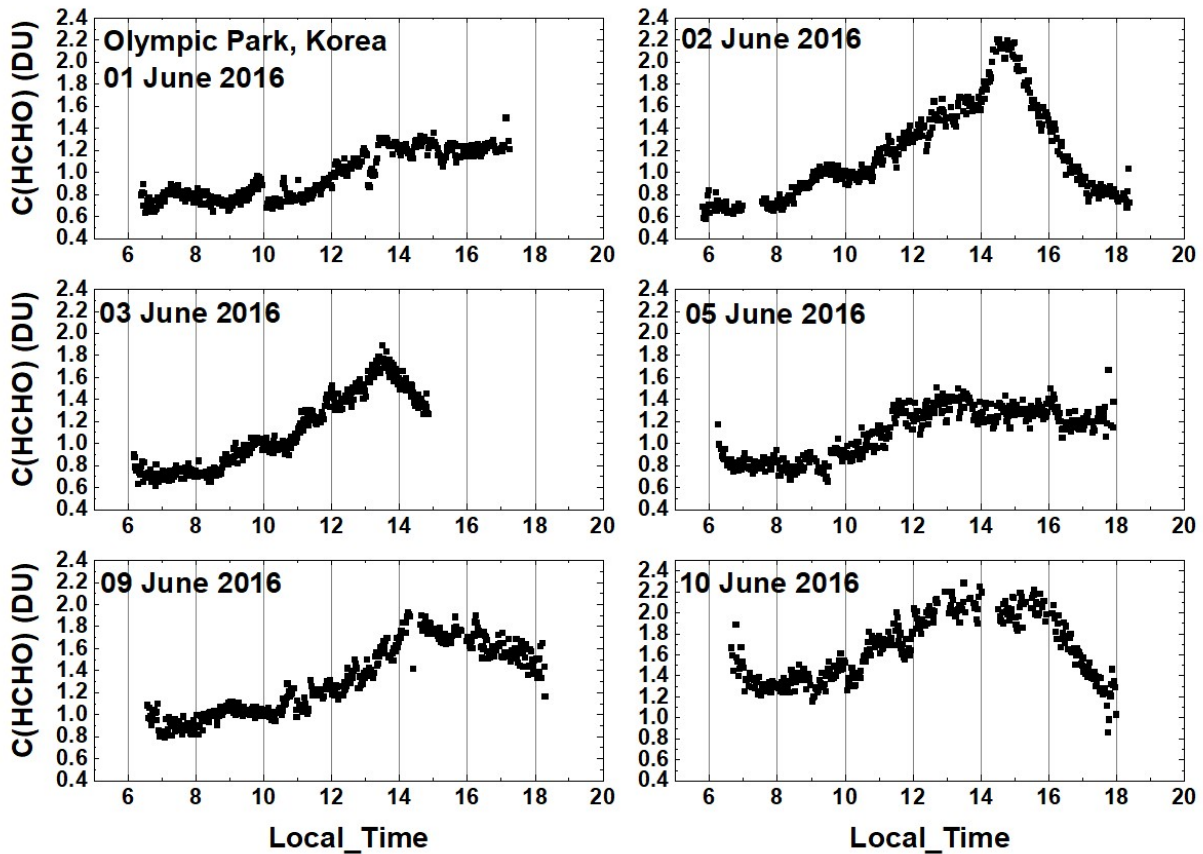


Fig. 12 C(HCHO) from PSI at Olympic Park for 6 days in June 2016. C(HCHO) on 2 June 2016 has a peak value of 2.3 DU at 14:30 hours.

940

941 **F12**

942

943

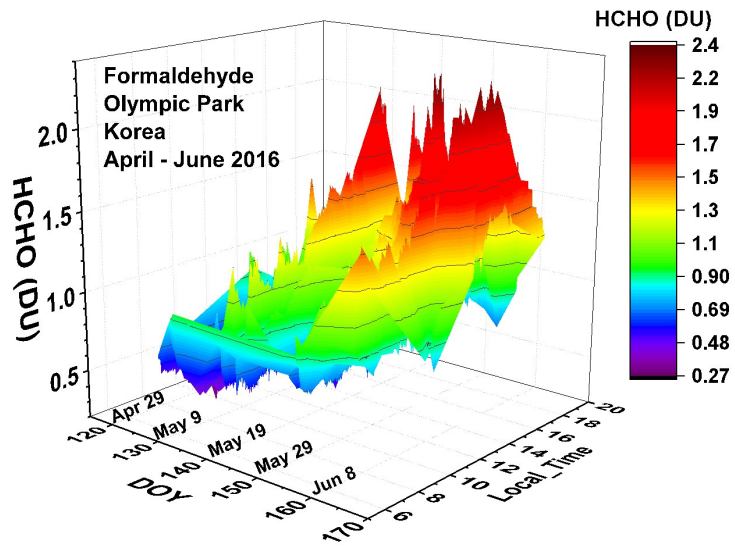


Fig. 13 Pandora measured formaldehyde amounts vs day of the year and local time for 29 April 2016 to 11 June 2016 in Olympic Park.

944

945 **F13**

946

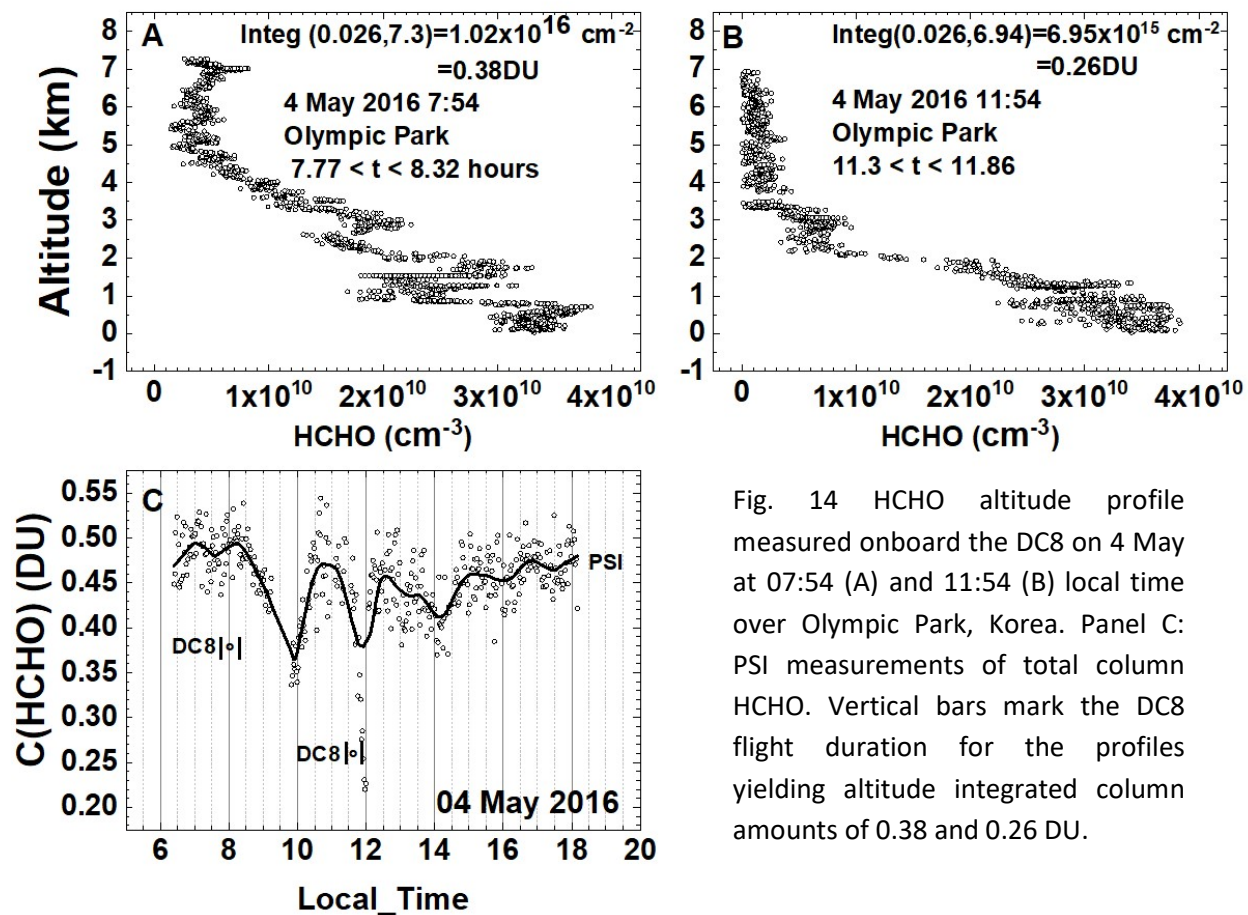


Fig. 14 HCHO altitude profile measured onboard the DC8 on 4 May at 07:54 (A) and 11:54 (B) local time over Olympic Park, Korea. Panel C: PSI measurements of total column HCHO. Vertical bars mark the DC8 flight duration for the profiles yielding altitude integrated column amounts of 0.38 and 0.26 DU.

947

948 **F14**

949

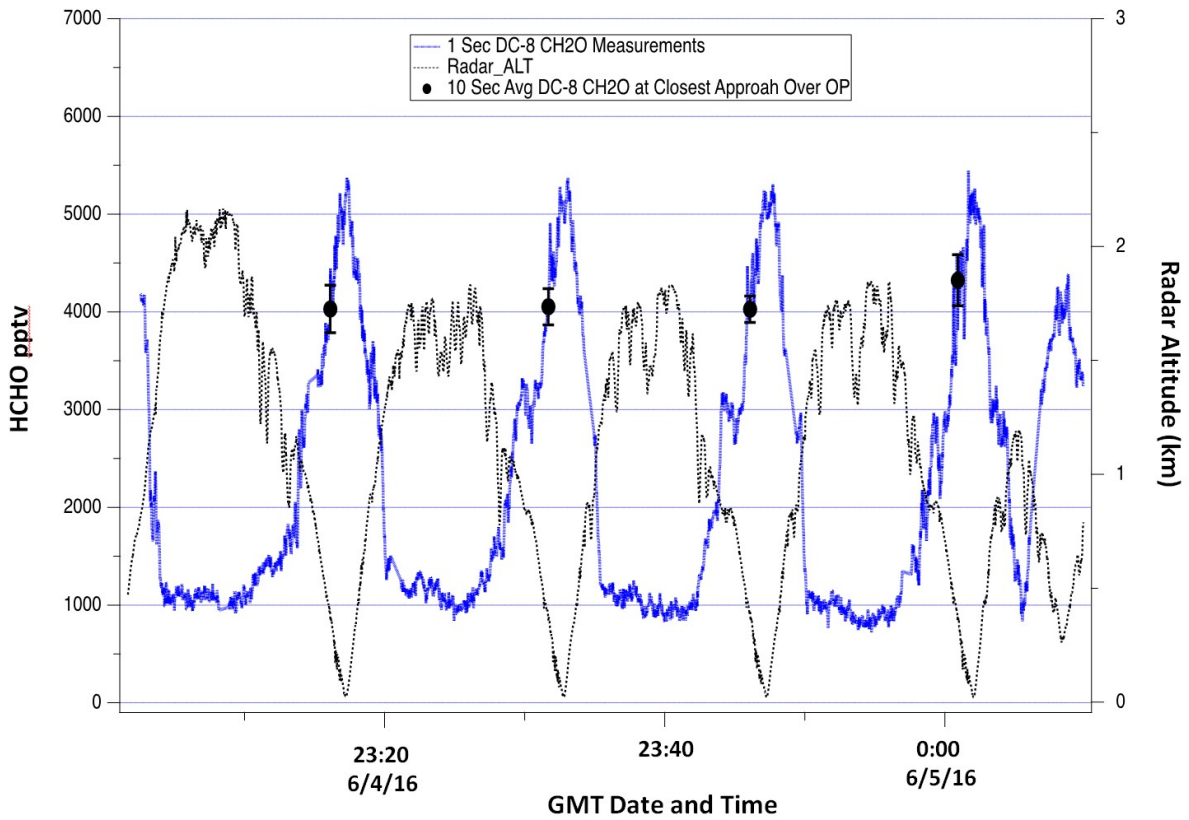


Fig. 15 DC-8 HCHO measurements over Olympic Park on June 4. The continuous blue profiles show the 1-second HCHO data while the black points with error bars show the 10-second average and standard deviation of this data at points of closest approach above the Olympic Park site.

950

951 **F15**

952

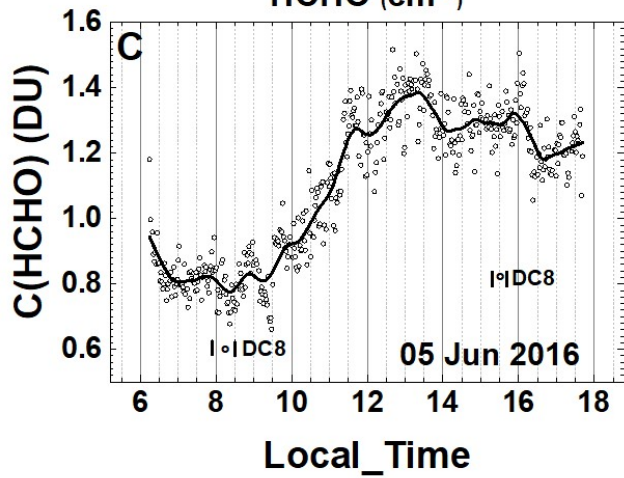
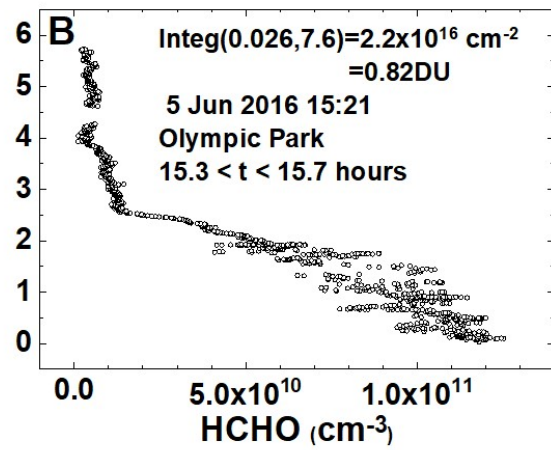
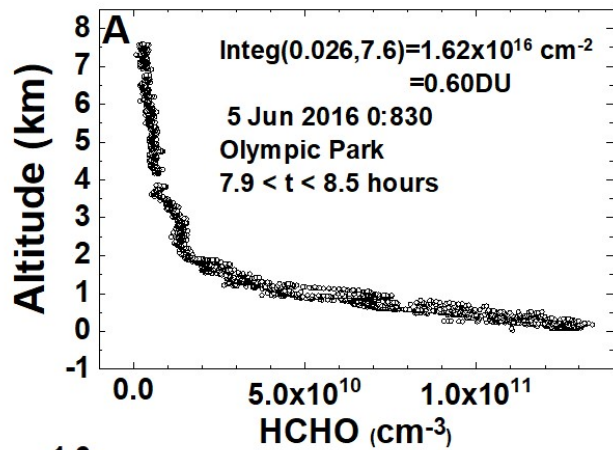


Fig. 16 HCHO altitude profile measured onboard the DC8 on 5 June at 8:30 (A) and 15:21 (B) local time over Olympic Park, Korea. Panel C: PSI measurements of total column HCHO. Vertical bars mark the DC8 flight duration for the profiles yielding column amounts of 0.60 and 0.82 DU.

953

954 **F16**

955

956

957

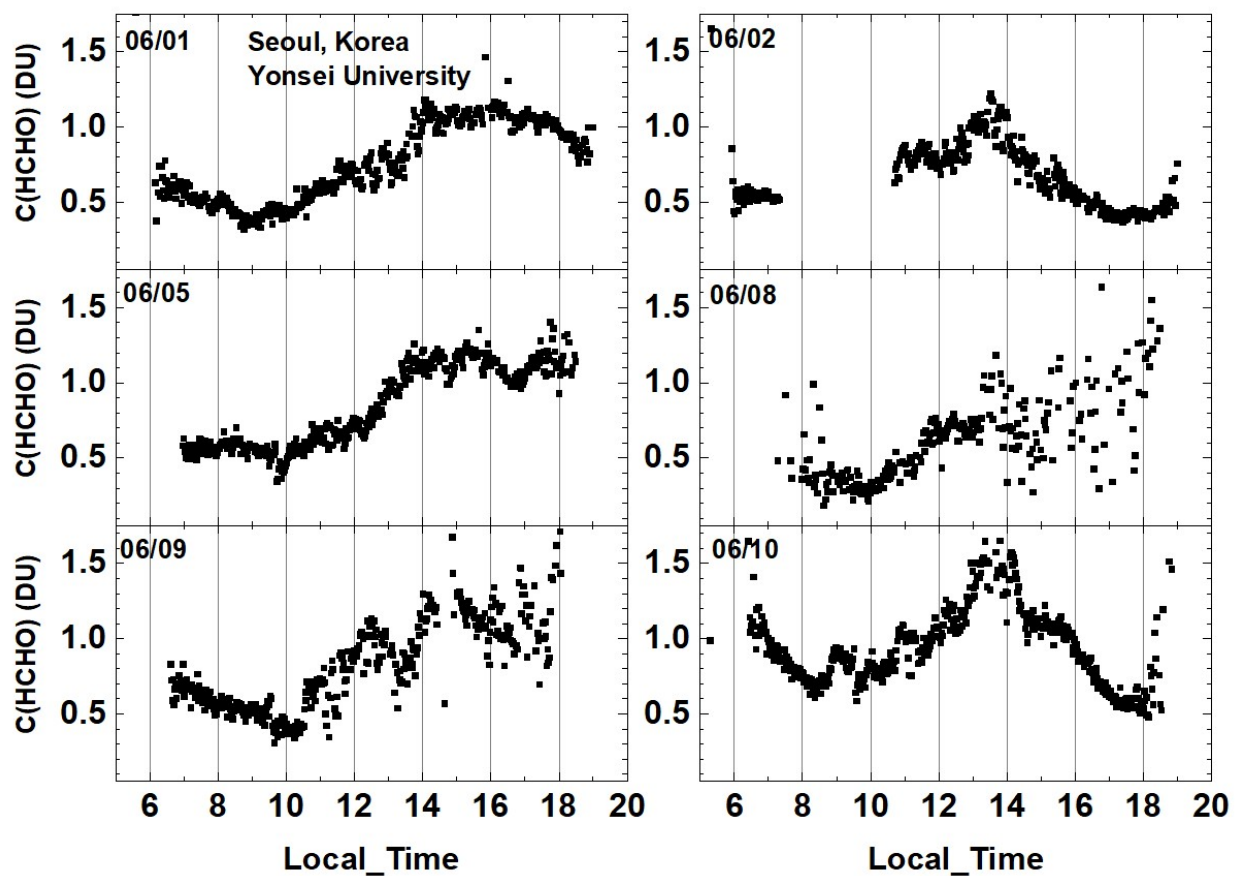


Fig. 17 Total column HCHO from Pandora Yonsei University, Seoul for 6 days in June 2016. C(HCHO) on 2 June 2016 has a peak value of 1.2 DU at 13:30 hours.

958

959 **F17**

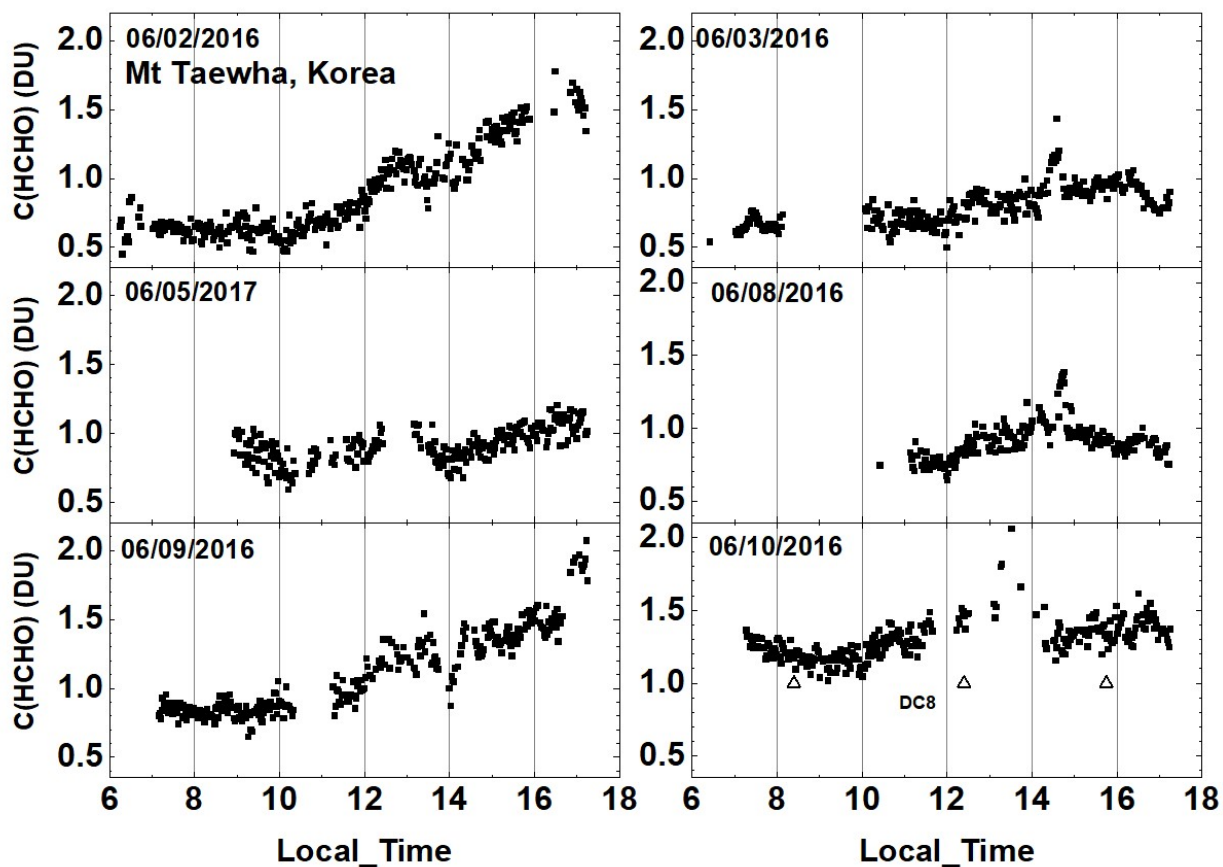


Fig. 18 Total column HCHO from Pandora at Taehwa Mountain for 6 days in June 2016. C(HCHO) on 2 June 2016 has a peak value of 1.7 DU at 16:20. △ are DC8 measurements on 10 June

960

961 **F18**

962

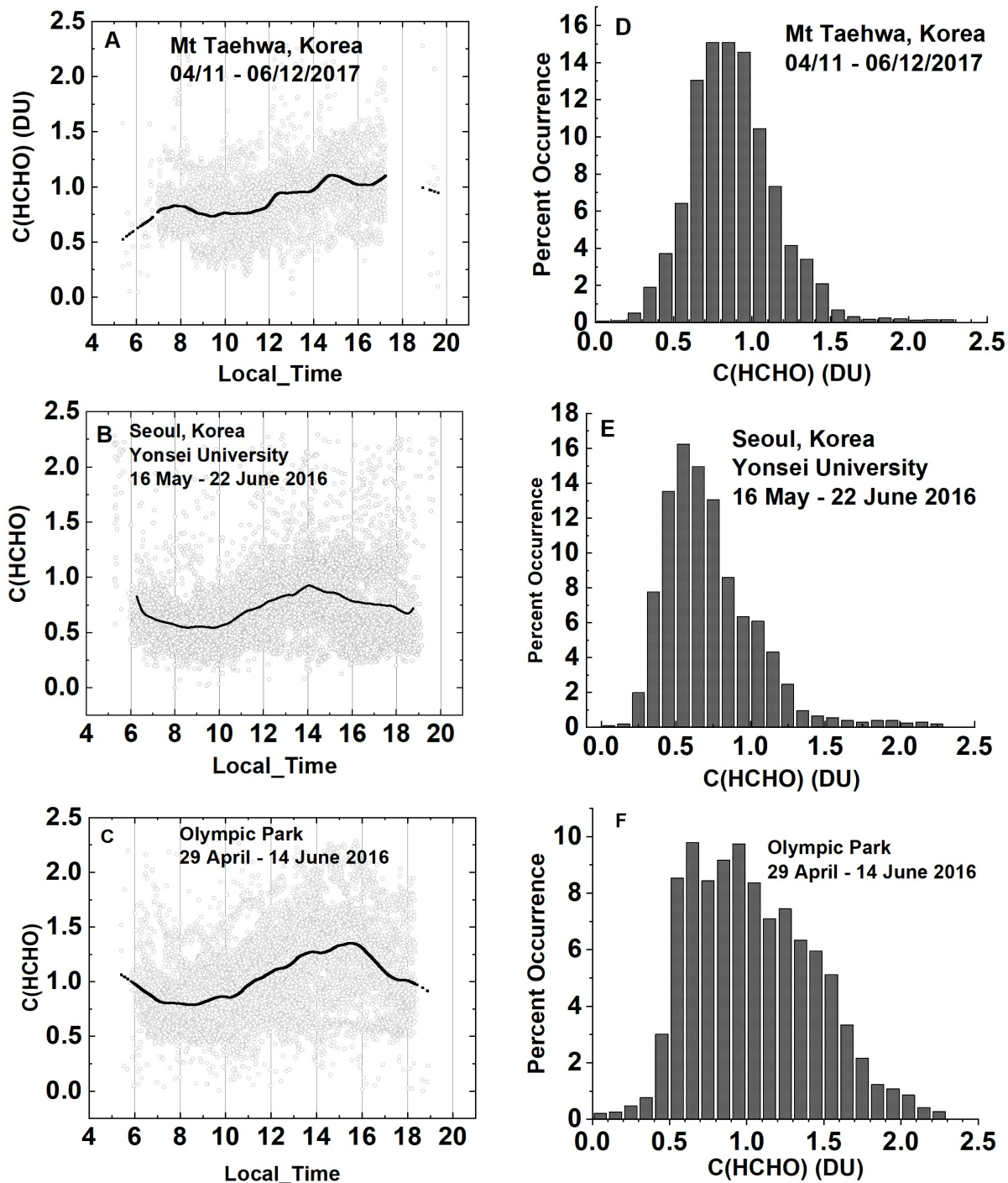


Fig. 19a Summary of total column HCHO for the stated dates during the KORUS-AQ campaign. The solid line is a Lowess(0.1) fit to the data. The sharp cutoffs in panel A, B, and C were caused by obstructions of the direct sun from the PSI FOV in the afternoon.

963

964 **F19a**

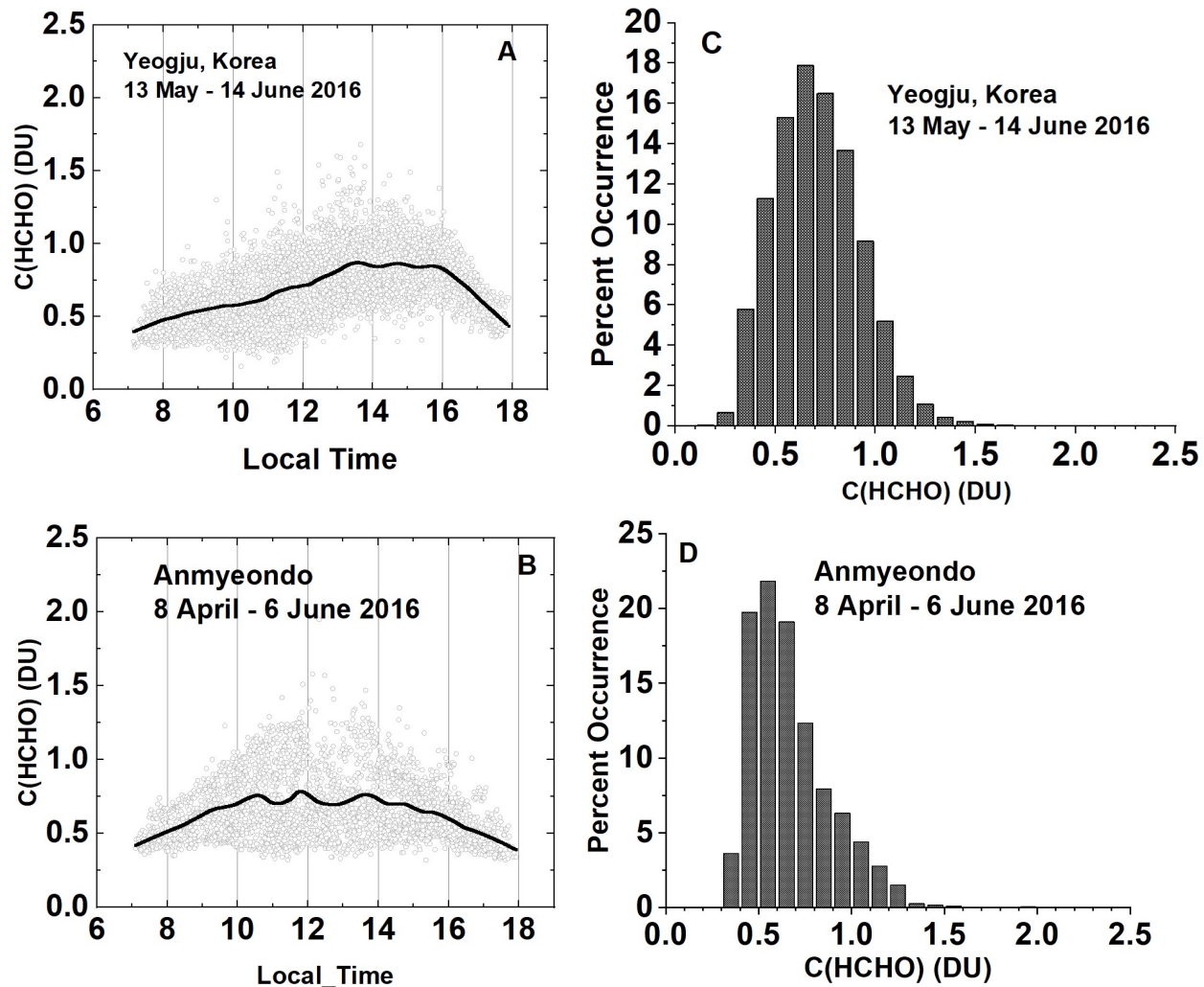


Fig. 19b Summary of total column HCHO for the stated dates during the KORUS-AQ campaign. Panels A and B represent the daily variation at a given local time. The solid line is a Lowess(0.1) fit to the data. Panels C and D show the frequency of occurrence (%) for different amounts of HCHO.

965

966

967 **F19b**

968

969

970

971

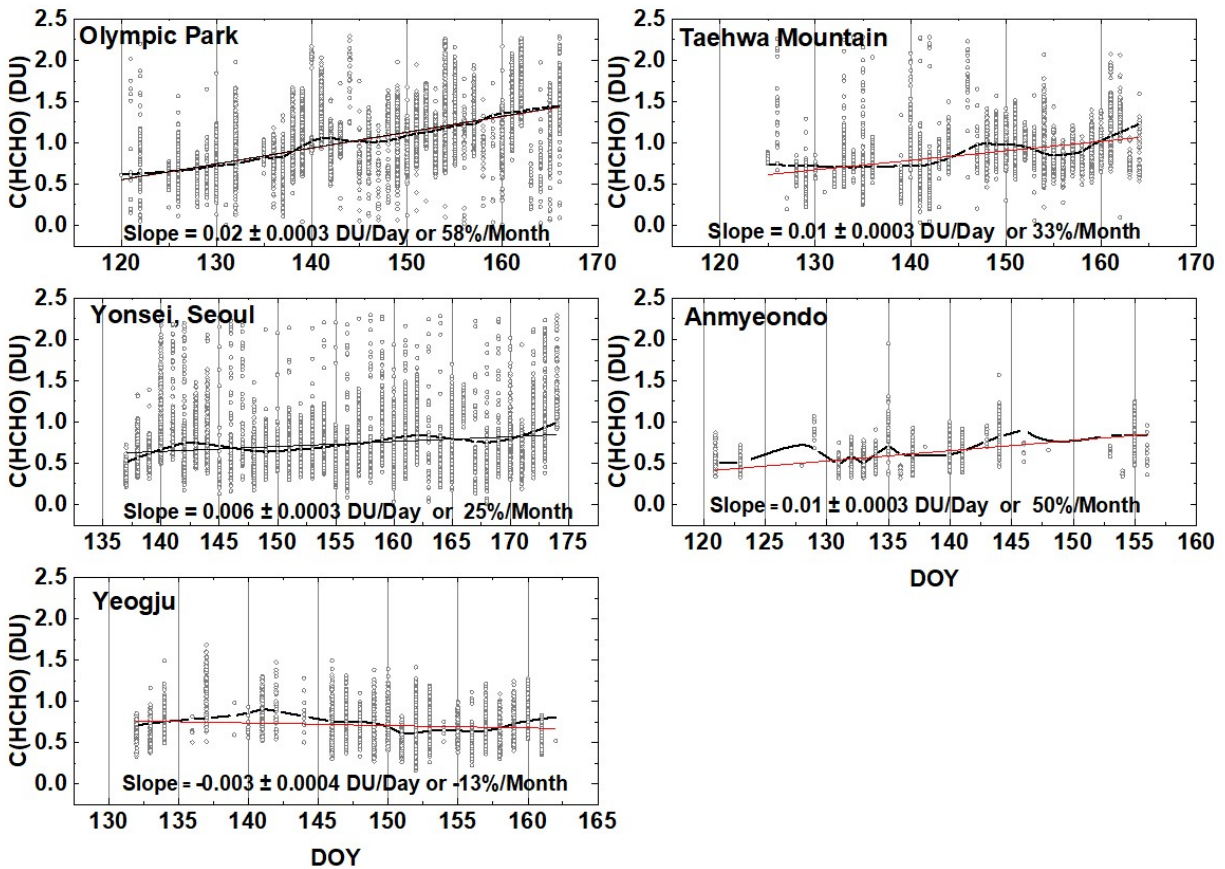


Fig. 20 The springtime change in C(HCHO) over about a 40 day period depending on the site. The “vertical bars” are the diurnal variation within each day of data. The thicker red curve is a Lowess(0.3) fit to the data, while the thin red line is a linear least squares fit. The Lowess(0.3) fit is approximately a 10-day local least-squares average.

972

973 **F20**

974

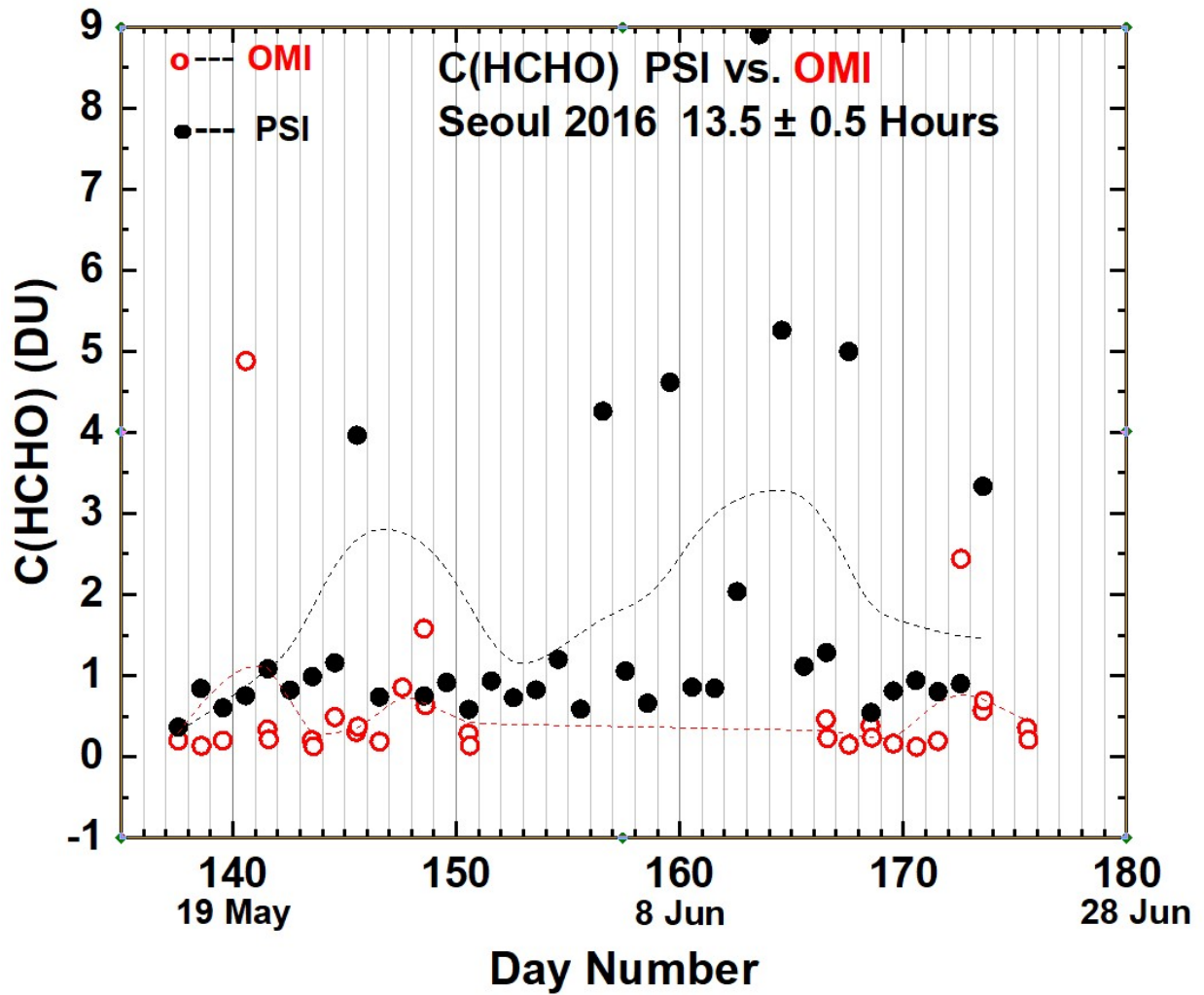


Fig. 21 Compare PSI • and OMI ◯ retrievals of C(HCHO) at 13.5 ± 0.5 hours. OMI overpass data, V03, are from <https://avdc.gsfc.nasa.gov/index.php?site=1113974256&id=81>

975

976 **F21**

977

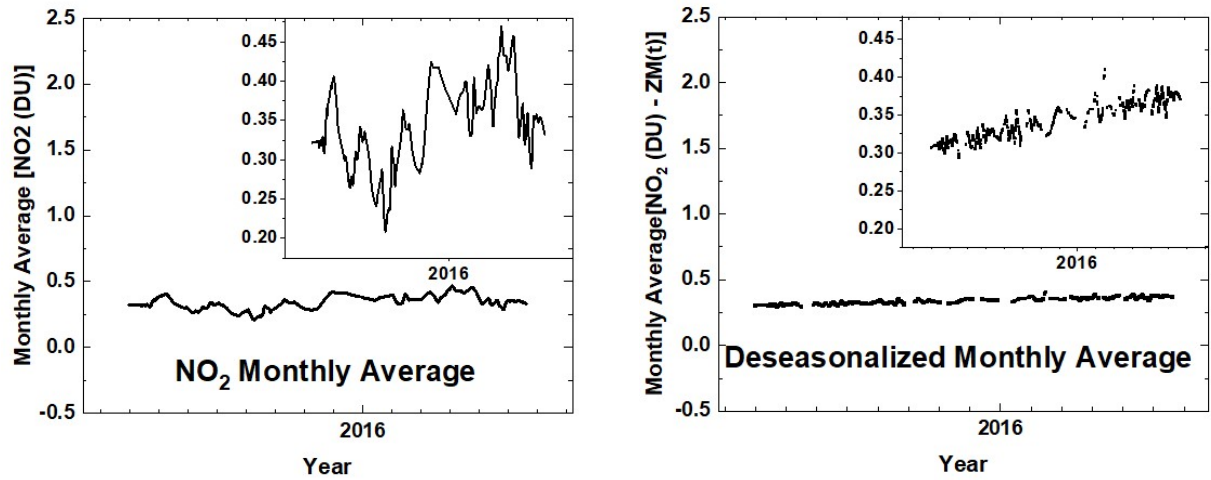


Fig. A1 An illustration of the deseasonalization (right panel) of the monthly running average of NO₂ (left panel) shown in Fig. 6. The insets are magnifications of the main plots.

978

979

980 **FA1**